DISSERTATION

NITRIC OXIDE-RELEASING OR GENERATING SURFACES FOR BLOOD-CONTACTING MEDICAL DEVICES

Submitted by

Yanyi Zang

School of Biomedical Engineering

In partial fulfillment of the requirements

For the Degree of Doctor of Philosophy

Colorado State University

Fort Collins, Colorado

Summer 2020

Doctoral Committee:

Advisor: Melissa Reynolds

Matt Kipper
Yan Vivian Li
Mark Zabel

ABSTRACT

NITRIC OXIDE-RELEASING OR GENERATING SURFACES FOR BLOOD-CONTACTING MEDICAL DEVICES

Medical device-induced thrombosis is a major complication that impairs the expected performance of blood-contacting medical devices. Traditional anticoagulation therapies are used to reduce thrombus formation; however, systemic anticoagulants such as heparin increase the risk of thrombocytopenia or even bleeding, which are detrimental to patients who already have injuries. To address these issues, surface modification has been widely studied to improve the performance of blood-contacting medical devices, ranging from biopassive surfaces to biomimetic surfaces. To date, such modifications are not sufficient to prevent blood clotting alone. Supplementary anticoagulation remains necessary to maintain clot-free surfaces. Nitric oxide (NO) is a well-known signaling molecule that has antiplatelet properties. Our approach is to use surfaces that can either release NO via NO donors or promote NO production via an NO catalyst. In this work, a NO-releasing polyelectrolyte multilayer coating effectively reduces platelet adhesion, platelet activation and delay blood clotting on titania nanotube array surfaces. In addition, NO-releasing polymeric surfaces mediate blood serum protein deposition in a manner that prevents platelet adhesion and platelet activation. However, the NO donors used in these two coatings are photo- and thermo- sensitive, and the NO release is limited by the amount of NO donor added to the coating. To overcome these shortcomings, a copper-based metal organic framework (MOF) was used to infinitely promote NO production from NO donors in the blood. The copper-based MOF polymer coating was successfully applied to the surfaces of extracorporeal life support catheters and circulation tubing via custom coating systems. These

copper-based MOF-coating also exhibited inherent antibacterial properties under both static and dynamic flow conditions.

ACKNOWLEDGEMENTS

I would like to express my sincere appreciation and gratitude to my advisor, Prof. Melissa Reynolds, for her endless help and support throughout my time at Colorado State University. It has been five years, but I can still remember the first time I met you during my interview. You have been such a wonderful advisor that I couldn't ask for anything more. You provided me with unique collaborative opportunities and supported all of my research work and professional development. Most importantly, you taught me how to move forward in life and made me a better person. You influenced me much more than you could imaging. I am so blessed to have you as my advisor.

I would like to thank my committee members, Prof. Matt Kipper, Prof. Yan Vivian Li, and Prof. Mark Zabel for their active participation and invaluable inputs. I would also like to acknowledge Prof. Matt Kipper, Prof. Christine Olver and Prof. Ketul Popat for their insightful advices during our collaborative project. I would like to give my special thanks to Dr. Alec Lutzke, who proofread and provided invaluable input to all of my writings. For all previous and current group members, thank you all for your support. I would also like to thank our collaborator Dr. Andriy Batchinsky from the U.S. Army Institute of Surgical Research who provided me with the opportunity to transfer our benchtop research into real application and showed me how surgeons perform ECLS procedures on animal models when I visited his lab.

I would like to thank my birding friends who distracted me every week and provided me all with delicious food. You treated me like family.

Finally, I would like to thank my parents and my uncle who are always there and support me. To my mom: You unlocked my interests in science and engineering when I was five. You taught me right from wrong and how to love myself and others. To my dad: I know you wanted me to have an easy life and provided me with the best you can, but still supported whatever I

decided to do. To my uncle: I enjoyed the time with you and in your lab every summer when I was in high school. You always encouraged me to take on new challenges.

TABLE OF CONTENTS

ABSTRACT ii
ACKNOWLEDGEMENTS iv
CHAPTER 1 1
LITERATURE REVIEW 1
1.1 Blood-contacting medical devices and complications 1
1.1.1 Coronary stents 2
1.1.2 ECMO 3
1.2 Medical device-induced thrombosis 5
1.3 Systemic antiplatelet agents and anticoagulants 7
1.4 Surface modification 8
1.1.3 Biopassive surfaces 8
1.1.4 Biomimetic surfaces 9
1.5 Nitric oxide 10
1.6 Dissertation overview 13
REFERENCES 14
CHAPTER 2 30
HYPOTHESIS AND RESEARCH AIMS 30
CHAPTER 3 32
FABRICATION AND EX VIVO EVALUATION OF GLYCOCALYX-INSPIRED NITRIC OXIDE-RELEASING POLYELECTROLYTE MULTILAYER COATING ON TITANIA SURFACE 32
3.1 Introduction 32
3.2 Material and methods 35
3.2.1 Materials 35
3.2.2 Fabrication of titania nanotube arrays 36
3.2.3 Synthesis of chitosan thioglycolic acid (Chitosan-TGA) 37
3.2.4 Polyelectrolyte multilayer (PEM) preparation 38
3.2.5 Nitrosation 38
3.2.6 Surface characterization by SEM and XPS 38

3.2.7 Endotoxin assay 39
3.2.8 Nitric oxide detection 39
3.2.9 Human whole blood collection and platelet-rich plasma preparation 40
3.2.10 Cytotoxicity 40
3.2.11 Platelet adhesion 41
3.2.12 Platelet activation 42
3.2.13 Thromboelastography (TEG) 43
3.2.14 Statistical analysis 43
3.3 Results and discussion 44
3.3.1 Surface characterization by SEM and XPS 44
3.3.2 Endotoxin assay 47
3.3.3 Nitric oxide (NO) release 47
3.3.4 Cytotoxicity 49
3.3.5 Platelet adhesion 50
3.3.6 Platelet activation 52
3.3.7 Thromboelastography (TEG) 55
3.4 Conclusions 62
REFERENCES 64
CHAPTER 4 75
NITRIC OXIDE-MEDIATED FIBRINOGEN DEPOSITION PREVENTS PLATELET ADHESION AND ACTIVATION 75
4.1 Introduction 75
4.2 Materials and Methods 78
4.2.1 Materials 78
4.2.2 Synthesis and characterization of S-nitrosoglutathione 78
4.2.3 Fabrication of polymer films 79
4.2.4 Measurement of NO surface flux from polymer films 80
4.2.5 Isolation of platelet-rich plasma 80

4.2.6 Cytotoxicity of polymer films 81
4.2.7 Blood cell interaction with polymer films 81
4.2.8 Surface characterization of high NO flux films 82
4.2.9 Fb adsorption on high NO flux films 83
4.2.10 Blood interaction with high NO flux films with pre-adsorbed Fb 83
4.2.11 Statistical analysis 84
4.3 Results and discussion 84
4.3.1 Measurement of NO surface flux of polymer films 84
4.3.2 Cytotoxicity of polymer films 86
4.3.3 Blood cell interaction with polymer films 87
4.3.4 Surface characterization of high NO flux films 90
4.3.5 Fb adsorption on high NO flux films 92
4.3.6 Blood cell interaction with high NO flux films with pre-adsorbed Fb 95
4.4 Conclusions 97
REFERENCES 99
CHAPTER 5 106
METAL–ORGANIC FRAMEWORK POLYMER COATING ON EXTRACORPOREAL LIFE SUPPORT COMPONENTS AND ITS ANTIBACTERIAL ATTACHMENT PERFORMANCE 106
5.1 Introduction 106
5.2 Materials and methods 110
5.2.1 Materials 110
5.2.2 CuBTTri synthesis and characterization 111
5.2.3 Circulation tubing coating and characterization 112
5.2.4 Avalon catheter coating and characterization 119
5.2.5 OriGen catheter coating 120
5.2.6 Membrane oxygenation fiber coating 122
5.2.7 Bacterial attachment study 123
5.2.8 Statistical analysis 124

5.3 Results and discussion 124
5.3.1 Circulation tubing coating and characterization 124
5.3.2 Avalon catheter coating and coating catalytic property evaluation 132
5.3.3 OriGen catheter coating 134
5.3.4 Membrane oxygenation fiber coating 135
5.3.5 Static and dynamic flow bacterial attachment studies on CuBTTri-coated tubing 136
5.4 Conclusion 140
REFERENCES 141
CHAPTER 6 150
CONCLUSIONS AND FUTURE DIRECTIONS 150
6.1 Conclusions 150
6.2 Future directions 151
6.2.1 NO-releasing PEM coating 151
6.2.2 NO-mediated fibrinogen coating 152
6.2.3 NO-generating MOF-coating 153
REFERENCES 154

CHAPTER 1

LITERATURE REVIEW

1.1 Blood-contacting medical devices and complications

Blood-contacting medical devices have been widely used during clinical procedures and include vacutainer blood collection tubes, coronary stents, central venous catheters, heart valves, hemodialyzers, extracorporeal membrane oxygenators (ECMO), and others. Based on International Organization for Standardization (ISO) 10993-1: 2018 Biological evaluation of medical devices – Part 1: Evaluation and testing within a risk management process, these medical devices can be categorized by nature of body contact.[1] For examples, vacutainer blood collection tubes and *ex vivo* blood diagnostic equipment are non-contact devices, coronary stents and vascular grafts are implant medical devices, and ECMO are externally communicating medical devices. In addition, medical devices can be also categorized based on duration of contact, from limited exposure (<24 h) and prolonged exposure (24 h – 30 days) to long-term exposure (>30 days). For example, blood collection needles are used for less than a few minutes, the duration of patients on ECMO ranges from days to years based on patient's need, while coronary stents can be used for decades. Despite these different categorization methods, one identical feature of these blood-contacting medical devices is the exposure of blood to foreign surfaces, which induces thrombosis and further leads to the failure of medical devices. Among all blood-contacting medical devices, we focus on two medical devices based on their material composition: coronary stents with metallic surfaces, and extracorporeal life support (ECLS) with polymeric surfaces. Both metallic and polymeric surfaces may cause medical device-induced thrombosis during contact with blood.

1.1.1 Coronary stents

Coronary stents are small mesh-like tubes of thin wires that help to keep a blood vessel open and prevent it from narrowing again. The first implantation of a stent into human coronary arteries was performed by Sigwart et al. in 1986.[2,3] In 1993, the Gianturco-Roubin coil stent became the first Food and Drug Administration (FDA)-approved bare-metal stent for threatened or acute vessel closure in the United States.[4] The following year, the first bare-metal balloon-expandable stent developed by Palmaz and Schatz was approved by the FDA for elective use.[3,5] In 1999, the first drug (sirolimus)-eluting stent was implanted into a human coronary artery by Sousa in Brazil.[5,6] Since then, stents technology has developed significantly and is widely used in clinical practice.

Three main types of coronary stents are currently available: bare-metal stents, drug-eluting stents, and textured stents.[7] Traditional bare-metal stents are made from 316L stainless-steel (316L SS), tantalum (Ta), titanium alloys such as nitinol, and others.[7] 316L SS is the most commonly used material for manufacturing stents, with excellent mechanical properties and corrosion resistance.[8] However, 316L SS stents are not MRI compatible, have poorly fluoroscopic visibility, and release ions from the metal surface.[7] Ta stents lack the drawbacks of 316L SS stents, but tent to recoil or break during placement process. Nitinol alloys have been widely used to manufacture self-expanding stents, due to their superelastic and shape memory properties.[9] In addition, Nitinol stents exhibit equal corrosion resistance and biocompatibility to other metallic materials.[9] Although bare-metal stents are able to effectively keep narrowed arteries open, in-stent restenosis develops in approximately 30% of the patients who receives bare-metal stents implantation.[10,11] Drug-eluting stents coated with polymers containing therapeutic agents such as sirolimus and paclitaxel greatly reduce the risk of in-stent restenosis compared to bare-metal stents.[5,12–15] However, late-thrombosis which starts from 1 to 12 months after drug-eluting stent implantation has been observed in many clinical studies, increasing the risk of heart failure or

cardiogenic shock.[16–20] In recent years, textured stents with micro- or nano-topography have become an alternative to bare-metal stents and drug-eluting stents.[21] These textured surfaces are able to serve as drug reservoirs to sustain drug-release in the absence of polymer coatings.[22] In addition, physically or chemically changed surface topography has been shown to enhance corrosion resistance and reendothelialization. However, surfaces with texture oxides still induce late-thrombosis.[22]

By 2019, it was reported that over 1.8 million stents were implanted per year in the United State, including approximately 965,000 coronary stents.[23] However, in-stent restenosis and late-thrombosis remain important clinical problems. To address this, we explored a multifunctional nitric oxide (NO)-releasing polysaccharide-based textured titanium surface as a unique approach to improve the metallic surface of coronary stents.

1.1.2 ECMO

ECMO is extracorporeal circulation with mechanical devices that provides lung and/or heart support to patients with severe trauma injuries (**Figure 1.1**). It pumps blood from patient's body into a membrane lung to remove carbon dioxide and oxygenate blood and delivers the oxygenated blood from the membrane lung back to the patient's body. ECMO has four components: circulation tubing, catheters, membrane lung, and pump. Except the pump, all other components are polymeric surfaces and have direct contact with blood.

Figure 1.1 Extracorporeal membrane oxygenation (ECMO). Photos courtesy of Dr. Phillip Mason, Col (USAF) with permission.

The concept of an artificial lung support was established in 1930s by Carrel and Lindbergh.[24] In 1953, the first heart-lung machine was successfully used for an atrial septal defect repair by Gibbons who had been working on the development of this machine for approximately 25 years.[25] However, the first clinical use of ECMO for an adult patient with heart and lung failure did not occur until 1971.[26] Five years later, Bartlett reported the first neonatal survivor of ECMO with lung damage.[27] After these initial successes, ECMO made slow progress due to the low long-term survival rate of adult patients on ECMO reported in 1979 and 1994, even with a 50-60% survival rate in neonate and pediatric populations.[28–30] In the last decade, ECMO has regained interest with a better understanding of ventilator-associated lung injury and the improvement of pump and membrane lung technology.[31] A landmark was the 75% survival rate of ECMO in critically ill patients with H1N1-associated respiratory failure in 2009.[32] Since then, ECMO has been widely recognized and has grown rapidly in intensive care units for patients with acute respiratory disease syndrome.

In recent years, ECMO has been increasingly used for combat casualty critical care by the U.S. military.[31,33] The Department of Defense has established a programmatic focus to novel forms of ECMO at Role II, Role III, and other stages of ground and altitude evacuation.[31,33–36] However, there are challenges in the use of ECMO for military medical care, including complications related to the management of thrombosis and hemorrhage during prolonged field care.[37–39] This major complication limits the early initiation and wider utilization of ECMO for trauma patients. To address this, we establish coating methods for circulation tubing, catheters, and membrane lung and evaluate the performance of copper-based metal-organic framework (MOF) coating.

1.2 Medical device-induced thrombosis

Under physiological conditions, the endothelium layer lining on the interior wall of blood vessels inhibits protein adsorption and cell adhesion, and further prevents thrombus formation.[40] However, the surfaces of medical devices lack this endothelium layer and present as a foreign body to blood. The interaction between blood and the surfaces of medical devices ultimately results in thrombosis which commonly causes the failure of medical devices. Four major events lead to medical device-induced thrombosis as shown in **Figure 1.2**: (1) protein adsorption, (2) platelet adhesion, activation and aggregation, (3) blood coagulation, and (4) thrombus formation.[41]

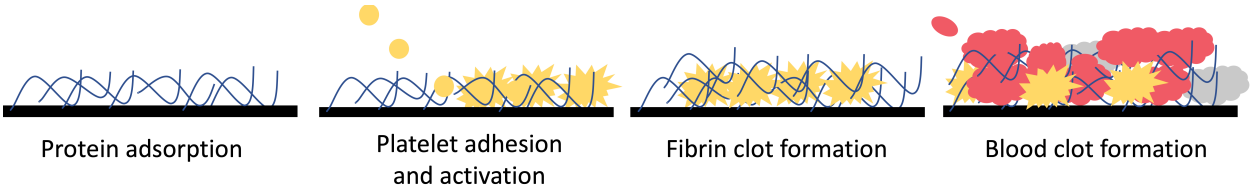

Figure 1.2 Schematic of blood clotting cascade.

Blood mainly contains plasma, platelets, red blood cells, and white blood cells. Blood serum proteins are one of the major components in plasma, including 55% of albumins, 38%of globulins, 7% of fibrinogen, and approximately 300 other types of proteins.[42,43] Within seconds to minutes of contact, blood proteins adsorb onto a material surface and form a 2-10 nm protein monolayer.[41] After attachment, the adsorbed proteins undergo conformational change through structure rearrangement and adapt an orientation in which part of the protein interacts with the material surface and another is exposed to the blood.[44] The ability of proteins to bind to cells is determined by the exposed part. It is believed that cells in blood recognize and respond to this adsorbed protein layer, rather than through direct contact with a foreign surface.[45]

Among these adsorbed proteins, fibrinogen is a prominent component in blood clotting and binds only to inactivated platelets.[46] Fibronectin, vitronectin, and von Willebrand factor are

also able to bind platelets, but are less important in mediation of platelet adhesion than fibrinogen.[47] Albumin has been considered as non-adhesive to platelets for a long time. However, certain studies have suggested that platelets adhere to albumin through receptor-mediated processes with the full mechanism remaining unclear.[48,49] The adsorbed proteins bind to platelets through integrin $\alpha IIb\beta_3$ (known as glycoprotein IIb/IIIa and the most abundant integrin on the platelet surface) and other receptors, leading to platelet adhesion.[50–52] Adhered platelets further spread or change shape, which is mediated by cytoskeletal reorganization.[53] This platelet activation can be recognized through pseudopod extension. In addition, the release of granule contents is able to further activate and induce platelet aggregation.[54]

Blood serum protein induced blood coagulation is also responsible for thrombus formation by converting fibrinogen into fibrin clots.[55] Two pathways are involved in coagulation cascades: an extrinsic pathway which is triggered by vessel injuries and responsible for hemostatic control, and an intrinsic pathway which is triggered by the interaction between blood and a foreign surface.[56,57] The initiation of the intrinsic pathway involves Factor XII, prekallikrein, high-molecular weight kininogen, and coagulation Factor XI.[55] Factor XII is first converted to Factor XIIa which then activates Factor XI to Factor XIa.[58] Factor XIa further converts Factor IX to Factor IXa which then convert Factor X to Factor Xa. Finally, Factor Xa activates thrombin which converts fibrinogen into fibrin clots.[59]

The aggregated platelets are stabilized by fibrin clots and form a platelet-fibrin thrombus. Such thrombi may lead to the failure of medical devices without proper treatment. To prevent medical device-induced thrombosis, strategies involved in systemic antiplatelet agents and anticoagulants, and cutting-edge surface modification techniques will be discussed in the following sections.

1.3 Systemic antiplatelet agents and anticoagulants

Systemic antiplatelet agents which inhibit platelet aggregation and anticoagulants which inhibit coagulation pathways are drugs that have been used to prevent thrombus formation or prolong clotting time in clinical procedures. The use of these drugs has both benefits and risks. The greatest risk is bleeding complications, especially in patients who have bleeding injuries or clotting disorders. Below are several examples of commonly used systemic antiplatelet agents and anticoagulants.

Dual antiplatelet therapy (DAPT), the combination of aspirin and a $P2Y_{12}$ inhibitor (clopidogrel, prasugrel, or ticagrelor), is commonly used for adult patients with bare-metal stent or drug-eluting stent implantation.[60] Aspirin exerts antithrombotic effects through irreversible acetylation of a serine residue of cyclooxygenase (COX). The COX enzyme family catalyzes a series of reactions to generate thromboxane A2 (TXA_2), which induces platelet aggregation.[61,62] Although the half-life of aspirin is 20 min, the duration of effect lasts through the approximate 10 day life cycle of platelets, since platelets cannot generate new COX.[61] $P2Y_{12}$ inhibitors block the $P2Y_{12}$ receptor, which is the primary receptor involved in adenosine diphosphate (ADP)-stimulated activation of the $\alpha IIb\beta_3$ receptor. Inactivation of the $\alpha IIb\beta_3$ receptor results in diminished platelet degranulation and thromboxane production, leading to reduced platelet aggregation.[63] DAPT is able to inhibit platelets more effectively than single antiplatelet therapy, reducing the degree of thrombus formation.[64] However, prolonged use of DAPT increases the risk of bleeding complications, which relates to the increased risk of both short- and long-term mortality.[65,66]

Unfractionated heparin (UNFH) is currently the main anticoagulant used in ECMO. It exerts anticoagulant effects by binding to antithrombin, an endogenous anticoagulant produced by the liver.[37] The UNFH + antithrombin complex is able to inactivate thrombin, activated Factor Xa, and coagulation factors.[67] However, this complex cannot bind to thrombin already existing in fibrin clots, due to the less accessible binding sites on clot-bound thrombin, leading to the

ineffectiveness of UNFH on pre-existing clots.[68] The use of UNFH also has the risk of bleeding complications. In clinical procedure, activated clotting time (ACT), thromboelastography, or activated partial thromboplastin time (aPTT) are monitored. Protamine is used as an antidote to reverse the effects of UNFH.[37] Direct thrombin inhibitors (DTIs) such as bivalirudin and argatroban are a class of new anticoagulants that are being used in patients with allergic reactions to UNFH. They are able to specifically bind both circulating and clot-bound thrombin, not other plasma proteins. However, there is no antidote to reverse the effects of DTIs. In addition, DTIs can destabilize existing clots in the patients, increasing the risk of destroying normal hemostasis and inducing bleeding complications.[37,69] Because the anticoagulation responses vary between patients, it is challenging to balance clotting and the effect of systemic anticoagulants.

1.4 Surface modification

Surface modification is another strategy to improve the performance of blood-contacting medical devices. Since the mechanism of thrombus formation has been well-studied over the past decades, different surface modification techniques have been investigated to prevent protein adsorption, inhibit platelet activity, and impede the blood coagulation cascade. Some of these surface modification techniques are already commercially available, while some remain under development. Surface modification can be classified into two groups: biopassive surfaces and biomimetic surfaces. Several common surface modification techniques used for blood-contacting medical devices are discussed below, including commercially available surfaces and novel surfaces that are currently being researched.

1.1.3 Biopassive surfaces

Trillium® Biosurface is a polymer coating used in extracorporeal circuits and catheters. This surface is hydrophilic and contains a polyethylene oxide layer with negatively charged sulfate/sulfonate groups and heparin.[70] Polyethylene oxide serves as a priming layer that strongly

binds to the artificial surface of the device. The sulfate/sulfonate and heparin layer is the functional layer that strongly binds to the priming layer and is able to hold water and repel blood cells.[71] The Trillium® Biosurface has been shown to significantly improve the biocompatibility of cardiopulmonary bypass circuits.[72–74] However, the Trillium® Biosurface failed to show clinical benefits or clinically important biochemical results in certain clinical trials.[75,76]

Phosphorylcholine (PPC) represents the predominant hydrophilic polar head group of zwitterionic phospholipids on the outside of plasma membranes of red blood cells and platelets.[77] It has been suggested that these polar head groups contribute to the interface between cell membrane and surrounding environment, maintaining the hemostatic balance.[77] PPC coated coronary stents have shown excellent biocompatibility in an animal study and favorable effects on blood platelets in a human clinical trial.[78,79] In addition, phosphorylcholine has been crosslinked with polymers to enhance its antithrombotic properties or act as a multifunctional copolymer.[80–82] However, in certain studies, PPC coatings did not show advantages compared to artificial surfaces with or without other coatings.[83,84]

Poly-2-methoxyethylacrylate (PMEA) coatings have been evaluated in cardiopulmonary bypass. PMEA is an amphiphilic polymer with a hydrophobic polyethylene backbone and mild residues with hydrophilic functional groups.[85] PMEA coatings have been shown to have similar performance as commercially available heparin coatings.[85,86] In contrast, unlike heparin coatings, some studies suggest that PMEA coatings may lead to post-procedural leukopenia and systemic inflammatory response syndrome in the pediatric population.[87]

1.1.4 Biomimetic surfaces

Heparin, a polysaccharide with a repeating disaccharide unit, belongs to the glycosaminoglycan (GAG) family.[88] Heparin is chemically and structurally similar to heparan sulfate, a proteoglycan that has an anticoagulative function in the vascular endothelium.[89] In 1963,

Gott et al. bound the anticoagulant drug heparin to a colloidal graphite coating and first discovered the thromboresistant properties of a heparin-coated surface.[90] Since then, heparin-bound surfaces have been widely studied and used on blood-contacting medical devices. Two types of heparin binding techniques are currently available: ionic binding and covalent binding.[91] Ionic binding through the ionic interaction between negatively charged heparin which localized to sulfate and carboxyl groups and positively charged quaternary ammonium ions on a device surface. However, this technique has a risk of heparin leaching and further damage the membrane lung fibers.[92] Covalent binding reduces the risk of heparin leaching and is able to permanently immobilize heparin onto the device surface. However, immobilized heparin has a relatively low binding affinity for antithrombin compared to free heparin, leading to insufficient antithrombotic activity. With this disadvantage, the heparin-bound surface cannot prevent blood clotting alone and supplemental systemic anticoagulants are needed during the ECMO procedure.[93,94] Therefore, treatment with covalently heparinized surfaces may result in the same complications associated with UNFH.

1.5 Nitric oxide

Nitric oxide (NO) was first identified as a simple gas molecule with one nitrogen atom and one oxygen atom by Joseph Priestly in 1772.[95] Since this first discovery, NO was primarily recognized as an atmospheric pollutant until the late 1970s,[96,97] the dawn of understanding NO from a pharmacological perspective.[98] Furchgott and Zawadzki first discovered blood vessel relaxation requires the presence of endothelial cells when studying the effects of acetylcholine on vasodilation.[98] In 1982, Furchgott et al. demonstrated the link between an unknown endothelium-derived relaxing factor (EDRF) and relaxation of arteries.[99] These results drew broad interest in identification of this unknown EDRF. In 1987, Ignarro et al. published two articles that demonstrated the chemical and biological properties of EDRF are equivalent to radical NO.[100,101]

During the same period, Murad et al. noticed that several nitrogen-containing chemicals were able to increase guanylate cyclase activity, and in 1977 they hypothesized that the mechanism might be due to the formation of NO.[102] In the same year, Murad et al. validated that it was NO alone or NO produced from nitro compounds activated by guanylate cyclase.[103] In 1998, Furchgott, Ignarro, and Murad shared The Nobel Prize in Physiology or Medicine for their identification of NO as a signaling molecule in the cardiovascular system.[104] Following these milestones, the study of NO biochemistry and the use of NO as a therapeutic agent have greatly expanded.

NO is a signaling molecule involved in many physiological processes, such as inhibition of platelet activation and aggregation, defense against bacteria, promotion of the wound healing process, and others. NO is synthesized through a series of enzymatic reactions promoted by a family of NO synthases (NOS) that convert the amino acid L-arginine to L-citrulline.[105] Three NOS are present in mammals: calcium-dependent endothelial NOS (eNOS) and neuronal NOS (nNOS), and calcium-independent inducible NOS (iNOS). The half-life of NO is between milliseconds to seconds depending on oxygen (O_2) concentration and distance from the blood vessel wall.[106] This short half-life is largely due to the interaction between NO and hemoglobin. Hemoglobin is a tetrameric protein with four iron-containing globular protein subunits.[107] In mammals, hemoglobin can bind up to four O_2 to form oxyhemoglobin, in which the heme group iron is ferrous (Fe^{2+}). When ferrous iron is oxidized to the ferric state (Fe^{3+}), hemoglobin cannot carry O_2, forming methemoglobin. However, NO is able to bind to ferrous iron heme to form nitrate and methemoglobin, as well as bind to ferric ions with a lower affinity.[108,109] Though such an interaction, hemoglobin can deplete NO and further mediate NO signaling pathway. In addition, NO can be consumed through the indirect interaction with other radicals such as superoxide O_2-, which widely occurs in nature, to form reactive nitrogen species such as nitrate (NO_3-), nitrite (NO_2-), peroxynitrite (ONOO), dinitrogen trioxide (N_2O_3) and dinitrogen tetroxide (N_2O_4).[110,111] The very short half-life makes NO a promising therapeutic agent that can locally target its effects. Some

examples include the addition of NO gas into ECMO circuits and fabrication of NO-releasing materials.[112,113]

Nitric oxide is well-known for its ability to inhibit platelet activity. The vascular endothelium cell can generate NO through calcium-dependent eNOS to protect blood vessels from platelet adhesion and aggregation.[114] NO performs its antiplatelet properties through the increased amount of intracellular cyclic guanosine monophosphate (cGMP) which can inhibit calcium mobilization.[115–117] Intracellular calcium has been shown to regulate platelet inhibition and further delay thrombus growth.[118,119] NO is also able to inhibit thromboxane A_2, a type of thromboxane secreted by activated platelets to stimulate new platelet activation and aggregation.[120] The inhibition of thromboxane A_2 is believed to occur through the phosphorylation of the thromboxane A_2 receptor by cGMP-dependent protein kinase.[121] In addition, both eNOS and iNOS isoforms are present in platelets, leading to the production of platelet-derived NO production.[122] Several studies have proposed that platelet-derived NO suppressed platelet activation less depends on intracellular Ca^{2+} than endothelium-derived NO.[123–125] Several stimuli are able to active eNOS in platelets through glycoprotein VI (GPVI), β_2-adrenoceptors (β_2AR), protein kinase B (Akt) or others without affected by intracellular Ca^{2+}, resulting in the conversion from L-arginine to L-citrulline and NO.[125] The NO-induced increased concentration of cGMP is also able to inhibit fibrinogen binding to the $\alpha IIb\beta_3$ receptor on the surfaces of platelet membranes through the decreased calcium ion concentration, which further inhibits platelet adhesion, activation and aggregation.[126] However, recent studies have shown that NO-releasing surfaces increase fibrinogen adsorption in a manner that prevents platelet adhesion and activation.[127,128] The mechanism is still unclear.

1.6 Dissertation overview

This dissertation focuses on the fabrication of various NO-generating coatings for different medical applications and their performance on protein, platelet, whole blood, and bacteria.

Multifunctional surfaces have become a new approach in the design of biomimetic surfaces for medical devices that prevent blood clotting. The endothelial glycocalyx presents a brush-like carbohydrate-rich lining on the surface of vascular endothelial cells.[129] Inspired by the glycocalyx, a NO-releasing polyelectrolyte multilayer coating on a titanium nanotube array surface is explored and evaluated using platelet-rich plasma and human whole blood in Chapter 3.

Protein adsorption marks the beginning of thrombus formation on blood-contacting medical devices. NO is well-known for its antiplatelet functions and its ability to prevent thrombus formation. However, it was observed that NO-releasing surfaces decrease clot formation despite the presence of a thin fibrin layer.[130] More interestingly, Lantvit et al. confirmed that a significant degree of fibrinogen adsorption occurs on NO-releasing surfaces.[127] There is a lack of information regarding how this fibrinogen would affect platelet activity. In Chapter 4, the effects of NO-exposed fibrinogen on platelets adhesion and activation are explored.

Thrombosis is a major complication that impede the performance of ECMO. Traditional heparinization is utilized to prevent thrombus formation in the ECMO circuit, however this treatment increases the risk of bleeding. Copper-based additives promote NO production from endogenous biomolecules present in blood, such as *S*-nitrosoglutathione (GSNO). Free copper-based additives have shown to inhibit collagen-stimulated platelet aggregation and reduce thrombus formation in human donor blood.[131] To date, the ability of copper-based additives to improve NO production has not been exploited in the design of ECMO systems that contain it as a coating. In Chapter 5, various coating methods are designed to coat a copper-based additive onto the surface of ECLS components with the aim to promote NO production from NO donors in the blood.

REFERENCES

1. ISO 10993-1:2018 - Biological evaluation of medical devices — Part 1: Evaluation and testing within a risk management process. https://www.iso.org/standard/68936.html. Accessed February 19, 2020.
2. Sigwart U, Puel J, Mirkovitch V, Joffre F, Kappenberger L. Intravascular Stents to Prevent Occlusion and Re-Stenosis after Transluminal Angioplasty. *N Engl J Med*. 1987;316(12):701-706. doi:10.1056/NEJM198703193161201
3. Tomberli B, Mattesini A, Baldereschi GI, Di Mario C. A Brief History of Coronary Artery Stents. *Rev Española Cardiol (English Ed*. 2018;71(5):312-319. doi:10.1016/j.rec.2017.11.022
4. Mueller RL, Sanborn TA. The history of interventional cardiology: Cardiac catheterization, angioplasty, and related interventions. *Am Heart J*. 1995;129(1):146-172. doi:10.1016/0002-8703(95)90055-1
5. Htay T, Liu MW. Drug-eluting stent: a review and update. *Vasc Health Risk Manag*. 2005;1(4):263-276. doi:10.2147/vhrm.2005.1.4.263
6. Iqbal J, Gunn J, Serruys PW. Coronary stents: historical development, current status and future directions. doi:10.1093/bmb/ldt009
7. Mani G, Feldman MD, Patel D, Agrawal CM. Coronary stents: A materials perspective. *Biomaterials*. 2007;28(9):1689-1710. doi:10.1016/j.biomaterials.2006.11.042
8. Navarro L, Luna J, Rintoul I. SURFACE CONDITIONING of CARDIOVASCULAR 316L STAINLESS STEEL STENTS: A REVIEW. *Surf Rev Lett*. 2017;24(1). doi:10.1142/S0218625X17300027
9. Stoeckel D, Pelton A, Duerig T. Self-expanding Nitinol stents: Material and design considerations. *Eur Radiol*. 2004;14(2):292-301. doi:10.1007/s00330-003-2022-5
10. Mehran R, Dangas G, Abizaid AS, et al. Angiographic patterns of in-stent restenosis:

Classification and implications for long-term outcome. *Circulation*. 1999;100(18):1872-1878. doi:10.1161/01.CIR.100.18.1872

11. Her AY, Shin ES. Current management of in-stent restenosis. *Korean Circ J*. 2018;48(5):337-349. doi:10.4070/kcj.2018.0103
12. Sousa JE, Costa MA, Abizaid AC, et al. Sustained suppression of neointimal proliferation by sirolimus-eluting stents: One-year angiographic and intravascular ultrasound follow-up. *Circulation*. 2001;104(17):2007-2011. doi:10.1161/hc4201.098056
13. Sousa JE, Costa MA, Sousa AGMR, et al. Two-year angiographic and intravascular ultrasound follow-up after implantation of sirolimus-eluting stents in human coronary arteries. *Circulation*. 2003;107(3):381-383. doi:10.1161/01.CIR.0000051720.59095.6D
14. Sousa JE, Serruys PW, Costa MA. New frontiers in cardiology: drug-eluting stents: Part I. *Circulation*. 2003;107(17):2274-2279. doi:10.1161/01.CIR.0000069330.41022.90
15. Sousa JE, Serruys PW, Costa MA. New frontiers in cardiology: Drug-eluting stents: Part II. *Circulation*. 2003;107(18):2383-2389. doi:10.1161/01.CIR.0000069331.67148.2F
16. Liistro F, Colombo A. Late acute thrombosis after paclitaxel eluting stent implantation. *Heart*. 2001;86(3):262-264. doi:10.1136/heart.86.3.262
17. McFadden EP, Stabile E, Regar E, et al. Late thrombosis in drug-eluting coronary stents after discontinuation of antiplatelet therapy. *Lancet*. 2004;364(9444):1519-1521. doi:10.1016/S0140-6736(04)17275-9
18. Bavry AA, Kumbhani DJ, Helton TJ, Borek PP, Mood GR, Bhatt DL. Late Thrombosis of Drug-Eluting Stents: A Meta-Analysis of Randomized Clinical Trials. *Am J Med*. 2006;119(12):1056-1061. doi:10.1016/j.amjmed.2006.01.023
19. Feres F, Ribamar Costa J, Abizaid A. Very late thrombosis after drug-eluting stents. *Catheter Cardiovasc Interv*. 2006;68(1):83-88. doi:10.1002/ccd.20692
20. Maisel WH. Unanswered Questions — Drug-Eluting Stents and the Risk of Late

Thrombosis. *N Engl J Med*. 2007;356(10):981-984. doi:10.1056/NEJMp068305

21. Caves JM, Chaikof EL. The evolving impact of microfabrication and nanotechnology on stent design. *J Vasc Surg*. 2006;44(6):1363-1368. doi:10.1016/j.jvs.2006.08.046
22. O'Brien B, Zafar H, Ibrahim A, Zafar J, Sharif F. Coronary Stent Materials and Coatings: A Technology and Performance Update. *Ann Biomed Eng*. 2016;44(2):523-535. doi:10.1007/s10439-015-1380-x
23. Interventional Cardiology Devices Market | US | Analysis, ASP, Size, Units Sold, Forecasts | 2018-2024. https://idataresearch.com/product/interventional-cardiology-market-united-states/. Accessed February 19, 2020.
24. Carrel A, Lindbergh CA. The culture of whole organs. *Science (80-)*. 1935;81(2112):621-623. doi:10.1126/science.81.2112.621
25. Stoney WS. Evolution of cardiopulmonary bypass. *Circulation*. 2009;119(21):2844-2853. doi:10.1161/CIRCULATIONAHA.108.830174
26. Hill JD, O'brien TG, Murray JJ, et al. Prolonged Extracorporeal Oxygenation for Acute Post-Traumatic Respiratory Failure (Shock-Lung Syndrome): Use of the Bramson Membrane Lung. *N Engl J Med*. 1972;286(12):629-634. doi:10.1056/NEJM197203232861204
27. Bartlett RH, Gazzaniga AB, Jefferies MR, Huxtable RF, Haiduc NJ, Fong SW. Extracorporeal Membrane Oxygenation (ECMO) Cardiopulmonary Support in Infancy. *Am Soc Artif Intern Organsrtificial Intern Organs*. 1976;22(1):80-92.
28. Zapol WM. Extracorporeal membrane oxygenation in severe acute respiratory failure. A randomized prospective study. *JAMA J Am Med Assoc*. 1979;242(20):2193-2196. doi:10.1001/jama.242.20.2193
29. Morris AH, Wallace CJ, Menlove RL, et al. Randomized clinical trial of pressure-controlled inverse ratio ventilation and extracorporeal CO2 removal for Adult Respiratory

Distress Syndrome. *Am J Respir Crit Care Med*. 1994;149(2 I):295-305. doi:10.1164/ajrccm.149.2.8306022

30. Cypel M, Keshavjee S. Artificial Lung Support. In: *Regenerative Medicine Applications in Organ Transplantation*. Elsevier Inc.; 2014:683-689. doi:10.1016/B978-0-12-398523-1.00047-1

31. Neff LP, Cannon JW, Stewart IJ, et al. Extracorporeal organ support following trauma: the dawn of a new era in combat casualty critical care. *J Trauma Acute Care Surg*. 2013;75(2 SUPPL. 2):S120-S129. doi:10.1097/TA.0b013e318299d0cb

32. Laudi S, Busch T, Kaisers U. Extracorporeal membrane oxygenation for ARDS due to 2009 influenza A(H1N1) [7]. *JAMA - J Am Med Assoc*. 2010;303(10):941. doi:10.1001/jama.2010.200

33. Cannon JW, Mason PE, Batchinsky AI. Past and present role of extracorporeal membrane oxygenation in combat casualty care. *J Trauma Acute Care Surg*. 2018;84(6S Suppl 1):S63-S68. doi:10.1097/TA.0000000000001846

34. Rasmussen TE, Baer DG, Remick KN, Ludwig G V. Combat casualty care research for the multidomain battlefield. *J Trauma Acute Care Surg*. 2017;83:S1-S3. doi:10.1097/TA.0000000000001469

35. Macku D, Hedvicak P, Quinn J, Bencko V. Prehospital Medicine and the Future Will ECMO Ever Play a Role? *J Spec Oper Med*. 18(1):133-138. http://www.ncbi.nlm.nih.gov/pubmed/29533448. Accessed February 21, 2020.

36. Allan PF, Osborn EC, Bloom BB, Wanek S, Cannon JW. The Introduction of Extracorporeal Membrane Oxygenation to Aeromedical Evacuation. *Mil Med*. 2011;176(8):932-937. doi:10.7205/milmed-d-10-00294

37. Coughlin MA, Bartlett RH. Anticoagulation for Extracorporeal Life Support. *ASAIO J*. 2015;61(6):652-655. doi:10.1097/MAT.0000000000000273

38. Oliver WC. Anticoagulation and coagulation management for ECMO. *Semin Cardiothorac Vasc Anesth*. 2009;13(3):154-175. doi:10.1177/1089253209347384

39. Tieu BH, Holcomb JB, Schreiber MA. Coagulopathy: Its pathophysiology and treatment in the injured patient. *World J Surg*. 2007;31(5):1055-1064. doi:10.1007/s00268-006-0653-9

40. Yau JW, Teoh H, Verma S. Endothelial cell control of thrombosis. *BMC Cardiovasc Disord*. 2015;15(1). doi:10.1186/s12872-015-0124-z

41. Jaffer IH, Fredenburgh JC, Hirsh J, Weitz JI. Medical device-induced thrombosis: what causes it and how can we prevent it? *J Thromb Haemost*. 2015;13(S1):S72-S81. doi:10.1111/jth.12961

42. Anderson NL, Anderson NG. The human plasma proteome: history, character, and diagnostic prospects. *Mol Cell Proteomics*. 2002;1(11):845-867. doi:10.1074/mcp.R200007-MCP200

43. 18.1 An Overview of Blood – Anatomy and Physiology. https://opentextbc.ca/anatomyandphysiology/chapter/an-overview-of-blood/. Accessed February 23, 2020.

44. Rabe M, Verdes D, Seeger S. Understanding protein adsorption phenomena at solid surfaces. *Adv Colloid Interface Sci*. 2011;162(1-2):87-106. doi:10.1016/j.cis.2010.12.007

45. Wilson CJ, Clegg RE, Leavesley DI, Pearcy MJ. Mediation of biomaterial-cell interactions by adsorbed proteins: A review. *Tissue Eng*. 2005;11(1-2):1-18. doi:10.1089/ten.2005.11.1

46. Wertz CF, Santore MM. Adsorption and relaxation kinetics of albumin and fibrinogen on hydrophobic surfaces: Single-species and competitive behavior. *Langmuir*. 1999;15(26):8884-8894. doi:10.1021/la990089q

47. Tsai WB, Grunkemeier JM, McFarland CD, Horbett TA. Platelet adhesion to polystyrene-based surfaces preadsorbed with plasmas selectively depleted in fibrinogen, fibronectin,

vitronectin, or von Willebrand's factor. *J Biomed Mater Res*. 2002;60(3):348-359. doi:10.1002/jbm.10048

48. Sivaraman B, Latour RA. The Adherence of platelets to adsorbed albumin by receptor-mediated recognition of binding sites exposed by adsorption-induced unfolding. doi:10.1016/j.biomaterials.2009.10.017

49. Hylton DM, Shalaby SW, Latour RA. Direct correlation between adsorption-induced changes in protein structure and platelet adhesion. *J Biomed Mater Res - Part A*. 2005;73(3):349-358. doi:10.1002/jbm.a.30295

50. Savage B, Ruggeri ZM. Selective recognition of adhesive sites in surface-bound fibrinogen by glycoprotein IIb-IIIa on nonactivated platelets. *J Biol Chem*. 1991;266(17):11227-11233. http://www.ncbi.nlm.nih.gov/pubmed/2040630. Accessed February 23, 2020.

51. Coller BS. αIIbβ3: Structure and function. *J Thromb Haemost*. 2015;13(S1):S17-S25. doi:10.1111/jth.12915

52. Goodman SL, Cooper SL, Albrecht RM. Integrin receptors and platelet adhesion to synthetic surfaces. *J Biomed Mater Res*. 1993;27(5):683-695. doi:10.1002/jbm.820270516

53. Park K, Park H. Application of video-enhanced interference reflection microscopy to the study of platelet-surface interactions. *Scanning Microsc Suppl*. 1989;3:137-145; discussion 145-6. http://www.ncbi.nlm.nih.gov/pubmed/2616950. Accessed February 23, 2020.

54. Friedman LI, Liem H, Grabowski EF, Leonard EF, McCord CW. Inconsequentiality of surface properties for initial platelet adhesion. *Trans Am Soc Artif Intern Organs*. 1970;16:63-73. http://www.ncbi.nlm.nih.gov/pubmed/5454212. Accessed February 23, 2020.

55. Xu L-CC, Bauer JW, Siedlecki CA. Proteins, platelets, and blood coagulation at biomaterial interfaces. *Colloids Surfaces B Biointerfaces*. 2014;124:49-68.

56. Mackman N, Tilley RE, Key NS. Role of the extrinsic pathway of blood coagulation in hemostasis and thrombosis. *Arterioscler Thromb Vasc Biol*. 2007;27(8):1687-1693. doi:10.1161/ATVBAHA.107.141911

57. Gailani D, Renné T. The intrinsic pathway of coagulation: A target for treating thromboembolic disease? *J Thromb Haemost*. 2007;5(6):1106-1112. doi:10.1111/j.1538-7836.2007.02446.x

58. Griffin JH. Role of surface in surface-dependent activation of Hageman factor (blood coagulation Factor XII). *Proc Natl Acad Sci U S A*. 1978;75(4):1998-2002. doi:10.1073/pnas.75.4.1998

59. Palta S, Saroa R, Palta A. Overview of the coagulation system. *Indian J Anaesth*. 2014;58(5):515-523. doi:10.4103/0019-5049.144643

60. Levine GN, Bates ER, Bittl JA, et al. 2016 ACC/AHA Guideline Focused Update on Duration of Dual Antiplatelet Therapy in Patients With Coronary Artery Disease: A Report of the American College of Cardiology/American Heart Association Task Force on Clinical Practice Guidelines. *J Am Coll Cardiol*. 2016;68(10):1082-1115. doi:10.1016/j.jacc.2016.03.513

61. Awtry EH, Loscalzo J. *Aspirin.*; 2000. http://www.circulationaha.org. Accessed February 25, 2020.

62. Altman R, Luciardi HL, Muntaner J, Herrera RN. The antithrombotic profile of aspirin. Aspirin resistance, or simply failure? *Thromb J*. 2004;2(1):1. doi:10.1186/1477-9560-2-1

63. Damman P, Woudstra P, Kuijt WJ, De Winter RJ, James SK. P2Y12 platelet inhibition in clinical practice. *J Thromb Thrombolysis*. 2012;33(2):143-153. doi:10.1007/s11239-011-0667-5

64. Degrauwe S, Pilgrim T, Aminian A, Noble S, Meier P, Iglesias JF. Dual antiplatelet therapy for secondary prevention of coronary artery disease. *Open Hear*. 2017;4(2). doi:10.1136/openhrt-2017-000651

65. Mehran R, Pocock S, Nikolsky E, et al. Impact of bleeding on mortality after percutaneous coronary intervention: Results from a patient-level pooled analysis of the REPLACE-2 (Randomized Evaluation of PCI Linking Angiomax to Reduced Clinical Events), ACUITY (Acute Catheterization and Urgent Intervention Triage Strategy), and HORIZONS-AMI (Harmonizing Outcomes with Revascularization and Stents in Acute Myocardial Infarction) trials. *JACC Cardiovasc Interv*. 2011;4(6):654-664. doi:10.1016/j.jcin.2011.02.011

66. Ndrepepa G, Schuster T, Hadamitzky M, et al. Validation of the bleeding academic research consortium definition of bleeding in patients with coronary artery disease undergoing percutaneous coronary intervention. *Circulation*. 2012;125(11):1424-1431. doi:10.1161/CIRCULATIONAHA.111.060871

67. Hirsh J, Anand SS, Halperin JL, Fuster V. *Mechanism of Action and Pharmacology of Unfractionated Heparin*.; 2001. http://www.atvb.org. Accessed February 25, 2020.

68. Weitz JI, Hudoba M, Massel D, Maraganore J, Hirsh J. Clot-bound thrombin is protected from inhibition by heparin-antithrombin III but is susceptible to inactivation by antithrombin III-independent inhibitors. *J Clin Invest*. 1990;86(2):385-391. doi:10.1172/JCI114723

69. Mulder M, Fawzy I. *ECMO and Anticoagulation: A Comprehensive Review*. Vol 26.; 2018.

70. Dwyer A. Surface-treated catheters - A review. *Semin Dial*. 2008;21(6):542-546. doi:10.1111/j.1525-139X.2008.00499.x

71. *Trillium Trillium ® Biosurface*.

72. Tevaearai HT, Mueller XM, Seigneul I, et al. Trillium coating of cardiopulmonary bypass circuits improves biocompatibility. *Int J Artif Organs*. 1999;22(9):629-634.

http://www.ncbi.nlm.nih.gov/pubmed/10532432. Accessed February 25, 2020.

73. Cazzaniga A, Ranucci M, Isgrò G, et al. Trillium biopassive surface: a new biocompatible treatment for extracorporeal circulation circuits. *Int J Artif Organs*. 2000;23(5):319-324. http://www.ncbi.nlm.nih.gov/pubmed/10872850. Accessed February 25, 2020.

74. Palanzo DA, Zarro DL, Manley NJ, et al. Effect of Carmeda® bioactive surface coating versus Trillium ™ biopassive surface coating of the oxygenator on circulating platelet count drop during cardiopulmonary bypass. *Perfusion*. 2001;16(4):279-283. doi:10.1177/026765910101600403

75. Ereth MH, Nuttall GA, Clarke SH, et al. Biocompatibility of trillium biopassive surface-coated oxygenator versus uncoated oxygenator during cardiopulmonary bypass. *J Cardiothorac Vasc Anesth*. 2001;15(5):545-550. doi:10.1053/jcan.2001.26525

76. van den Goor JM, van Oeveren W, Rutten PM, Tijssen JG, Eijsman L. Adhesion of thrombotic components to the surface of a clinically used oxygenator is not affected by Trillium coating. *Perfusion*. 2006;21(3):165-172. doi:10.1191/0267659106pf859oa

77. Hayward JA, Chapman D. Biomembrane surfaces as models for polymer design: the potential for haemocompatibility. *Biomaterials*. 1984;5(3):135-142. doi:10.1016/0142-9612(84)90047-4

78. Whelan DM, Van Der Giessen WJ, Krabbendam SC, et al. Biocompatibility of phosphorylcholine coated stents in normal porcine coronary arteries. *Heart*. 2000;83(3):338-345. doi:10.1136/heart.83.3.338

79. De Somer F, François K, van Oeveren W, et al. Phosphorylcholine coating of extracorporeal circuits provides natural protection against blood activation by the material surface. *Eur J Cardio-Thoracic Surg*. 2000;18(5):602-606. doi:10.1016/S1010-7940(00)00508-X

80. Iwasaki Y, Ishihara K. Phosphorylcholine-containing polymers for biomedical applications.

Anal Bioanal Chem. 2005;381(3):534-546. doi:10.1007/s00216-004-2805-9

81. Hirota K, Murakami K, Nemoto K, Miyake Y. Coating of a surface with 2-methacryloyloxyethyl phosphorylcholine (MPC) co-polymer significantly reduces retention of human pathogenic microorganisms. *FEMS Microbiol Lett*. 2005;248(1):37-45. doi:10.1016/j.femsle.2005.05.019

82. Liu Q, Singha P, Handa H, Locklin J. Covalent Grafting of Antifouling Phosphorylcholine-Based Copolymers with Antimicrobial Nitric Oxide Releasing Polymers to Enhance Infection-Resistant Properties of Medical Device Coatings. *Langmuir*. 2017;33(45):13105-13113. doi:10.1021/acs.langmuir.7b02970

83. Kuiper KKJ, Robinson KA, Chronos NAF, Cui J, Palmer SJ, Nordrehaug JE. Phosphorylcholine-coated metallic stents in rabbit iliac and porcine coronary arteries. *Scand Cardiovasc J*. 1998;32(5):261-268. doi:10.1080/14017439850139843

84. Thiara AS, Andersen VY, Videm V, et al. Comparable biocompatibility of Phisio- and Bioline-coated cardiopulmonary bypass circuits indicated by the inflammatory response. *Perfusion*. 2010;25(1):9-16. doi:10.1177/0267659110362822

85. Suhara H, Sawa Y, Nishimura M, et al. Efficacy of a new coating material, PMEA, for cardiopulmonary bypass circuits in a porcine model. *Ann Thorac Surg*. 2001;71(5):1603-1608. doi:10.1016/S0003-4975(01)02466-3

86. Ueyama K, Nishimura K, Nishina T, Nakamura T, Ikeda T, Komeda M. PMEA Coating of Pump Circuit and Oxygenator May Attenuate the Early Systemic Inflammatory Response in Cardiopulmonary Bypass Surgery. *ASAIO J*. 2004;50(4):369-372. doi:10.1097/01.MAT.0000130679.55946.4D

87. Itoh H, Ichiba S, Ujike Y, et al. A prospective randomized trial comparing the clinical effectiveness and biocompatibility of heparin-coated circuits and PMEA-coated circuits in pediatric cardiopulmonary bypass. *Perfus (United Kingdom)*. 2016;31(3):247-254.

doi:10.1177/0267659115598217

88. Casu B. Structure and Biological Activity of Heparin. *Adv Carbohydr Chem Biochem*. 1985;43(C):51-134. doi:10.1016/S0065-2318(08)60067-0

89. De Agostini AI, Watkins SC, Slayter HS, Youssoufian H, Rosenberg RD. Localization of anticoagulantly active heparan sulfate proteoglycans in vascular endothelium: Antithrombin binding on cultured endothelial cells and perfused rat aorta. *J Cell Biol*. 1990;111(3):1293-1304. doi:10.1083/jcb.111.3.1293

90. Gott VL, Whiffen JD, Dutton RC. Heparin Bonding on Colloidal Graphite Surfaces. *Science (80-)*. 1963;142(3597):1297-1298. doi:10.1126/science.142.3597.1297

91. Biran R, Pond D. Heparin coatings for improving blood compatibility of medical devices. *Adv Drug Deliv Rev*. 2017;112:12-23. doi:10.1016/j.addr.2016.12.002

92. Gravlee GP. Heparin-coated cardiopulmonary bypass circuits. *J Cardiothorac Vasc Anesth*. 1994;8(2):213-222. doi:10.1016/1053-0770(94)90066-3

93. Gorman RC, Ziats N, Rao AK, et al. Surface-bound heparin fails to reduce thrombin formation during clinical cardiopulmonary bypass. *J Thorac Cardiovasc Surg*. 1996;111(1):1-11; discussion 11-2. doi:10.1016/s0022-5223(96)70395-1

94. Reynolds MM, Annich GM. The artificial endothelium. *Organogenesis*. 2011;7(1):42-49. doi:10.4161/org.7.1.14029

95. Yetik-Anacak G, Catravas JD. Nitric oxide and the endothelium: History and impact on cardiovascular disease. *Vascul Pharmacol*. 2006;45(5):268-276. doi:10.1016/j.vph.2006.08.002

96. Fontijn A, Sabadell AJ, Ronco RJ. Homogeneous Chemiluminescent Measurement of Nitric Oxide with Ozone: Implications for Continuous Selective Monitoring of Gaseous Air Pollutants. *Anal Chem*. 1970;42(6):575-579. doi:10.1021/ac60288a034

97. Kreuzer LB, Patel CKN. Nitric oxide air pollution: Detection by optoacoustic spectroscopy.

Science (80-). 1971;173(3991):45-47. doi:10.1126/science.173.3991.45

98. Furchgott RF, Zawadzki J V. The obligatory role of endothelial cells in the relaxation of arterial smooth muscle by acetylcholine. *Nature*. 1980;288(5789):373-376. doi:10.1038/288373a0

99. Cherry PD, Furchgott RF, Zawadzki J V., Jothianandan D. Role of endothelial cells in relaxation of isolated arteries by bradykinin. *Proc Natl Acad Sci U S A*. 1982;79(6 I):2106-2110. doi:10.1073/pnas.79.6.2106

100. Ignarro LJ, Byrns RE, Buga GM, Wood KS. Endothelium-derived relaxing factor from pulmonary artery and vein possesses pharmacologic and chemical properties identical to those of nitric oxide radical. *Circ Res*. 1987;61(6):866-879. doi:10.1161/01.RES.61.6.866

101. Ignarro LJ, Buga GM, Wood KS, Byrns RE, Chaudhuri G. Endothelium-derived relaxing factor produced and released from artery and vein is nitric oxide. *Proc Natl Acad Sci U S A*. 1987;84(24):9265-9269. doi:10.1073/pnas.84.24.9265

102. Katsuki S, Arnold W, Mittal C, Murad F. Stimulation of guanylate cyclase by sodium nitroprusside, nitroglycerin and nitric oxide in various tissue preparations and comparison to the effects of sodium azide and hydroxylamine. *J Cyclic Nucleotide Res*. 1977;3(1):23-35.

103. Arnold WP, Mittal CK, Katsuki S, Murad F. Nitric oxide activates guanylate cyclase and increases guanosine 3':5'-cyclic monophosphate levels in various tissue preparations. *Proc Natl Acad Sci U S A*. 1977;74(8):3203-3207. doi:10.1073/pnas.74.8.3203

104. The Nobel Prize in Physiology or Medicine 1998. https://www.nobelprize.org/prizes/medicine/1998/7543-the-nobel-prize-in-physiology-or-medicine-1998/. Accessed February 26, 2020.

105. Mayer B, Hemmens B. Biosynthesis and action of nitric oxide in mammalian cells. *Trends Biochem Sci*. 1997;22(12):477-481. doi:10.1016/S0968-0004(97)01147-X

106. Thomas DD. The biological lifetime of nitric oxide: Implications for the perivascular dynamics of NO and O2. *Proc Natl Acad Sci*. 2001;98(1):355-360. doi:10.1073/pnas.011379598

107. Weissbluth M. Hemoglobin. In: Springer, Berlin, Heidelberg; 1974:10-26. doi:10.1007/978-3-642-80801-2_2

108. Eich RF, Li T, Lemon DD, et al. Mechanism of NO-induced oxidation of myoglobin and hemoglobin. *Biochemistry*. 1996;35(22):6976-6983. doi:10.1021/bi960442g

109. Doyle MP, Hoekstra JW. Oxidation of nitrogen oxides by bound dioxygen in hemoproteins. *J Inorg Biochem*. 1981;14(4):351-358. doi:10.1016/S0162-0134(00)80291-3

110. Rubanyi GM, Vanhoutte PM. Oxygen-derived free radicals, endothelium, and responsiveness of vascular smooth muscle. *Am J Physiol - Hear Circ Physiol*. 1986;250(5). doi:10.1152/ajpheart.1986.250.5.h815

111. Gryglewski RJ, Palmer RMJ, Moncada S. Superoxide anion is involved in the breakdown of endothelium-derived vascular relaxing factor. *Nature*. 1986;320(6061):454-456. doi:10.1038/320454a0

112. Mellgren K, Friberg LG, Mellgren G, Hedner T, Wennmalm Å, Wadenvik H. Nitric oxide in the oxygenator sweep gas reduces platelet activation during experimental perfusion. *Ann Thorac Surg*. 1996;61(4):1194-1198. doi:10.1016/0003-4975(96)00017-3

113. Major TC, Brant DO, Reynolds MM, et al. The attenuation of platelet and monocyte activation in a rabbit model of extracorporeal circulation by a nitric oxide releasing polymer. *Biomaterials*. 2010;31(10):2736-2745. doi:10.1016/j.biomaterials.2009.12.028

114. Tousoulis D, Kampoli A-M, Tentolouris Nikolaos Papageorgiou C, Stefanadis C. The Role of Nitric Oxide on Endothelial Function. *Curr Vasc Pharmacol*. 2011;10(1):4-18. doi:10.2174/157016112798829760

115. Durante W, Kroll MH, Vanhoutte PM, Schafer AI. Endothelium-derived relaxing factor inhibits thrombin-induced platelet aggregation by inhibiting platelet phospholipase C. *Blood*. 1992;79(1):110-116. http://www.ncbi.nlm.nih.gov/pubmed/1309423. Accessed February 26, 2020.

116. Nakashima S, Tohmatsu T, Hattori H, Okano Y, Nozawa Y. Inhibitory action of cyclic GMP on secretion, polyphosphoinositide hydrolysis and calcium mobilization in thrombin-stimulated human platelets. *Biochem Biophys Res Commun*. 1986;135(3):1099-1104. doi:10.1016/0006-291x(86)91041-7

117. Geiger J, Nolte C, Butt E, Sage SO, Walter U. Role of cGMP and cGMP-dependent protein kinase in nitrovasodilator inhibition of agonist-evoked calcium elevation in human platelets. *Proc Natl Acad Sci U S A*. 1992;89(3):1031-1035. doi:10.1073/pnas.89.3.1031

118. Nesbitt WS, Giuliano S, Kulkarni S, Dopheide SM, Harper IS, Jackson SP. Intercellular calcium communication regulates platelet aggregation and thrombus growth. *J Cell Biol*. 2003;160(7):1151-1161. doi:10.1083/jcb.200207119

119. Varga-Szabo D, Braun A, Nieswandt B. Calcium signaling in platelets. *J Thromb Haemost*. 2009;7(7):1057-1066. doi:10.1111/j.1538-7836.2009.03455.x

120. FitzGerald GA. Mechanisms of platelet activation: Thromboxane A2 as an amplifying signal for other agonists. *Am J Cardiol*. 1991;68(7). doi:10.1016/0002-9149(91)90379-Y

121. Wang GR, Zhu Y, Halushka P V., Lincoln TM, Mendelsohn ME. Mechanism of platelet inhibition by nitric oxide: In vivo phosphorylation of thromboxane receptor by cyclic GMP-dependent protein kinase. *Proc Natl Acad Sci U S A*. 1998;95(9):4888-4893. doi:10.1073/pnas.95.9.4888

122. Mehta JL, Chen LY, Kone BC, Mehta P, Turner P. Identification of constitutive and inducible forms of nitric oxide synthase in human platelets. *J Lab Clin Med*. 1995;125(3):370-377. http://www.ncbi.nlm.nih.gov/pubmed/7534807. Accessed February

28, 2020.

123. Freedman JE, Ting B, Hankin B, Loscalzo J, Keaney JF, Vita JA. Impaired platelet production of nitric oxide predicts presence of acute coronary syndromes. *Circulation*. 1998;98(15):1481-1486. doi:10.1161/01.cir.98.15.1481

124. Freedman JE, Loscalzo J, Barnard MR, Alpert C, Keaney JF, Michelson AD. Nitric oxide released from activated platelets inhibits platelet recruitment. *J Clin Invest*. 1997;100(2):350-356. doi:10.1172/JCI119540

125. Gkaliagkousi E, Ritter J, Ferro A. Platelet-derived nitric oxide signaling and regulation. *Circ Res*. 2007;101(7):654-662. doi:10.1161/CIRCRESAHA.107.158410

126. Michelson AD, Benoit SE, Furman MI, et al. Effects of nitric oxide/EDRF on platelet surface glycoproteins. *Am J Physiol*. 1996;270(5 PART 2). doi:10.1152/ajpheart.1996.270.5.h1640

127. Lantvit SM, Barrett BJ, Reynolds MM. Nitric oxide releasing material adsorbs more fibrinogen. *J Biomed Mater Res - Part A*. 2013;101(11):3201-3210. doi:10.1002/jbm.a.34627

128. Zang Y, Popat KC, Reynolds MM. Nitric oxide-mediated fibrinogen deposition prevents platelet adhesion and activation ARTICLES YOU MAY BE INTERESTED IN. *Biointerphases*. 2018;13:6-403. doi:10.1116/1.5042752

129. Reitsma S, Slaaf DW, Vink H, M J van Zandvoort MA, A oude Egbrink MG. The endothelial glycocalyx: composition, functions, and visualization. doi:10.1007/s00424-007-0212-8

130. Fleser PS, Nuthakki VK, Malinzak LE, et al. Nitric oxide-releasing biopolymers inhibit thrombus formation in a sheep model of arteriovenous bridge grafts. *J Vasc Surg*. 2004;40(4):803-811. doi:10.1016/j.jvs.2004.07.007

131. Roberts TR, Neufeld MJ, Meledeo MA, et al. A metal organic framework reduces

thrombus formation and platelet aggregation ex vivo. *J Trauma Acute Care Surg*. 2018;85(3):572-579. doi:10.1097/TA.0000000000001982

CHAPTER 2

HYPOTHESIS AND RESEARCH AIMS

Fundamental Hypothesis: Nitric oxide (NO)-releasing or generating surfaces exhibit antiplatelet properties, improving the performance of medical devices.

Hypothesis 1: A NO releasing polyelectrolyte multilayer (PEM) coating deposited on titanium nanotube array (TiO_2NT) surfaces inhibits platelet adhesion and activation, as well as blood clot formation.

Aim 1: Develop a NO releasing PEM coating on TiO_2NT surfaces, evaluate its antiplatelet performance, and investigate its effects on real-time blood clot formation. This work is discussed in Chapter 3.

- Develop the NO-releasing PEM coating on TiO_2NT surfaces.
- Perform platelet adhesion and platelet activation studies using platelet-rich plasma.
- Perform *ex vivo* thromboelastographic studies using human whole blood.

Hypothesis 2: NO-releasing polymer films mediate fibrinogen adsorption to further prevent platelet adhesion and activation.

Aim 2: Investigate the effects of the NO-releasing surface on fibrinogen adsorption and subsequent platelet adhesion and activation. This work is discussed in Chapter 4.

- Prepare NO releasing polymer films.
- Perform fibrinogen adsorption studies on NO releasing polymer films.
- Perform platelet adhesion and activation studies on adsorbed NO-mediated fibrinogen surface in the absence of NO.

Hypothesis 3: A copper-based metal-organic framework (MOF) coating promotes NO production from the surface of extracorporeal life support (ECLS) components and inhibits bacterial attachment under both static and dynamic flow conditions.

Aim 3: Coat copper-based MOF onto ECLS circulation tubing, catheters, and membrane lung fibers using different coating techniques and evaluate the ability of MOF coating to inhibit bacterial attachment under static and dynamic flow conditions. This work is discussed in **Chapter 5**.

- Coating ECLS circulation tubing, catheter, and membrane lung fibers.
- Characterize copper-based MOF coating.
- Perform bacterial attachment study under static and dynamic flow conditions.

CHAPTER 3

FABRICATION AND *EX VIVO* EVALUATION OF GLYCOCALYX-INSPIRED NITRIC OXIDE-RELEASING POLYELECTROLYTE MULTILAYER COATING ON TITANIA SURFACE[1]

3.1 Introduction

Since the first attempt of using "Lane plates" for bone fracture repair in 1895, metal implants have become increasingly popular because of their specific advantages, such as excellent corrosion resistance, ease of sterilization, and others.[1–4] Currently, metal implants have been used in a variety of blood-contacting applications, for example, biosensors, vascular stents, and pacemakers. However, coagulation at the interface between human whole blood and the surface of metal implants is still an unsolved limitation that impedes their performance.[5] The coagulation cascade starts when human whole blood interacts with implant surfaces, resulting in the deposition of blood serum proteins such as fibrinogen. The adsorbed proteins on the material surface are then converted into a fibrin clot in the presence of thrombin. The fibrin clots further induce platelet adhesion, activation and aggregation, and finally lead to thrombus formation.[6] Without proper anticoagulant intervention, continuous blood clot formation places patients at high risk of medical device-induced thrombosis and leads to an additional surgery to replace the implanted medical devices.[7]

---

[1] Part of the following work (except Thromboelastographic studies) was adapted with permission from Simon-Walker R, Romero R, Staver JM, Zang Y, Reynolds MM, Popat, KC, Kipper MJ. Glycocalyx-Inspired Nitric Oxide-Releasing Surfaces Reduce Platelet Adhesion and Activation on Titanium. *ACS Biomater Sci Eng*. 2017;3(1):68-77. Copyright 2017 American Chemistry Society. This work was supported in part by the Office of the Vice President for Research at Colorado State University and by the National Science Foundation (award number 1511830). Surface characterization and endotoxin assay were performed by Raimundo Romero. Nitric oxide detection was performed by Joseph Staver. PF-4 study was performed by Rachael Simon-Walker. All other experimentation was performed by Joseph Staver and Yanyi Zang.

The other part the following work (Thromboelastorgraphic studies) has been developed partially and will be submitted with authors Dr. Christine Olver, Dr. Ketul C. Popat, Dr. Matt J. Kipper, and Dr. Melissa M. Reynolds. All experimentation was performed by Yanyi Zang.

Strategies for improving blood–material interactions include the development of “bioinert” surfaces that have reduced interactions with blood proteins, and “bioactive” surfaces activated with specific anticoagulant or antiplatelet functions.[8] Over 35 years ago, Olsson and co-workers began investigating the interactions of blood components with heparinized surfaces. While heparinized surfaces could reduce platelet adhesion,[9,10] reduced platelet adhesion alone was not sufficient to eliminate thrombus formation; the morphology of the heparinized surface at the nanoscale also plays a strong role in reducing thrombosis.[11] Surface-bound heparin can also potentiate the activity of antithrombin III.[9,10,12,13] This has led to the extensive use of adsorbed glycosaminoglycans, particularly heparin, to improve the hemocompatibility of surfaces, including dialysis membranes, venous implants, arterio-artery shunts, microfluidic channels, vascular grafts, and arterial stents.[9–24] Chitosan is a polycationic polysaccharide that can also improve blood-compatibility. Chitosan can promote wound healing, reduce platelet adhesion, and encourage endothelialization of surfaces.[21,25–27]

Despite these advances, to date all blood-contacting materials used in biomedical devices induce thrombosis and inflammation.[28,29] Approaches to development of new blood-compatible surfaces are largely “one-dimensional” in the sense that they often focus on a single surface feature to address one blood-material interaction, such as a chemistry that reduces protein adsorption or a signal that reduces cell adhesion. After reviewing the development of blood-compatible surfaces over the past three decades, Brash et al. concluded that new approaches should focus on multifunctional surfaces containing key features of the blood vessel wall.[8]

In contrast to current biomaterials, the luminal surface of healthy blood vessels is a dynamic multifunctional surface that prevents inflammation and coagulation, while in continuous contact with flowing whole blood. Endothelial cells lining blood vessels actively maintain the presentation of a glycosaminoglycan-rich brush-like layer called the glycocalyx and can change the glycocalyx structure and composition in response to physiological cues.[30] The hierarchical

organization of the glycocalyx at the nanoscale and microscale is an important determinant of its multiple biological functions.[31–33] The glycosaminoglycans (GAGs) in the glycocalyx such as heparin and heparan sulfate are polysaccharides that modulate enzymes in the coagulation cascade, have antimicrobial activity, and interact with circulating blood cells and proteins. The glycocalyx also regulates the production and transport of nitric oxide (NO), a small signaling molecule produced by endothelial cells.[34] NO also has antiplatelet and antimicrobial activity.[35,36] These multiple, synergistic, biological functions of the blood vessel wall prevent thrombosis and inflammation by (i) governing protein adsorption, (ii) presenting biochemical signals that prevent adhesion and activation of platelets to reduce coagulation, and (iii) regulating cell–cell interactions that prevent leukocyte activation that leads to inflammation. Since synthetic polymers and metals do not have these dynamic features and functions, they cannot obviate the undesirable blood–material interactions of thrombosis and inflammation.

This work proposes a new approach to developing blood-contacting surfaces with three important features inspired by features of the endothelial glycocalyx. First, nanoscale and microscale topography are introduced on titanium by anodization to produce titania nanotubes. Surface nanotopographical features on titanium have been shown to reduce platelet adhesion and activation and platelet–leukocyte interactions.[37–40] Second, these nanotubes are conformally coated with heparin and chitosan-thioglycolic acid polyelectrolyte multilayers (PEMs), providing a GAG-functionalized surface. The Kipper lab has previously demonstrated similar coatings on polymers, bone, metals, glass, and nanostructured materials, to provide controlled modulation of cell surface interactions and antimicrobial activity.[41–49] Third, the surfaces are nitrosated to provide a physiologically relevant and sustained release of NO. The Reynolds lab has developed NO-donor functionalization of polysaccharides. In particular, thiolated chitosan derivatives from the Reynolds lab are converted to an *S*-nitrosothiol, which provides extended release of NO under physiological conditions.[50] We hypothesize that by combining nanostructured surfaces,

polysaccharide-based PEMs, and NO-donor chemistry to introduce multiple functions on a biomaterial surface, platelet adhesion and activation can be substantially reduced. In the present work, we demonstrate that the combination of these topographical and biochemical surface features, inspired by the endothelial glycocalyx, can improve the blood compatibility of titanium surfaces by reducing platelet adhesion and activation.

In addition, we report the first real-time clot formation evaluation on NO-releasing PEM coating on a titania nanotube array surface using human whole blood. In this work, thromboelastography (TEG) was performed, since TEG has been widely used in various applications, ranging from coagulation management in clinical testing to the evaluation of newly designed biomaterials.[51–53] Several clinically-relevant clot formation parameters were measured: reaction time (R), the amount of time required for the first detection of a 2 mm amplitude clot in blood; initial clot formation time (K), the amount of time required for R to progress to a 20 mm amplitude clot; amplification rate (α-angle), the speed of fibrin formation and cross-linking; and clot strength (MA), the maximum amplitude detected and related to clot stability. For all modified surfaces, 2 mm amplitude blood clot formation was never detected on TiO_2NT+PEM surfaces after either 15 min or 60 min incubation time. Blood clotting was delayed on TiO_2NT+PEM+NO surfaces after both 15 min and 60 min incubation time. However, this material still induced the formation of clots. Based on these results, we have been able to evaluate our coating for further development.

3.2 Material and methods

3.2.1 Materials

All chemicals and solvents were purchased from commercial vendors and used without further purification unless otherwise noted. Ti sheets (CP grade 1, 0.025 inch thickness) was purchased from Titanium Joe (Kingston, Ontario, Canada). Platinum foil was purchased from

Surepure Chemetals (Florham Park, NJ, USA). Low molecular weight chitosan (96.1% deacetylated, 50–190 kDa), thioglycolic acid (TGA; ≥ 98%), tris(2-carboxyethyl)phosphine (≥98%), glutaraldehyde (Grade II, 25 % in H_2O), sucrose, and hexamethyldisilazane (HDMS; reagent grade, 99%) were obtained from Sigma-Aldrich (St. Louis, MO USA). *N*-(3-(Dimethylamino)propyl)-*N′*-ethylcarbodiimide hydrochloride (EDAC; 99.23%) was purchased from Chem-Impex International (Wood Lawn, IL, USA). Heparin sodium was purchased from Celsus Laboratories, Inc. (from porcine intestinal mucosa, 14.4 kDa, 12.5% sulfur; Cincinnati, OH, USA). Sodium cacodylate was purchased from Polysicences (Warrington, PA, USA). Acetic acid (≥99%) was purchased from ACROS organics (Geel, Belgium). Corning™ 0.22 μm PES vacuum filter/storage systems were purchased from Corning (Corning, NT, USA). Diethylene glycol (DEG; 99%), methanol, ethanol, and 50 mL conical tubes were purchased from Fisher Scientific (Hampton, NH, USA). Nitric acid (100%) and diethyl ether was purchased from EMD Millipore (Burlington, MA, USA). *tert*-Butyl nitrite was purchased from Sigma-Aldrich (90%; St. Louis, MO, USA). Hydrofluoric acid (HF; 48-51%) and Spectrapor 7 8000 MWCO dialysis tubing were obtained from VWR International (Radnor, PA USA). Deionized water (18.2 MΩ·cm) (H_2O) was prepared using a Millipore Direct-Q5 ultrapure water purification system purchased from EMD Millipore (Burlington, MA, USA).

3.2.2 Fabrication of titania nanotube arrays

Titania nanotube arrays (TiO_2NT) were fabricated similar to the diethylene glycol (DEG)-based electrochemical anodization process outlined elsewhere.[40,54] The titanium substrates served as the anode, and the platinum foil served as the cathode. All experiments were carried out at room temperature. Commercially pure titanium sheets were cut into 2 cm × 2 cm square substrates and used as the anode. Titanium substrates were cleaned with acetone, Micro 90, and isopropyl alcohol. Platinum foil was cleaned by isopropyl alcohol and nitric acid and used as the

cathode. The DEG-based electrolyte was composed of 95 v/v% DEG with 2 v/v% HF and 3 v/v% DI water. Anodization was performed at 55 V for 22 h to form nanotubes on titanium substrates. After anodization, the TiO_2NT were rinsed with DI water, isopropyl alcohol, and DI water, and dried with nitrogen gas. The TiO_2NT were annealed in an oven at 530 °C at a ramp rate of 15 °C per min for 5 h to induce crystallization. The anodization conditions used here result in titania nanotubes, containing both rutile and anatase phases, approximately 3.7 μm long and 120 nm in diameter, completely covering the surface of the titanium.[40,54] The TiO_2NT samples were cut into 0.5 cm × 0.5 cm squares and separated into 24-well trays. They were then washed using an Alconox solution and rinsed in DI water before use.

3.2.3 Synthesis of chitosan thioglycolic acid (Chitosan-TGA)

Chitosan thioglycolic acid (TGA) was synthesized using the following method. Chitosan (1.000 g) was suspended in 100 mL of DI water and 1.00 mL of glacial acetic acid in a 250 mL round-bottomed flask (RBF) at room temperature. The suspension was stirred until it became visually clear. TGA (1.508 mL) was added to the suspension and stirred for 5 min. EDAC (3.800 g) was then added to the suspension. The RBF was covered with aluminum foil to protect from light exposure and stirred overnight. The solution was then transferred to dialysis tubing and dialyzed against 5 L of DI water at pH 4–5 for 24 h. The water was changed 4 times over the 24-h dialysis. The solution was then transferred to a 250 mL RBF, and 100 mg tris(2-carboxyethyl)phosphine was added. The solution was covered with aluminum foil and stirred for 1 h. The solution was then transferred to dialysis tubing and dialyzed in 5 L of DI water at pH 4–5 for 7 days, with daily water changes. For the first 2 days, the dialysis water had 1% m/v NaCl added. After dialysis, the chitosan-TGA was lyophilized using a FreeZone Plus 2.5 L Cascade Console Freeze-Dry System (Labconco; Kansas City, MO) with a collector temperature of –89 °C at 0.01 mbar.

3.2.4 Polyelectrolyte multilayer (PEM) preparation

A 0.01 M (on a saccharide unit basis) chitosan-TGA solution was made by dissolving the chitosan-TGA in 0.2 M acetate buffer, with pH adjusted to 5 using glacial acetic acid. A 0.01 M solution of heparin (on a saccharide unit basis) was prepared using the same acetate buffer solution, with pH 5. Both polymer solutions were filtered using Thermo Scientific (Waltham, MA USA) 0.2 μm Nalgene Rapid Flow filters. An acidified rinse was prepared with DI water, using glacial acetic acid to adjust pH to 4. The samples were coated using a layer-by-layer process, using the following order: acidified rinse, chitosan-TGA, acidified rinse, and heparin. For each step, 500 μL of solution was added to each well, and the 24-well tray was placed onto a shaker for 5 min. The solution was then aspirated off, and the next solution was added, for a total of 10 bilayers, followed by a final acidified water rinse. Ten PEM bilayers are sufficient to completely coat the nanotubes and provide a physiologically relevant dose of the NO-donor group, while still preserving the nanotube structure and high surface area. Samples were then dried using a 5-step ethanol series (50%, 70%, 90%, 100%, and 100%) for 5 min intervals. The samples were then dried in a chemical fume hood and stored wrapped in foil in a vacuum desiccator before nitrosation step.

3.2.5 Nitrosation

Each sample was soaked in 300 μL of *tert*-butyl nitrite overnight on a shaker. The next day, samples were rinsed with 300 μL of methanol followed by 300 μL of diethyl ether before being dried under vacuum for 30 min. Nitrosated samples were then covered with aluminum foil and used within 1 h.

3.2.6 Surface characterization by SEM and XPS

The structure of titania nanotubes before and after PEM modification and after nitrosation was evaluated by scanning electron microscopy (SEM), using a JEOL JSM-6500F (Tokyo, Japan).

Samples were coated with 10 nm of gold for imaging. Using separate samples from those used for SEM, surface chemistry was evaluated by X-ray photoelectron spectroscopy (XPS) using a Phi Electronics 5800 Spectrometer (Chanhassen, MN). Spectra were obtained with a monochromatic Al Kα X-ray source (ηv = 1486.6 eV), a hemispherical analyzer, and multichannel detector. High-resolution spectra were obtained using 23.5 eV analyzer pass energy with 0.1 eV steps and an X-ray spot of 800 μm. All spectra were obtained with a photoelectron takeoff angle of 45°. A low-energy electron gun was used for charge neutralization. Spectra curve fitting was done using Phi Electronics Multipak version 9.3 (Chanhassen, MN). All spectra were shifted according to the aliphatic carbon peak at 284.8 eV. Curve fitting of all spectra used a Shirley background. Gaussian–Lorentzian peaks in the Ti 2p, C 1s, and N 1s envelopes were fit according to expected functional groups.

3.2.7 Endotoxin assay

Endotoxin presence on TiO_2 nanotubes coated with 10 bilayers of chitosan-TGA and heparin was evaluated using a limulus amebocyte lysate (LAL) chromogenic assay (Thermo Scientific Waltham, MA). This assay detects Gram-negative bacterial endotoxins. Three TiO_2 nanotube samples coated with 10 bilayers of chitosan-TGA and heparin were immersed in 1 mL of endotoxin-free water for 2 h at room temperature to determine extractable endotoxins. The endotoxin concentration in the supernatant was then assayed in duplicate according the manufacturer's instructions, which has a sensitivity lower limit of 0.1 EU/mL.

3.2.8 Nitric oxide detection

NO release from nitrosated chitosan-TGA powder and from nitrosated PEMs on titania nanotubes was measured as previously described.[50] NO release was recorded in real-time using Sievers nitric oxide analyzers (NOA 280i, GE Analytical, Boulder, CO, USA). Calibration was performed with nitrogen (zero gas) and 46.3 ppm of NO/nitrogen. NO release was assayed under

simulated physiological conditions. *S*-Nitrosated chitosan-TGA (2–3 mg) or 2 cm × 2 cm PEM-coated titania nanotube samples were suspended in 10 mM PBS (pH 7.4) at 37 °C. NO release experiments were replicated 3 times on both *S*-nitrosated chitosan-TGA and PEM-coated titania nanotube samples.

3.2.9 Human whole blood collection and platelet-rich plasma preparation

Whole human blood was drawn via venous phlebotomy, by a trained phlebotomist, from healthy donors who had refrained from taking thromboxane inhibitors (aspirin, ibuprofen, and naproxen) for at least 2 weeks. The protocol for blood isolation from healthy individuals was approved by Colorado State University Institutional Review Board.

For cytotoxicity, platelet adhesion, and platelet activation studies, blood was collected into 10 mL BD vacutainers® EDTA tubes (K_2EDTA 18 mg). Plasma containing platelets and leukocytes were isolated by centrifugation at 100g for 15 min to remove red blood cells; the plasma and the buffy coat containing the platelets and leukocytes were removed and allowed to rest for 10 min prior to use. Plasma and cells were pooled into a sterilized 50 mL conical tube. For all cell adhesion, cytotoxicity, and platelet factor-4 assays described below, samples were placed into a 24-well plate and incubated with 500 µL of pooled plasma and cells on a horizontal shaker plate (100 rpm) for 2 h at 37 °C and 5% CO_2.

For TEG studies, blood was collected into 4.5 mL citrated BD vacutainers® venous blood collection tubes (12.35 mg sodium citrate, 2.21 mg citric acid). After blood collection, human whole blood in each tube was transferred into a 50 mL conical tube and allowed to rest for 20 min prior to use. All blood was used within 4 h of collection time.

3.2.10 Cytotoxicity

Cytotoxicity was determined using a commercially available lactate dehydrogenase (LDH) assay kit (Cayman Chemical, Ann Arbor, MI), on six or more samples for each condition, prepared

separately from the samples used for SEM, XPS, and NO release assays. This assay measures the relative concentration of LDH, which is released upon cell lysis. This is a relevant measure of cytotoxicity in this context because platelet lysis is associated with platelet activation during blood clot formation. After 2 h of incubation in plasma containing cells, the samples were further shaken on a horizontal shaker plate (100 rpm) for 5 min at room temperature, to resuspend settled components. Sample-exposed plasma (100 μL) and manufacturer-supplied standards were transferred to a 96-well plate. A reaction solution consisting of 96% v/v assay buffer, 1% v/v NAD+, 1% v/v lactic acid, 1% v/v INT, and 1% v/v LDH diaphorase was added in equal amounts (1:1) to all the standards and sample-exposed plasma. This was followed by gentle shaking on a horizontal shaker (100 rpm) for 30 min at room temperature, to achieve mixing. Experimental sample surfaces were compared to pooled plasma containing cells treated with 2% Triton X in DI water (to achieve maximal lysing and release of LDH), to plasma containing cells on tissue culture polystyrene (a nontoxic control surface), and to HEPES buffer with no cells (to provide absorbance readings on a solution containing no cells, representing no cell lysis). The absorbance was immediately measured at a wavelength of 490 nm using a plate reader.

3.2.11 Platelet adhesion

Platelet adhesion was investigated using fluorescence microscopy. At least five separate samples of each type were prepared for fluorescence microscopy, and at least two samples of each type were used for SEM imaging to qualitatively assess platelet adhesion and activation. After 2 h of incubation in plasma containing cells, the surfaces were stained with calcein-AM (Thermo-Scientific). CalceinAM is an acetoxymethyl ester fluorescein derivative that stains the cytoplasm of live cells. Only live cells are able to convert calcein-AM to the fluorescent calcein. The unadhered cells were gently aspirated, and the surfaces were rinsed twice with phosphate-buffered saline (Hyclone, 0.0067 M PO_4, without Ca and Mg, PBS). One milliliter of a 5 μM solution

of calcien-AM in PBS was added to the substrates. The samples were allowed to incubate for 20 min at room temperature in the stain solution. After 20 min, the stain solution was gently aspirated, and the substrates were rinsed twice with PBS. The surfaces were immediately imaged using a Zeiss Axiovision fluorescent microscope using a 493/514 nm filter. Two nonoverlapping images were taken on each of 5 replicate surfaces for each experimental condition. All 10 images representing each condition were processed using ImageJ software to quantify the percentage of the surface covered with cells.

3.2.12 Platelet activation

Platelet activation was qualitatively evaluated using scanning electron microscopy (SEM; JEOL JSM-6500F), and quantitatively evaluated by an ELISA for platelet factor-4. For SEM imaging, after 2 h of incubation in plasma, substrates were fixed with a primary fixative [6% glutaraldehyde, 0.1 M sodium cacodylate, and 0.1 M sucrose] for 45 min at room temperature. The substrates were then transferred to a secondary fixative (primary fixative without glutaraldehyde) for 10 min. This was followed by exposing the substrates to consecutive solutions of ethanol (35%, 50%, 70%, and 100%) for 10 min each followed by a final incubation in HMDS for 10 min at room temperature. The substrates were then air-dried and stored in a desiccator until imaging by SEM. Surfaces were coated with a 10 nm layer of gold and imaged at 15 kV.

Fully activated platelets express platelet factor-4 (PF-4). PF-4 expression was quantified using a commercially available enzyme linked immunosorbent assay kit (ELISA, RayBio), according to the manufacturer's recommended protocol. Substrate-exposed plasma was diluted 1:200 in the provided assay diluent and then transferred along with the provided PF-4 standards to an antibody-coated microassay well plate. The assay plate was incubated for 2.5 h at room temperature. The wells were subsequently washed (4×) with wash buffer and incubated with biotinylated antibody for 1 h on a horizontal shaker plate (100 rpm) at room temperature. The

wells were then washed (4×) to remove unbound biotinylated antibody. This was followed by incubating the wells with a diluted horseradish peroxidase (HRP)-streptavidin solution for 45 min on a horizontal shaker plate (100 rpm) at room temperature. Wells were then washed (4×) with the wash buffer. 3,3′,5,5′-Tetramethylbenzene (TMB) solution was immediately added to each well and incubated for 30 min on a horizontal shaker plate (100 rpm) at room temperature with no exposure to light. The reaction was stopped with a stop solution, and the optical density was measured at 450 nm to determine the amount of PF-4 released by platelets on each of the substrates.

3.2.13 Thromboelastography (TEG)

Citrated human whole blood without any added sample was gently shaken and tested at 1 h intervals until the blood became hypercoagulative or 5 h had elapsed since collection to ensure the blood duration of use ($n = 2$ 50 mL tubes of blood). 1 mL of citrated human whole blood was incubated with modified samples in microcentrifuge tubes for 15 min and 60 min at room temperature with gentle shaking, and unmodified Ti samples were used as controls ($n \geq 5$ samples). After incubation, 340 μL of citrated human whole blood was transferred into TEG disposable cups with 20 μL of $CaCl_2$. TEG was then performed without activating reagents at 37 °C until clot maximum amplitude (MA) was detected or until 60 min after TEG was started. Reaction time (R), initial clot formation time (K), amplification rate (α-angle), and clot strength (MA) were recorded.

3.2.14 Statistical analysis

Separate two-tailed, one-way ANOVAs were used to compare treatment means on cytotoxicity, platelet adhesion, and TEG data with a post-hoc Tukey's multiple comparisons test. For cytotoxicity, six samples of each type were evaluated. Data are reported as the mean ± standard deviation. For blood cell adhesion studies, two nonoverlapping areas on each of five

samples of each type were evaluated. Images from the median sample of each type are reported. Data are reported as the mean ± standard deviation. Three samples from each treatment group were imaged by SEM to characterize platelet adhesion, and representative SEM images are presented.

3.3 Results and discussion

3.3.1 Surface characterization by SEM and XPS

Figure 3.1 shows scanning electron micrographs of TiO_2 nanotubes (left), PEM-modified nanotubes (center), and nitrosated PEM-modified nanotubes (right) at two different magnifications. Hereafter, these are identified as TiO_2NT, TiO_2NT+PEM, and TiO_2NT+PEM+NO, respectively. The 10-bilayer PEM modification conformally coats the nanotubes and blocks the individual nanotube pores. However, the nanotubes remain distinct, with space between the nanotubes remaining. Subsequent nitrosation does not physically alter the PEM structure at a length scale observable by SEM. Complete coverage of the nanotubes is further confirmed by XPS. **Figure 3.2** shows representative high-resolution spectra of the Ti 2p and O 1s envelopes of the TiO_2NT, TiO_2NT+PEM, and TiO_2NT +PEM+NO samples. TiO_2NTs have the expected titanium signature in both the Ti 2p and O 1s envelopes. Addition of the PEM completely attenuates the TiO_2 signal, in both the Ti 2p and O 1s envelopes of the TiO_2NT+PEM and TiO_2NT+PEM +NO samples. This confirms complete coating of the surface. The O 1s envelope of these spectra is broad, due to contributions from sulfate (expected at 532 eV) and alcohol, ether, amide, and carboxylic acid groups in the 533–534 eV range.

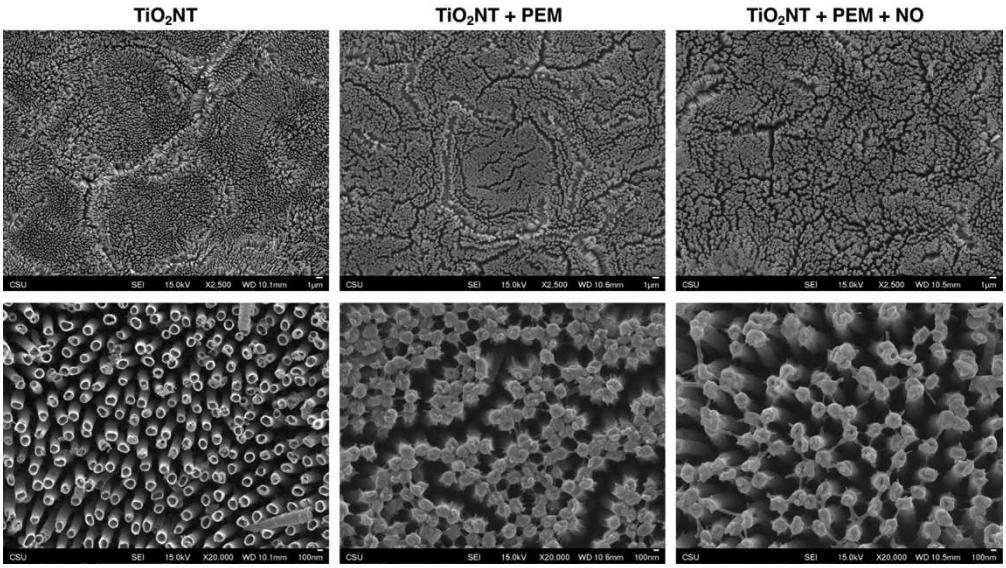

Figure 3.1 Scanning electron micrographs of different surface modifications.

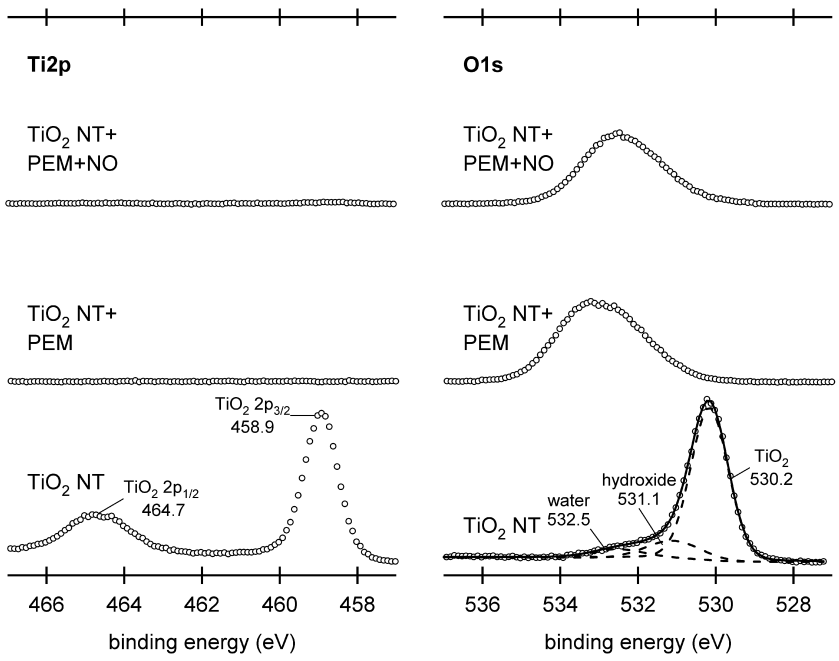

Figure 3.2 High-resolution X-ray photoelectron spectra of the Ti 2p (left) and O 1s (right) envelopes of all three modified surfaces. Data are circles, individual peaks in the curve fits are broken lines, and sums of individual peaks from the curve fit are solid lines.

The chemistry of the PEM coating and nitrosation is further confirmed by the N 1s, C 1s, and S 2p envelopes from XPS, shown in **Figure 3.3**. TiO_2NT has a small amount of adventitious

aliphatic carbon, with no discernible nitrogen or sulfur. Addition of the PEM results in expected nitrogen species, characteristic of the PEM, and oxidized sulfur (sulfate) at ~168.5 eV. The nitrogen species in the TiO_2NT+PEM sample includes both amide (400.4 eV) and amine (398.9 eV) contributions from the heparin and thioglycolic acid chitosan. Some of the amine is protonated (ammonium at 402.6 eV), indicating ionic interaction with the heparin and small counterions in the multilayer. The sulfate confirms the addition of heparin. Reduced sulfur (thiol) species at lower binding energy are not resolvable above the noise. The nitrosated TiO_2NT+PEM+NO sample has the same species present as the TiO_2NT+PEM sample. Nitrosation results in a relative increase in the ammonium in the TiO_2NT+PEM+NO sample and a new nitrogen peak at higher binding energy associated with oxides of nitrogen. The relative amounts of these nitrogen species are summarized in **Table 3.1**. Nitrosation also results in minor apparent changes in the C 1s and O 1s envelopes that are difficult to precisely assign, due to the convolution of multiple species.

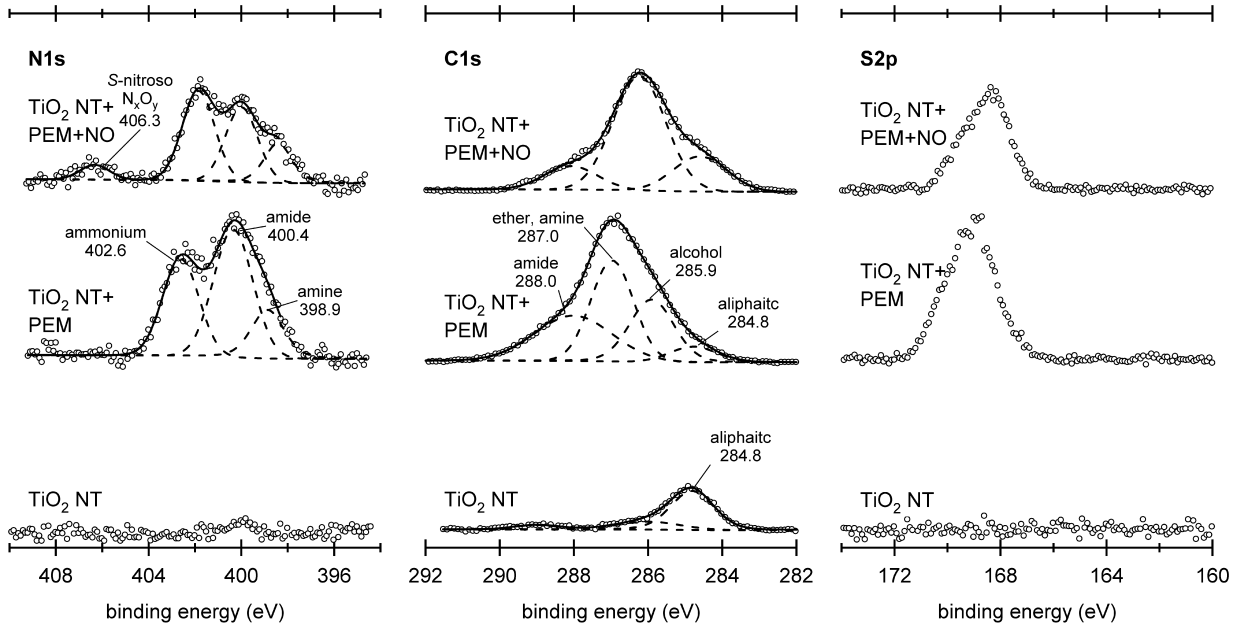

Figure 3.3 High-resolution X-ray photoelectron spectra of the N 1s (left), C 1s (center), and S 2p (right) envelopes of modified surfaces. Data are circles, individual peaks in the curve fits are broken lines, and sums of individual peaks from the curve fit are solid lines.

Table 3.1 Relative amounts of nitrogen species from XPS data.

surface	amine		amide		ammonium		N_xO_y	
	Pos. (eV)	%	Pos. (eV)	%	Pos. (eV)	%	Pos. (eV)	%
TiO_2NT+PEM	398.9	17.6	400.4	48.5	402.6	33.9	-	0
TiO_2NT+PEM+NO	398.4	18.0	400.0	34.4	401.9	41.5	406.3	6.2

3.3.2 Endotoxin assay

The endotoxin assay showed no detectable levels of endotoxin contamination. (**Table 3.2**) The TiO_2NT+PEM contain less than 0.1 EU mL^{-1}.

Table 3.2 Blank-corrected average absorbance for LAL standards and samples.

Endotoxin standard or sample	Blank corrected average absorbance
1.0 EU mL^{-1} standard	1.241
0.5 EU mL^{-1} standard	0.383
0.25 EU mL^{-1} standard	0.081
Endotoxin free water	0
TiO_2NT+PEM Sample 1	-0.001
TiO_2NT+PEM Sample 2	0.002
TiO_2NT+PEM Sample 3	0.001

3.3.3 Nitric oxide (NO) release

The NO release from *S*-nitrosated chitosan-TGA and from *S*-nitrosated TiO_2NT+PEM+NO was evaluated at 37 °C, in pH 7.4 PBS. The *S*-nitrosated chitosan-TGA releases 335 nmol/g over the first 1 h 45 min of the release experiment (**Figure 3.4**). The three TiO_2NT+PEM+NO samples released an average of about 40 pmol cm^{-2} over the first 20 min. In these experiments, the limit of quantitation (LOQ) is about 1 pmol cm^{-2} min^{-1}. After 15 min, the NO flux falls to below the LOQ (**Figure 3.5**). Endothelial cells are estimated to produce NO on the order of 10s to 100s of pmol cm^{-2} min^{-1}.[55,56] Some of this NO diffuses into the underlying smooth muscle cells, where it acts as a vasodilator. Some of the NO also diffuses into the blood vessel, where its antiplatelet activity is important. In blood, NO is rapidly consumed, in part by hemoglobin.[55,56] The resulting reaction–diffusion gradient is thought to produce antiplatelet activity only very close to the blood vessel wall. Materials that release on the order of 10 s to 100 s of pmol cm^{-2} min^{-1} of NO have

been shown to reduce platelet activation.[35,55,57] The NO flux required to affect platelet aggregation may depend upon the shear rate.[58] The very thin coatings used here (**Figure 3.1**) release at a maximum rate just below this range. The high surface area of the TiO_2NT+PEM+NO (**Figure 3.1**) may result in rapid early release of NO from the *S*-nitrosothiol donor group. On the basis of the release kinetics from the *S*-nitrosated chitosan-TGA, we conjecture that our TiO_2NT+PEM+NO samples continue to release NO for longer than 20 min, albeit at levels below the LOQ. However, the PEM coating thickness and the donor group chemistry used here might be modified to further optimize NO delivery.

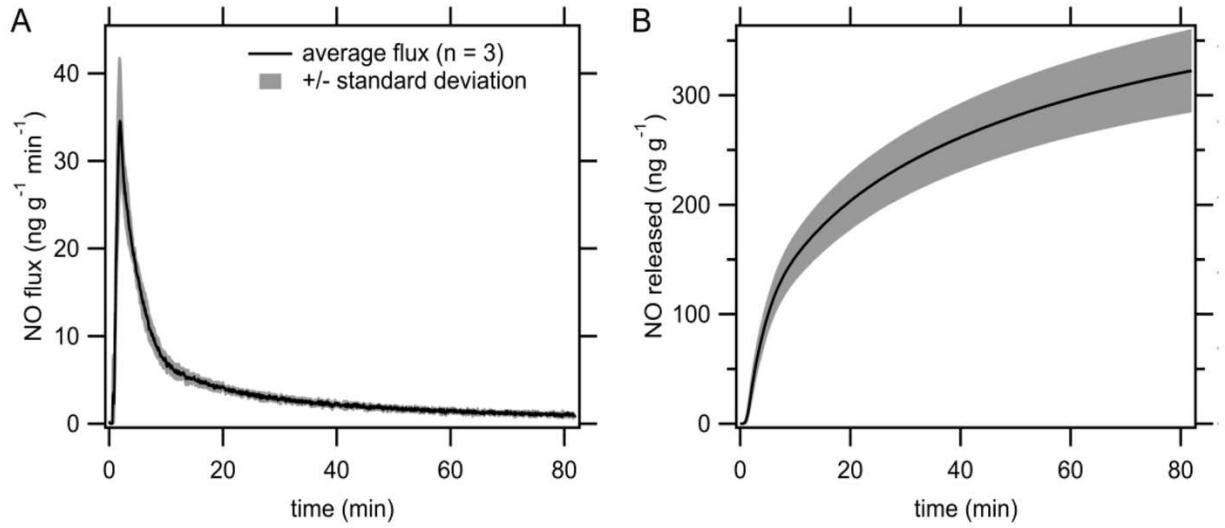

Figure 3.4 NO flux and (B) cumulative NO release from nitrosated chitosan-TGA.

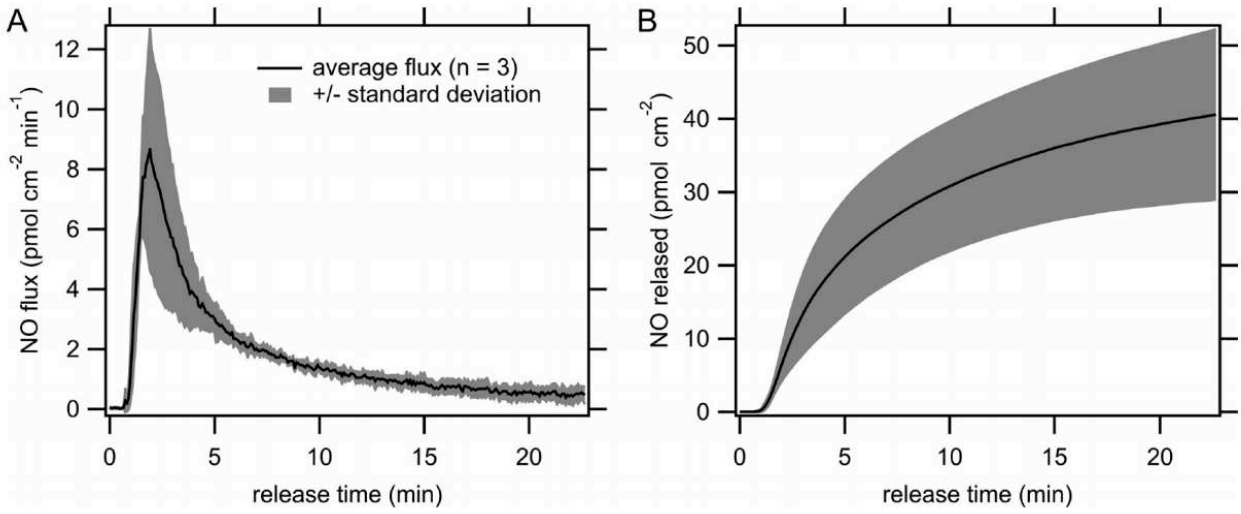

Figure 3.5 NO flux and (B) cumulative NO release from TiO_2NT+PEM+NO surfaces.

3.3.4 Cytotoxicity

Cytotoxicity of different surfaces after 2 h of incubation in whole blood plasma containing platelets and leukocytes was determined using a commercially available lactate dehydrogenase (LDH) assay kit. Upon exposure to a toxic surface, cell necrosis is induced resulting in swelling of the cell membrane and the organelles. This results in cell lysis and release of an enzyme, LDH, that is located in the cytoplasm of the cells. The LDH assay measures the amount of formazan crystals formed following a two-step reduction reaction, where the released LDH catalyzes NAD^+ to NADH and H^+ by oxidation and a subsequent catalyst reaction by diaphorase converting tetrazolium salt to a colored formazan, that can be spectrophotometrically measured. Adhered cells on all experimental sample surfaces have no significant differences in their cytotoxicity, nor are they different from either the PS or the HEPES buffer control containing no cells (**Figure 3.6**). All experimental surfaces, the noncytotoxic PS control, and the HEPES (no cells) control were significantly less cytotoxic than the cytotoxic control (Triton X). Since titanium and PS are not cytotoxic, and since other surfaces had comparable absorbance to the PS and HEPES controls, we conclude that none of the experimental surfaces will have any short-term cytotoxic effects on platelets and leukocytes.

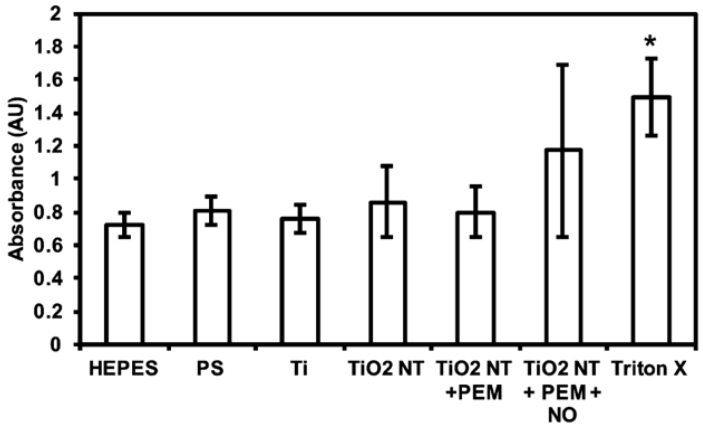

Figure 3.6 Quantification of LDH after 2 h of incubation in whole blood plasma containing platelets and leukocytes (mean LDH activity ± standard deviation). No significant difference in LDH activity was observed among the HEPES (no cells), PS (noncytotoxic control), and experimental sample types. Experiments were replicated with at least two difference cell populations on at least three different samples (n = 6). Triton X (positive control for cell lysis) is significantly different from all other conditions (* indicates $p < 0.05$).

3.3.5 Platelet adhesion

Platelet adhesion on surfaces was investigated after 2 h of incubation in whole blood plasma containing platelets and leukocytes using fluorescence microscopy. The cells were stained with calcein-AM, a cell-permeate stain that labels viable cells by converting the nonfluorescent calcein-AM into a green fluorescent calcein (**Figure 3.7**). The fluorescence micrographs were further processed using the ImageJ software to determine cell coverage (**Figure 3.8**). There is significantly lower cell adhesion on TiO_2NT, TiO_2NT+PEM, and TiO_2NT+PEM +NO surfaces ($p \leq 0.01$) compared to that on Ti surfaces. Several studies have shown that nanostructured surfaces reduce blood plasma cell adhesion.[37–40] This is due to the presence of nanotopography on the surface, which results in changes in surface area and surface energy.[37,40] The cell adhesion on TiO_2NT surfaces reported here is similar to these previous studies. The lack of nanotopography on Ti surfaces resulted in significantly higher cell adhesion. Chitosan surfaces may enhance platelet adhesion in the presence of adsorbed plasma.[59] This was found to be primarily mediated by α(IIb)β(3) integrins on the platelet surface. However, in

this work, we observe a decrease in cell adhesion on TiO_2NT+PEM surfaces. This may be due to the combined effect of nanotopography of TiO_2NT and the chitosan present in the form of PEMs. The cell adhesion is further reduced on TiO_2NT+PEM+NO compared to TiO_2NT ($p \leq 0.01$) and TiO_2NT+PEM ($p \leq 0.05$) surfaces. This is due to the effect of NO release from the surfaces. In the body, endothelium-derived NO inhibits platelet adhesion and aggregation.[60] NO-activated soluble guanylate cyclase, which catalyzes the formation of cGMP from GTP, and NO both inhibit platelet function via this cGMP-dependent mechanism.[61,62] Thus, the reduction in cell adhesion on TiO_2NT+PEM+NO surfaces may be beneficial in controlling subsequent thrombogenic events on surfaces.

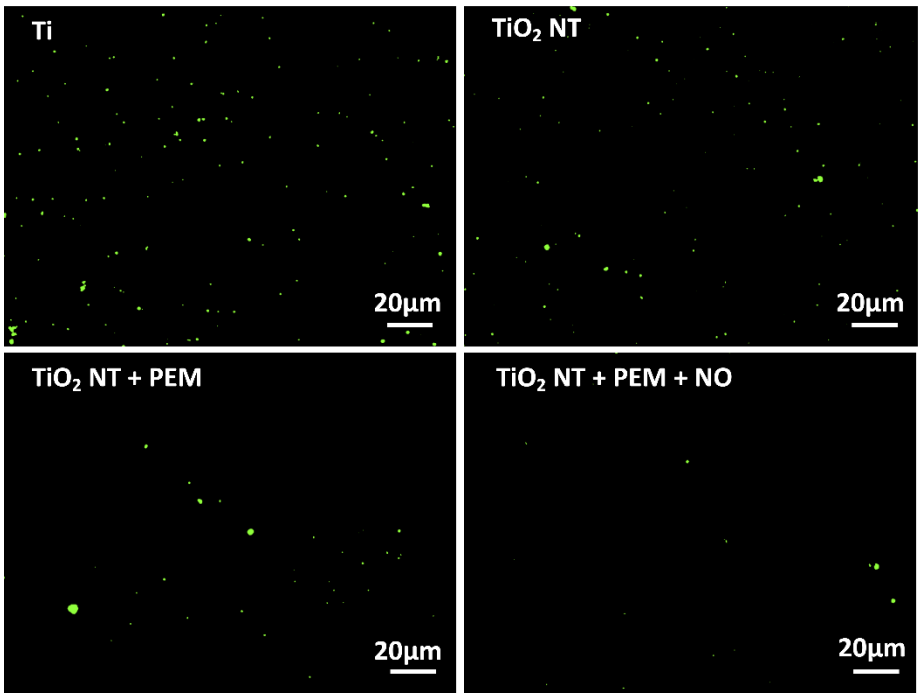

Figure 3.7 Representative (median from at least 5 samples for each experimental group) fluorescence micrographs of adhered cells stained with calcein-AM on Ti, TiO2NT, TiO2NT+PEM, and TiO2NT+PEM+NO surfaces.

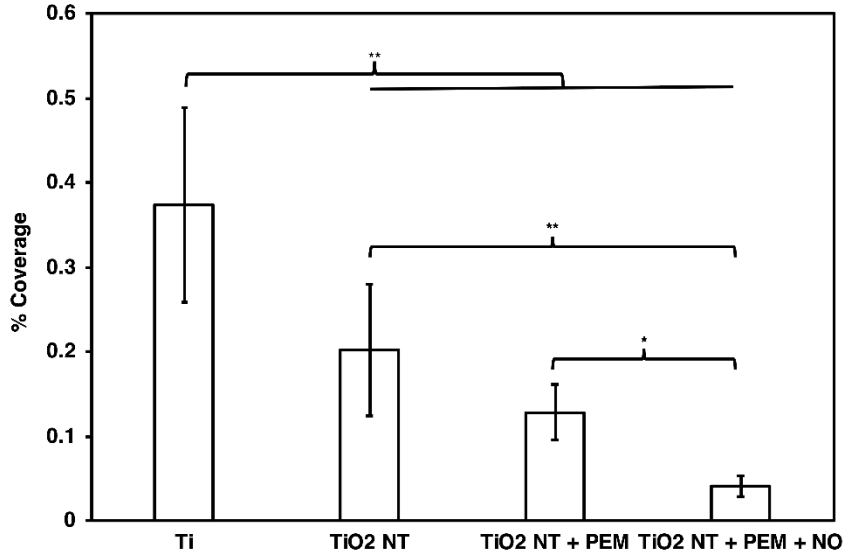

Figure 3.8 Percentage coverage analysis of cells adhered to surfaces visualized by calcein-AM staining on Ti, TiO_2NT, TiO_2NT+PEM, and TiO_2NT+PEM+NO surfaces (mean ± standard deviation). All NT surfaces have significantly lower cell adhesion than the Ti surfaces. The TiO_2NT+PEM+NO surfaces have significantly lower cell adhesion than the TiO_2NT+PEM and TiO_2NT surfaces. (n = 10 images from each experimental group; * indicates $p < 0.05$; ** indicates $p < 0.01$).

3.3.6 Platelet activation

Platelet adhesion and activation were characterized qualitatively by scanning electron microscopy. During activation, platelets undergo cytoskeletal-dependent membranous shape changes. This commences with the disassembly of the microtubule ring followed by actin polymerization to form dendritic extensions that are thought to release chemo-attractants and summon additional platelets to form aggregates and commence the production of the platelet plug.[63] Five morphological groups of dendritic expressions on implant surfaces have been identified corresponding with four levels of activation: *round* (unactivated), disc shaped with no pseudopodia present; *dendritic* (partially activated), early pseudopodia, i.e., short reversible dendritic extensions; *spread-dendritic* (moderately activated), irreversible long-dendritic extensions with some spreading and some pseudopodial flattening; *spreading* (fully activated), pseudopodia almost fully flattened, hyaloplasmic spreading; and *fully spread* (fully activated), no

pseudopodia present and full hyaloplasmic spreading.[64,65] Ti surfaces exhibit moderate activation of platelets with mostly short dendritic extensions. TiO_2NT surfaces exhibit a large amount of platelet aggregation; however, there are no visible dendritic extensions (**Figure 3.9**). This may be because TiO_2NT surfaces are hydrophilic compared to Ti surfaces, limiting platelet activation. Previous studies have shown that platelet activation is mitigated on TiO_2NT surfaces indicating lower propensity for subsequent thrombogenic events on surfaces.[40] We also observe a drastic decrease in platelet aggregation and activation on TiO_2NT+PEM and TiO_2NT+PEM+NO surfaces. The very few platelets on these surfaces have mostly round morphologies with minimal dendritic extensions. Studies have shown that platelets are activated by chitosan; however, the extent of activation is modulated by the presence of blood serum proteins such as fibrinogen.[59] The hydrophilic nature of TiO_2NT+PEM surfaces as well as the presence of nanotopography will result in lower fibrinogen adsorption, thus resulting in lower platelet adhesion and aggregation. Further, NO is a potent inhibitor of platelet function.[60] In the presence of NO multiple pathways of platelet activation are inhibited. NO binds with the hemoprotein, soluble guanylate cyclase (SGC), which results in increased production of cGMP that directly affects platelet function by inhibiting Ca^{2+} influx into the platelets, inhibiting GPIIb/IIIa expression and binding with fibrinogen, inhibiting phosphorylation of myosin light chains, inhibiting phosphorylation of protein kinase C, and modulating phospholipase A_2- and phospholipase C-mediated responses.[62,66] Further, the binding of NO to SGC also results in decrease in local Ca^{2+} concentration. The oxidation products of NO also reacts with thiols in blood resulting in the formation of *S*-nitrosothiols, which enhances the half-life and biological activity of NO, further inhibiting platelet function.[62,66] Thus, the drastic decrease in platelet aggregation and activation is due to the release of NO from TiO_2NT+PEM+NO surfaces.

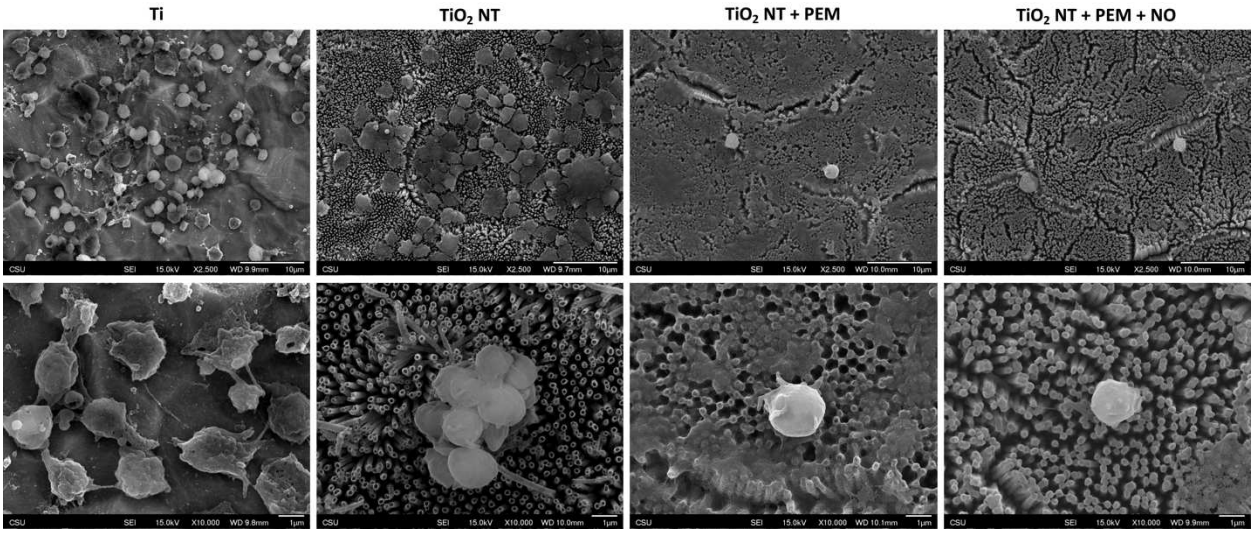

Figure 3.9 Representative SEM images of adhered cells on Ti, TiO_2NT, TiO_2NT+PEM, and TiO_2NT+PEM+NO surfaces.

Platelet activation was also quantified by measuring platelet factor-4 (PF-4) expression. During the late stages of activation and aggregation, PF-4 is released from alpha-granules (degranulation) present within the bodies of platelets and binds to heparin to assist in clotting. Thus, it is an indicator of the late stages of platelet activation, including degranulation. After 2 h of exposure of experimental surfaces to plasma containing platelets and leukocytes, no significant differences are observed in the release of PF-4, nor were differences noted between these groups and the negative controls (PS and HEPES). (**Figure 3.10**) The PF-4 confirms observations in the calcein-AM (**Figure 3.7**) and SEM (**Figure 3.9**) images, i.e., surfaces result in low amounts of adhesion, and surfaces do not significantly induce degranulation. Future work will investigate surface contact with plasma containing platelets and leukocytes for longer time periods to investigate whether increased adhesion, aggregation, and activation could occur with increased exposure.

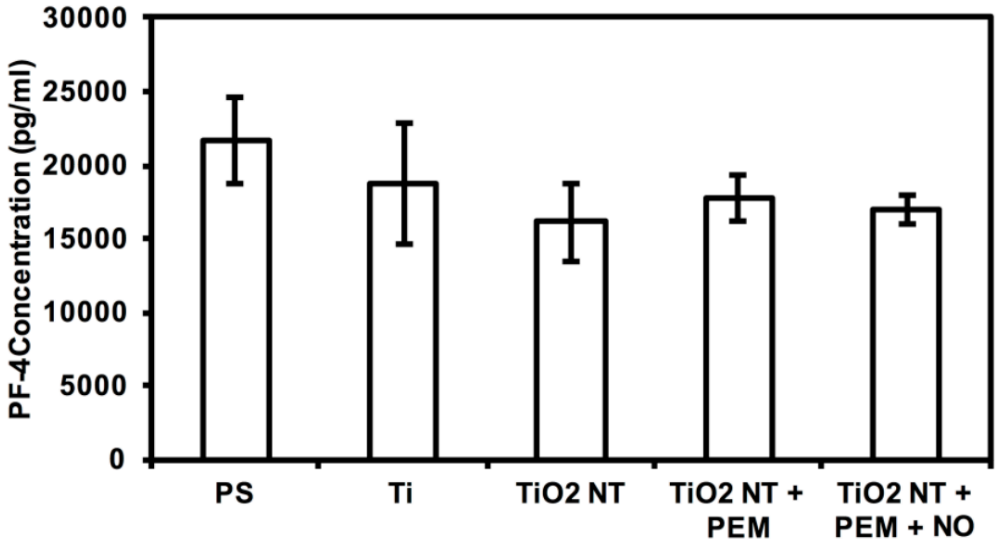

Figure 3.10 Quantification of platelet factor-4 released after surface exposure to plasma containing platelets and leukocytes for 2 h. No significant platelet activation amongst the experimental groups, nor differences between experimental surfaces and negative control (PS) in observed.

3.3.7 Thromboelastography (TEG)

The reaction time, initial clot formation time, amplification rate, and clot strength determined by TEG at 1 h intervals after human whole blood collection are shown in **Table 3.3**. The clot strength kept relatively similar value and less than 68 mm until 5 h had elapsed, which indicated that human whole blood did not become hypercoagulative and could be used within 5 h of collection.[67]

Table 3.3 Reaction time, initial clot formation time, amplification rate, and clot strength determined by TEG at 1 h intervals after human whole blood was collected.

Time interval after blood collection (h)	Reaction time (min)	Initial clot formation time (min)	Amplification rate (deg)	Clot strength (mm)
1	9.7 ± 1.6	4.4 ± 0.4	40.8 ± 4.0	52.5 ± 2.1
2	9.8 ± 2.2	4.9 ± 1.5	40.7 ± 3.3	54.5 ± 1.4
3	9.0 ± 0.0	4.1 ± 0.1	40.9 ± 1.6	54.8 ± 0.4
4	12.7 ± 0.7	3.6 ± 0.1	42.2 ± 6.4	55.0 ± 0.0
5	9.9 ± 3.1	3.2 ± 0.2	48.8 ± 3.0	52.5 ± 4.9

A 2 mm amplitude of blood clot formation was not reached on TiO_2NT+PEM surfaces after 15 min and 60 min incubation in human whole blood (**Figure 3.11**). Chitosan and its derivatives are suggested to be effective hemostatic agents that enhance the blood coagulation cascade to accelerate the wound healing process.[68–74] It is believed that at low pH, the positive charge density on chitosan and its derivatives interacts with negatively charged proteins and glycolipids in the red blood cell membrane, inducing the aggregation of red blood cells.[69,75] Some studies also show that chitosan and its derivatives are able to trigger platelet adhesion and aggregation, through the interaction between positively charged chitosan and negatively charged phosphatidyl serine in the platelet membrane.[59,76,77] The complete hemostasis mechanism of chitosan and its derivatives is still unclear.[78] However, in this study, we observed no blood clot formation on TiO_2NT+PEM surfaces. This may be due to the presence of heparin in the multilayer coating, since heparin is well-known for its anticoagulation function and has been widely used in clinics.[79–81] Two potential pathways of heparin from the PEM coating may contribute to the non-clotting phenomenon, heparin on top of the coating and leached heparin from the coating. During the PEM coating process, heparin is the top coating layer and increases the surface interaction with human whole blood compared to the lower chitosan layer. It is also possible that heparin is released from the PEM coating and leaches into surrounding blood. Further investigation is required, including *ex vivo* testing using anti-factor Xa assay, to measure the heparin level in human platelet-rich-plasma and determine the heparin source.

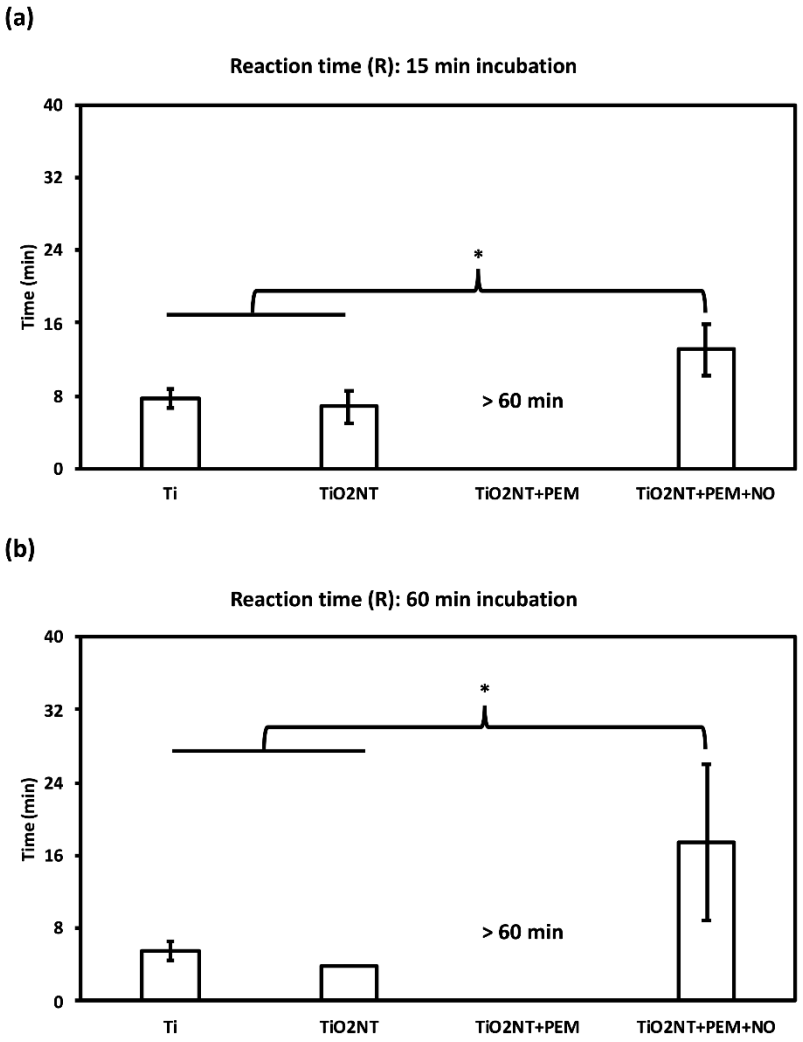

Figure 3.11 Reaction time (R) of modified surfaces after 15 min and 60 min incubation in human whole blood (n ≥ 5 samples, * indicates $p < 0.05$, > 60 min indicates no end-point value was provided by TEG during 60 min test).

Except for TiO_2NT+PEM surfaces, the time until clot formation was significantly prolonged on TiO_2NT+PEM+NO surfaces (13.1 ± 2.8 min) compared to Ti (7.7 ± 1.1 min) and TiO_2NT (6.8 ± 1.8 min) surfaces (**Figure 3.12 a**); TiO_2NT+PEM+NO surface (3.9 ± 0.8 min) showed an increase in initial clot formation time (K) compared to Ti (2.5 ± 0.6 min) and TiO_2NT surfaces (2.6 ± 0.9 min) (**Figure 3.12 a**); a lower α-angle of TiO_2NT+PEM+NO surface (40.9 ± 7.0°) compared to Ti surfaces (54.3 ± 7.5°), but no difference from TiO_2NT surfaces (51.4 ± 10.6°) (**Figure 3.12 b**); and no significant difference between Ti (57.4 ± 1.5 mm), TiO_2NT (55.4 ± 7.5 mm), and

TiO_2NT+PEM+NO (54.1 ± 1.9 mm) on clot strength (MA) after 15 min incubation in human whole blood (**Figure 3.12 c**).

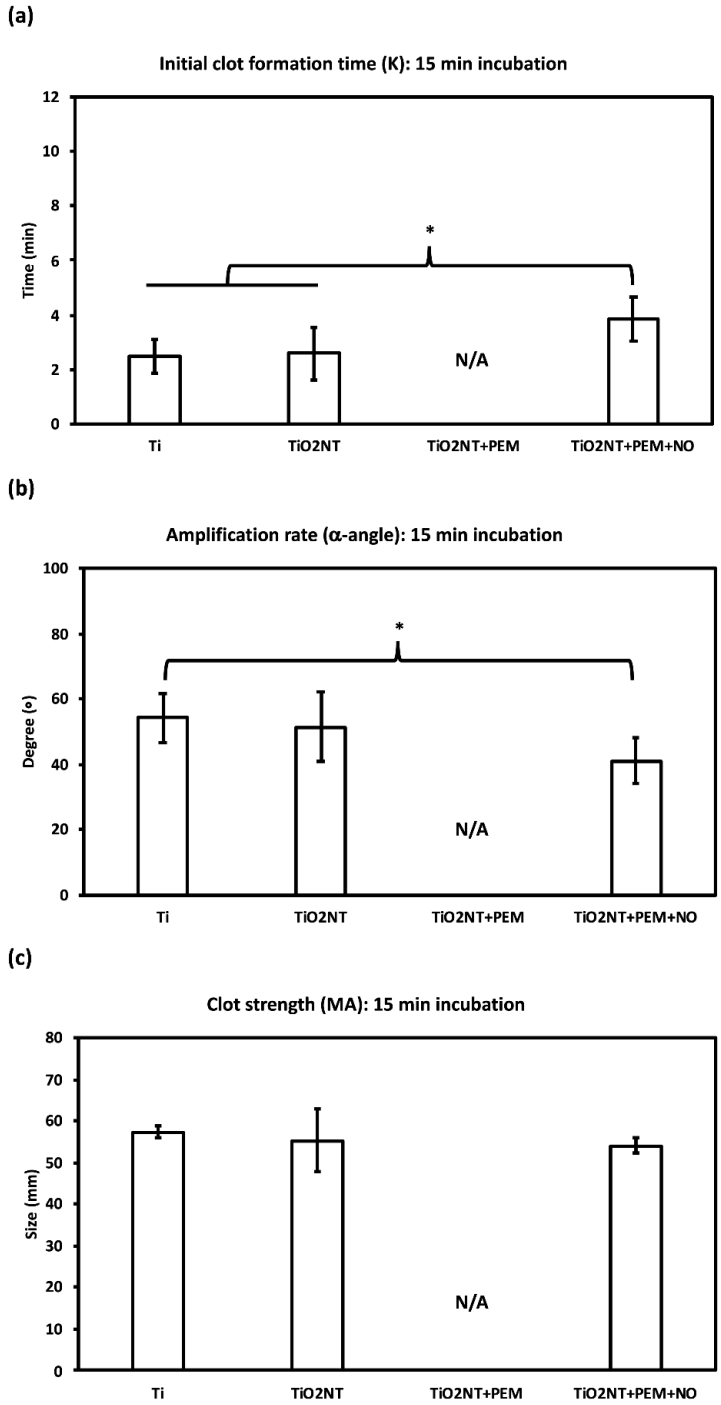

Figure 3.12 Initial clot formation time (K), amplification rate (α-angle), and clot strength (MA) of modified surfaces after 15 min incubation in human whole blood (n ≥ 5 samples, * indicated $p < 0.05$, N/A indicates no value was provided by TEG during the 60 min test).

Except for TiO_2NT+PEM surfaces, the time to initial clot formation (R) was significantly prolonged on TiO_2NT+PEM+NO surfaces (17.5 ± 8.6 min) compared to Ti (5.6 ± 1.0 min) and TiO_2NT (3.8 ± 0.0 min) surfaces (**Figure 3.13 b**); TiO_2NT+PEM+NO surfaces (5.1 ± 3.2 min) showed an increase in initial clot formation time (K) compared to TiO_2NT surfaces (1.4 ± 0.2 min), but not Ti surfaces (1.9 ± 0.4 min) (**Figure 3.13 a**); a lower α-angle of TiO_2NT+PEM+NO surface (40.4 ± 12.8°) compared to Ti surfaces (63.3 ± 5.5°) and TiO_2NT surfaces (69.4 ± 2.5°) (**Figure 3.13b**); and TiO_2NT+PEM+NO (53.1 ± 3.3 mm) with a significant lower clot strength (MA) compared to Ti (57.8 ± 2.1 mm) and TiO_2NT (59.2 ± 1.0 mm) after 60 min incubation in human whole blood (**Figure 3.13 c**).

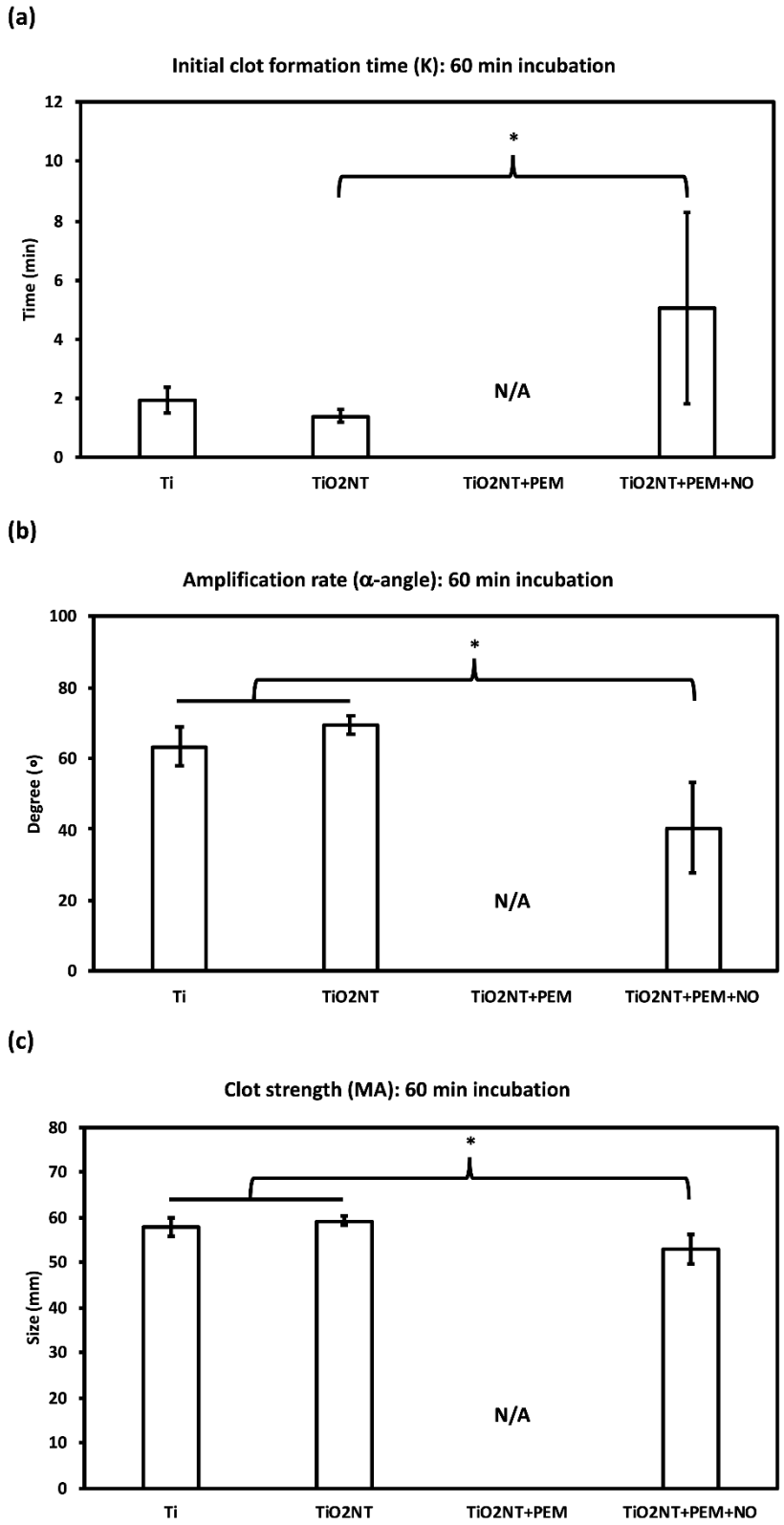

Figure 3.13 Initial clot formation time (K), amplification rate (α-angle), and clot strength (MA) of modified surfaces after 60 min incubation in human whole blood ($n \geq 5$ samples, * indicated $p < 0.05$, N/A indicates no value was provided by TEG during 60 min test).

NO is well-known for antiplatelet properties.[62,82,83] However, it was difficult to reach conclusions regarding the effects of NO on human whole blood in this work. Since NO has a short half-life (milliseconds range),[84,85] blood will not contain NO for any length of time during the transfer of human whole blood from microcentrifuge tubes containing incubated samples into TEG cups. Instead, the blood will contain NO oxidation products and probably methemoglobin within red blood cells. Blood incubated with TiO_2NT+PEM+NO surfaces for 15 min should be exposed to less NO than blood incubated for 60 min, contain lower quantities of NO oxidation products and methemoglobin, which probably leads to the different results observed between these two groups. An additional study without this transfer process is required. For example, direct coating of TEG cups with PEM and nitrosation of this coating to study the effects of NO release. Chitosan has been shown to be chemically degraded by certain nitrosating agents including nitrous acid (HNO_2). However, the use of an alkyl nitrite (*t*-buONO) as the nitrosating agent did not result in any apparent changes to the structure of chitosan.[86] This result indicates that our nitrosation process using *tert*-butyl nitrite is unlikely to affect PEM structure. In addition, the release of NO from *S*-nitrosated thioglycolic acid moieties may be accompanied by formation of disulfide bonds that link TGA units and perhaps chitosan-TGA chains.[87] It is possible that the inter- and intramolecular disulfide bonds in the coating partially prevent heparin leaching and reduce the effects of heparin on human whole blood. However, to form disulfide bonds, the TGA residues must be close together. The probability of two TGA residues reacting in such a way in a solid is unclear. Further investigation is needed to study the chemical and physical interaction between PEM coating layers during NO releasing process.

The present study establishes that the combination of surface nanotography, biologically derived coating chemistry, and release of a small molecule signal at physiologically relevant doses can improve the blood compatibility of titanium for short-term blood exposure. Design of biomedical device coatings for therapeutic delivery must also consider (i) off-target effects of the

therapeutic, (ii) the duration of delivery of the therapeutic, and (iii) possible side effects and longevity of the coating itself. For example, several recent studies suggest that drug-eluting stents designed to deliver cytostatic drugs from their surfaces may increase the risk of late thrombosis (3 years after implantation and beyond) compared to bare metal stents.[88–90] These cytostatic drugs are intended to perform for a long period of time, preventing smooth muscle cell proliferation and restenosis, while re-endothelialization occurs. However, the increased risk of late thrombosis may be attributed to delayed re-endothelialization and to local persistent inflammatory responses caused by the durable polymer coatings used to provide the cytostatic drug reservoir.[91–93] Delayed re-endothelialization is an off-target effect of the cytostatic drug, and the inflammatory response is a side effect of the coating persisting long after the drug reservoir is depleted.

The glycocalyx-inspired coatings proposed here are designed to obviate off-target effects of the therapeutic, could be tuned to regulate the NO release rate, and are composed of biodegradable, biologically derived polysaccharides. NO is a free radical with a short half-life, which ensures that it is active only very locally near the vessel wall. Since it is naturally produced by the healthy endothelium to cause both smooth muscle cell senescence and antiplatelet signals, the physiologically similar doses provided here are anticipated to neither have exhibit off-target effects nor to retard endothelialization. Further work should confirm these design criteria. Further work should also be pursued to optimize the NO release rate and duration, and the coating degradation kinetics to correspond to re-endothelialization time frame.

3.4 Conclusions

In this work, we have shown that surfaces with multiple functions inspired by blood vessel endothelium provide an alternative to one-dimensional surfaces for improving blood– material interactions. Here, we combine surface nanotopography, glycosaminoglycan-based surfaces, and NO-donor chemistry to demonstrate substantial reduction in platelet adhesion and activation

on titanium. From the ex vivo real-time blood clotting thromboelastographic performance of modified surfaces using human whole blood, TiO_2NT+PEM surfaces effectively inhibited blood clot formation. However, this raises concern of hemorrhage for patients who already have thrombocytopenia issue. In comparison, NO-releasing TiO_2NT+PEM+NO surfaces delayed blood clot formation without causing bleeding concerns. This study enables us to re-evaluate the multidimensional strategies like the one proposed here for further development of blood-compatible surfaces.

REFERENCES

1. Lane WA. Some remarks on the treatment of fractures. *Br Med J*. 1895;1(1790):861-863. doi:10.1136/bmj.1.1790.861
2. Özcan M, Hämmerle C. Titanium as a Reconstruction and Implant Material in Dentistry: Advantages and Pitfalls. *Materials (Basel)*. 2012;5(9):1528-1545. doi:10.3390/ma5091528
3. Balamurugan A, Rajeswari S, Balossier G, Rebelo AHS, Ferreira JMF. Corrosion aspects of metallic implants - An overview. *Mater Corros*. 2008;59(11):855-869. doi:10.1002/maco.200804173
4. Chen Q, Thouas GA. Metallic implant biomaterials. *Mater Sci Eng R Reports*. 2015;87:1-57. doi:10.1016/j.mser.2014.10.001
5. U.S. Food & Drug Administration. *Biological Responses to Metal Implants.*; 2019. www.fda.gov. Accessed January 12, 2020.
6. Gorbet MB, Sefton M V. Biomaterial-associated thrombosis: Roles of coagulation factors, complement, platelets and leukocytes. *Biomaterials*. 2004;25(26):5681-5703. doi:10.1016/j.biomaterials.2004.01.023
7. Jaffer IH, Fredenburgh JC, Hirsh J, Weitz JI. Medical device-induced thrombosis: what causes it and how can we prevent it? *J Thromb Haemost*. 2015;13(S1):S72-S81. doi:10.1111/jth.12961
8. Liu X, Yuan L, Li D, et al. Blood compatible materials: State of the art. *J Mater Chem B*. 2014;2(35):5718-5738. doi:10.1039/c4tb00881b
9. Lagergren H, Olsson P, Swedenborg J. Inhibited platelet adhesion: A non-thrombogenic characteristic of a heparin-coated surface. *Surgery*. 1974;75(5):643-650. doi:10.5555/uri:pii:0039606074902694

10. Olsson P, Lagergren H, Larsson R, Rådegran K. Prevention of Platelet Adhesion and Aggregation by a Glutardialdehyde-Stabilized Heparin Surface. *Thromb Haemost*. 1977;37(02):274-282. doi:10.1055/s-0038-1649228

11. Larsson R, Eriksson JC, Lagergren H, Olsson P. Platelet and plasma coagulation compatibility of heparinized and sulphated surfaces. *Thromb Res*. 1979;15(1-2):157-167. doi:10.1016/0049-3848(79)90061-6

12. Larsson R, Olsson P, Lindahl U. Inhibition of thrombin on surfaces coated with immobilized heparin and heparin-like polysaccharides: A crucial non-thrombogenic principle. *Thromb Res*. 1980;19(1-2):43-54. doi:10.1016/0049-3848(80)90402-8

13. Pasche B, Kodama K, Larm O, Olsson P, Swedenborg J. Thrombin inactivation on surfaces with covalently bonded heparin. *Thromb Res*. 1986;44(6):739-748. doi:10.1016/0049-3848(86)90020-4

14. Björck CG, Bergövist D, Esquivel CO, Larsson R, Rudsvik Y. In vitro evaluation of a biologic graft surface. Effect of treatment with conventional and low molecular weight (LMW) heparin. *Thromb Res*. 1984;35(6):653-663. doi:10.1016/0049-3848(84)90268-8

15. Ito Y, Imanishi Y. In vitro platelet adhesion and in vivo antithrombogenicity of heparinized polyetherurethaneureas. *Biomaterials*. 1988;9(3):235-240. doi:10.1016/0142-9612(88)90090-7

16. Park KD, Kim WG, Jacobs H, Okano T, Kim SW. Blood compatibility of SUUU-PEO-heparin graft copolymers. *J Biomed Mater Res*. 1992;26(6):739-756. doi:10.1002/jbm.820260605

17. Kito H, Matsuda T. Biocompatible coatings for luminal and outer surfaces of small-caliber artificial grafts. *J Biomed Mater Res*. 1996;30(3):321-330. doi:10.1002/(SICI)1097-4636(199603)30:3<321::AID-JBM6>3.0.CO;2-S

18. Kim YJ, Kang IK, Huh MW, Yoon SC. Surface characterization and in vitro blood

compatibility of poly(ethylene terephthalate) immobilized with insulin and/or heparin using plasma glow discharge. *Biomaterials*. 2000;21(2):121-130. doi:10.1016/S0142-9612(99)00137-4

19. Magnani A, Barbucci R, Montanaro L, Acriola CR, Lamponi S. In vitro study of blood-contacting properties and effect on bacterial adhesion of a polymeric surface with immobilized heparin and sulphated hyaluronic acid. *J Biomater Sci Polym Ed*. 2000;11(8):801-815. doi:10.1163/156856200744020
20. Tan Q, Ji J, Barbosa MA, Fonseca C, Shen J. Constructing thromboresistant surface on biomedical stainless steel via layer-by-layer deposition anticoagulant. *Biomaterials*. 2003;24(25):4699-4705. doi:10.1016/S0142-9612(03)00363-6
21. Yang M-C, Lin W-C. Protein adsorption and platelet adhesion of polysulfone membrane immobilized with chitosan and heparin conjugate. *Polym Adv Technol*. 2003;14(2):103-113. doi:10.1002/pat.337
22. Lin WC, Liu TY, Yang MC. Hemocompatibility of polyacrylonitrile dialysis membrane immobilized with chitosan and heparin conjugate. *Biomaterials*. 2004;25(10):1947-1957. doi:10.1016/j.biomaterials.2003.08.027
23. Thorslund S, Sanchez J, Larsson R, Nikolajeff F, Bergquist J. Bioactive heparin immobilized onto microfluidic channels in poly(dimethylsiloxane) results in hydrophilic surface properties. *Colloids Surfaces B Biointerfaces*. 2005;46(4):240-247. doi:10.1016/j.colsurfb.2005.10.009
24. Chen JL, Li QL, Chen JY, Chen C, Huang N. Improving blood-compatibility of titanium by coating collagen-heparin multilayers. *Appl Surf Sci*. 2009;255(15):6894-6900. doi:10.1016/j.apsusc.2009.03.011
25. Francis Suh JK, Matthew HWT. Application of chitosan-based polysaccharide biomaterials in cartilage tissue engineering: A review. *Biomaterials*. 2000;21(24):2589-

2598. doi:10.1016/S0142-9612(00)00126-5

26. Şenel S, McClure SJ. Potential applications of chitosan in veterinary medicine. *Adv Drug Deliv Rev*. 2004;56(10):1467-1480. doi:10.1016/j.addr.2004.02.007

27. Li Q-L, Nan Huang, Jialong Chen, Cheng Chen, Junying Chen, Hui Chen. Endothelial Cell and Platelet Behavior on Titanium Modified with a Mutilayer of Polyelectrolytes. *J Bioact Compat Polym*. 2009;24(2):129-150. doi:10.1177/0883911508101553

28. Jackson CM, Nemerson Y. Blood Coagulation. *Annu Rev Biochem*. 1980;49(1):765-811. doi:10.1146/annurev.bi.49.070180.004001

29. Anderson JM, Rodriguez A, Chang DT. Foreign body reaction to biomaterials. *Semin Immunol*. 2008;20(2):86-100. doi:10.1016/j.smim.2007.11.004

30. Reitsma S, Slaaf DW, Vink H, M J van Zandvoort MA, A oude Egbrink MG. The endothelial glycocalyx: composition, functions, and visualization. doi:10.1007/s00424-007-0212-8

31. Nieuwdorp M, Meuwese MC, Mooij HL, et al. Measuring endothelial glycocalyx dimensions in humans: A potential novel tool to monitor vascular vulnerability. *J Appl Physiol*. 2008;104(3):845-852. doi:10.1152/japplphysiol.00440.2007

32. van den Berg BM, Vink H, Spaan JAE. The endothelial glycocalyx protects against myocardial edema. *Circ Res*. 2003;92(6):592-594. doi:10.1161/01.RES.0000065917.53950.75

33. Boddohi S, Kipper MJ. Engineering Nanoassemblies of Polysaccharides. *Adv Mater*. 2010;22(28):2998-3016. doi:10.1002/adma.200903790

34. Nieuwdorp M, Meuwese MC, Vink H, Hoekstra JBL, Kastelein JJP, Stroes ESG. The endothelial glycocalyx: A potential barrier between health and vascular disease. *Curr Opin Lipidol*. 2005;16(5):507-511. doi:10.1097/01.mol.0000181325.08926.9c

35. Damodaran VB, Leszczak V, Wold KA, Lantvit SM, Popat KC, Reynolds MM.

Antithrombogenic properties of a nitric oxide-releasing dextran derivative: Evaluation of platelet activation and whole blood clotting kinetics. *RSC Adv*. 2013;3(46):24406-24414. doi:10.1039/c3ra45521a

36. Pegalajar-Jurado A, Wold KA, Joslin JM, et al. Nitric oxide-releasing polysaccharide derivative exhibits 8-log reduction against Escherichia coli, Acinetobacter baumannii and Staphylococcus aureus. *J Control Release*. 2015;217:228-234. doi:10.1016/j.jconrel.2015.09.015
37. Leszczak V, Popat KC. Improved in Vitro Blood Compatibility of Polycaprolactone Nanowire Surfaces. *ACS Appl Mater Interfaces*. 2014;6(18):15913-15924. doi:10.1021/am503508r
38. Leszczak V, Smith BS, Popat KC. Hemocompatibility of Polymeric Nanostructured Surfaces. doi:10.1080/09205063.2013.777228
39. Smith BS, Capellato P, Kelley S, Gonzalez-Juarrero M, Popat KC. Reduced in vitro immune response on titania nanotube arrays compared to titanium surface. *Biomater Sci*. 2013;1(3):322-332. doi:10.1039/c2bm00079b
40. Smith BS, Popat KC. Titania Nanotube Arrays as Interfaces for Blood-Contacting Implantable Devices: A Study Evaluating the Nanotopography-Associated Activation and Expression of Blood Plasma Components. *J Biomed Nanotechnol*. 2012;8(4):642-658. doi:10.1166/jbn.2012.1421
41. Almodóvar J, Kipper MJ. Coating Electrospun Chitosan Nanofibers with Polyelectrolyte Multilayers Using the Polysaccharides Heparin and N,N,N-Trimethyl Chitosan. *Macromol Biosci*. 2011;11(1):72-76. doi:10.1002/mabi.201000261
42. Boddohi S, Almodóvar J, Zhang H, Johnson PA, Kipper MJ. Layer-by-layer assembly of polysaccharide-based nanostructured surfaces containing polyelectrolyte complex nanoparticles. *Colloids Surfaces B Biointerfaces*. 2010;77(1):60-68.

doi:10.1016/j.colsurfb.2010.01.006

43. Boddohi S, Killingsworth CE, Kipper MJ. Polyelectrolyte multilayer assembly as a function of pH and ionic strength using the polysaccharides chitosan and heparin. *Biomacromolecules*. 2008;9(7):2021-2028. doi:10.1021/bm8002573

44. Almodóvar J, Place LW, Gogolski J, Erickson K, Kipper MJ. Layer-by-layer assembly of polysaccharide-based polyelectrolyte multilayers: A spectroscopic study of hydrophilicity, composition, and ion pairing. *Biomacromolecules*. 2011;12(7):2755-2765. doi:10.1021/bm200519y

45. Almodóvar J, Bacon S, Gogolski J, Kisiday JD, Kipper MJ. Polysaccharide-Based Polyelectrolyte Multilayer Surface Coatings can Enhance Mesenchymal Stem Cell Response to Adsorbed Growth Factors. *Biomacromolecules*. 2010;11(10):2629-2639. doi:10.1021/bm1005799

46. Almodóvar J, Mower J, Banerjee A, Sarkar AK, Ehrhart NP, Kipper MJ. Chitosan-heparin polyelectrolyte multilayers on cortical bone: Periosteum-mimetic, cytophilic, antibacterial coatings. *Biotechnol Bioeng*. 2013;110(2):609-618. doi:10.1002/bit.24710

47. Romero R, Chubb L, Travers JK, Gonzales TR, Ehrhart NP, Kipper MJ. Coating cortical bone allografts with periosteum-mimetic scaffolds made of chitosan, trimethyl chitosan, and heparin. *Carbohydr Polym*. 2015;122:144-151. doi:10.1016/j.carbpol.2015.01.015

48. Zomer Volpato F, Almodóvar J, Erickson K, Popat KC, Migliaresi C, Kipper MJ. Preservation of FGF-2 bioactivity using heparin-based nanoparticles, and their delivery from electrospun chitosan fibers. *Acta Biomater*. 2012;8(4):1551-1559. doi:10.1016/j.actbio.2011.12.023

49. Place LW, Kelly SM, Kipper MJ. Synthesis and Characterization of Proteoglycan-Mimetic Graft Copolymers with Tunable Glycosaminoglycan Density. *Biomacromolecules*. 2014;15(10):3772-3780. doi:10.1021/bm501045k

50. Lutzke A, Pegalajar-Jurado A, Neufeld BH, Reynolds MM. Nitric oxide-releasing S-nitrosated derivatives of chitin and chitosan for biomedical applications. *J Mater Chem B*. 2014;2(42):7449-7458. doi:10.1039/c4tb01340a

51. Peng HT. Thromboelastographic study of biomaterials. *J Biomed Mater Res Part B Appl Biomater*. 2010;94B(2):469-485. doi:10.1002/jbm.b.31626

52. Roberts TR, Leslie DC, Cap AP, Cancio LC, Batchinsky AI. Tethered-liquid omniphobic surface coating reduces surface thrombogenicity, delays clot formation and decreases clot strength ex vivo. *J Biomed Mater Res Part B Appl Biomater*. 2020;108(2):496-502. doi:10.1002/jbm.b.34406

53. Hawker MJ, Olver CS, Fisher ER. Modification of a commercial thromboelastography instrument to measure coagulation dynamics with three-dimensional biomaterials. *Biointerphases*. 2016;11(2):029602. doi:10.1116/1.4948339

54. Sorkin JA, Hughes S, Soares P, Popat KC. Titania nanotube arrays as interfaces for neural prostheses. 2015. doi:10.1016/j.msec.2015.01.077

55. Skrzypchak AM, Lafayette NG, Bartlett RH, et al. Effect of varying nitric oxide release to prevent platelet consumption and preserve platelet function in an in vivo model of extracorporeal circulation. *Perfusion*. 2007;22(3):193-200. doi:10.1177/0267659107080877

56. Vaughn MW, Kuo L, Liao JC. Estimation of nitric oxide production and reaction rates in tissue by use of a mathematical model. *Am J Physiol - Hear Circ Physiol*. 1998;274(6 43-6). doi:10.1152/ajpheart.1998.274.6.h2163

57. Wu Y, Zhou Z, Meyerhoff ME. In vitro platelet adhesion on polymeric surfaces with varying fluxes of continuous nitric oxide release. *J Biomed Mater Res Part A*. 2007;81A(4):956-963. doi:10.1002/jbm.a.31105

58. Sylman JL, Lantvit SM, Vedepo MC, Reynolds MM, Neeves KB. Transport limitations of

nitric oxide inhibition of platelet aggregation under flow. *Ann Biomed Eng*. 2013;41(10):2193-2205. doi:10.1007/s10439-013-0803-9

59. Lord MS, Cheng B, McCarthy SJ, Jung MS, Whitelock JM. The modulation of platelet adhesion and activation by chitosan through plasma and extracellular matrix proteins. *Biomaterials*. 2011;32(28):6655-6662. doi:10.1016/j.biomaterials.2011.05.062

60. Reynolds MM, Annich GM. The artificial endothelium. *Organogenesis*. 2011;7(1):42-49. doi:10.4161/org.7.1.14029

61. Moncada S, Palmer RM, Higgs EA. Nitric oxide: physiology, pathophysiology, and pharmacology. *Pharmacol Rev*. 1991;43(2).

62. Radomski MW, Moncada S. The biological and pharmacological role of nitric oxide in platelet function. In: *Advances in Experimental Medicine and Biology*. Vol 344. ; 1993:251-264. doi:10.1007/978-1-4615-2994-1_20

63. Paul BZS, Daniel JL, Kunapuli SP. Platelet shape change is mediated by both calcium-dependent and - independent signaling pathways. Role of p160 Rho-associated coiled-coil- containing protein kinase in platelet shape change. *J Biol Chem*. 1999;274(40):28293-28300. doi:10.1074/jbc.274.40.28293

64. Goodman SL, Grasel TG, Cooper SL, Albrecht RM. Platelet shape change and cytoskeletal reorganization on polyurethaneureas. *J Biomed Mater Res*. 1989;23(1):105-123. doi:10.1002/jbm.820230109

65. Ko T-M, Cooper SL. Surface properties and platelet adhesion characteristics of acrylic acid and allylamine plasma-treated polyethylene. *J Appl Polym Sci*. 1993;47(9):1601-1619. doi:10.1002/app.1993.070470908

66. Radomski MW, Palmer RMJ, Moncada S. The role of nitric oxide and cGMP in platelet adhesion to vascular endothelium. *Biochem Biophys Res Commun*. 1987;148(3):1482-1489. doi:10.1016/S0006-291X(87)80299-1

67. Kupcinskiene K, Trepenaitis D, Petereit R, et al. Monitoring of hypercoagulability by thromboelastography in bariatric surgery. *Med Sci Monit*. 2017;23:1819-1826. doi:10.12659/MSM.900769

68. Brandenberg G, Leibrock LG, Shuman R, Malette WG, Quigley H. Chitosan: A new topical hemostatic agent for diffuse capillary bleeding in brain tissue. *Neurosurgery*. 1984;15(1):9-13. doi:10.1227/00006123-198407000-00004

69. Rao SB, Sharma CP. Use of chitosan as a biomaterial: Studies on its safety and hemostatic potential. *J Biomed Mater Res*. 1997;34(1):21-28. doi:10.1002/(SICI)1097-4636(199701)34:1<21::AID-JBM4>3.0.CO;2-P

70. Benesch J, Tengvall P. Blood protein adsorption onto chitosan. *Biomaterials*. 2002;23(12):2561-2568. doi:10.1016/S0142-9612(01)00391-X

71. Okamoto Y, Yano R, Miyatake K, Tomohiro I, Shigemasa Y, Minami S. Effects of chitin and chitosan on blood coagulation. *Carbohydr Polym*. 2003;53(3):337-342. doi:10.1016/S0144-8617(03)00076-6

72. Wedmore I, McManus JG, Pusateri AE, Holcomb JB. A special report on the chitosan-based hemostatic dressing: Experience in current combat operations. *J Trauma - Inj Infect Crit Care*. 2006;60(3):655-658. doi:10.1097/01.ta.0000199392.91772.44

73. Ong SY, Wu J, Moochhala SM, Tan MH, Lu J. Development of a chitosan-based wound dressing with improved hemostatic and antimicrobial properties. *Biomaterials*. 2008;29(32):4323-4332. doi:10.1016/j.biomaterials.2008.07.034

74. Hattori H, Ishihara M. Changes in blood aggregation with differences in molecular weight and degree of deacetylation of chitosan. *Biomed Mater*. 2015;10(1):015014. doi:10.1088/1748-6041/10/1/015014

75. Mirzadeh L(') H, Yaghobi N, Amanpour2 S, Ahmadi2 H, Mohagheghi2 MA, Hormozi F. *Preparation of Chitosan Derived from Shrimp's Shell of Persian Gulf as a Blood*

Hemostasis Agent. Vol 11.; 2002.

76. Chou TC, Fu E, Wu CJ, Yeh JH. Chitosan enhances platelet adhesion and aggregation. *Biochem Biophys Res Commun*. 2003;302(3):480-483. doi:10.1016/S0006-291X(03)00173-6

77. Sagnella S, Mai-Ngam K. Chitosan based surfactant polymers designed to improve blood compatibility on biomaterials. *Colloids Surfaces B Biointerfaces*. 2005;42(2):147-155. doi:10.1016/j.colsurfb.2004.07.001

78. Hu Z, Zhang D-Y, Lu S-T, Li P-W, Li S-D. marine drugs Chitosan-Based Composite Materials for Prospective Hemostatic Applications. doi:10.3390/md16080273

79. Oduah EI, Linhardt RJ, Sharfstein ST, Pinto MMM, Emília De Sousa M. pharmaceuticals Heparin: Past, Present, and Future. doi:10.3390/ph9030038

80. Murugesan S, Xie J, Linhardt RJ. *Immobilization of Heparin: Approaches and Applications*.; 2008.

81. Oliver WC. Anticoagulation and coagulation management for ECMO. *Semin Cardiothorac Vasc Anesth*. 2009;13(3):154-175. doi:10.1177/1089253209347384

82. Radomski M., Palmer RM., Moncada S. Endogenous nitric oxide inhibits human platelet adhesion to vascular endothelium. *Lancet*. 1987;330(8567):1057-1058.

83. Fleser PS, Nuthakki VK, Malinzak LE, et al. Nitric oxide-releasing biopolymers inhibit thrombus formation in a sheep model of arteriovenous bridge grafts. *J Vasc Surg*. 2004;40(4):803-811. doi:10.1016/j.jvs.2004.07.007

84. Archer S. *Measurement of Iitric Oxide in. Biological Models*. www.fasebj.org. Accessed February 15, 2020.

85. Hakim TS, Sugimori K, Camporesi EM, Anderson G. *Half-Life of Nitric Oxide in Aqueous Solutions with and without Haemoglobin*. Vol 17.; 1996.

86. Allison CL, Lutzke A, Reynolds MM. Examining the effect of common nitrosating agents

on chitosan using a glucosamine oligosaccharide model system. *Carbohydr Polym*. 2019;203:285-291. doi:https://doi.org/10.1016/j.carbpol.2018.09.052

87. Kast CE, Bernkop-Schnürch A. Thiolated polymers - thiomers: Development and in vitro evaluation of chitosan-thioglycolic acid conjugates. *Biomaterials*. 2001;22(17):2345-2352. doi:10.1016/S0142-9612(00)00421-X

88. Shuchman M. Trading Restenosis for Thrombosis? New Questions about Drug-Eluting Stents. *N Engl J Med*. 2006;355(19):1949-1952. doi:10.1056/NEJMp068234

89. McFadden EP, Stabile E, Regar E, et al. Late thrombosis in drug-eluting coronary stents after discontinuation of antiplatelet therapy. *Lancet*. 2004;364(9444):1519-1521. doi:10.1016/S0140-6736(04)17275-9

90. Moreno R, Fernández C, Hernández R, et al. Drug-eluting stent thrombosis: Results from a pooled analysis including 10 randomized studies. *J Am Coll Cardiol*. 2005;45(6):954-959. doi:10.1016/j.jacc.2004.11.065

91. Ma X, Hibbert B, Dhaliwal B, et al. Delayed re-endothelialization with rapamycin-coated stents is rescued by the addition of a glycogen synthase kinase-3β inhibitor. *Cardiovasc Res*. 2010;86(2):338-345. doi:10.1093/cvr/cvq047

92. Joner M, Finn A V., Farb A, et al. Pathology of Drug-Eluting Stents in Humans. Delayed Healing and Late Thrombotic Risk. *J Am Coll Cardiol*. 2006;48(1):193-202. doi:10.1016/j.jacc.2006.03.042

93. Nebeker JR, Virmani R, Bennett CL, et al. Hypersensitivity cases associated with drug-eluting coronary stents: A review of available cases from the Research on Adverse Drug Events and Reports (RADAR) project. *J Am Coll Cardiol*. 2006;47(1):175-181. doi:10.1016/j.jacc.2005.07.071

CHAPTER 4

NITRIC OXIDE-MEDIATED FIBRINOGEN DEPOSITION PREVENTS PLATELET ADHESION AND ACTIVATION[2]

4.1 Introduction

Blood-contacting medical devices such as extracorporeal circuits (ECCs), vascular grafts, stents, and catheters have been widely used in critical medical procedures. However, these medical devices have one major complication: thrombosis. Initially, key blood serum proteins such as fibrinogen (Fb) adsorb on the device surface within seconds of contact with the blood.[1] The adsorbed Fb binds to platelets through the glycoprotein IIb/IIIa receptors and induces platelet adhesion, activation, and aggregation.[2] Further, adsorbed Fb is converted to fibrin via thrombin, thereby cross-linking platelets to each other, which ultimately results in thrombus formation.[3] Without intervention, platelets will continue to accumulate on the surface, leading to overall low platelet counts, obstruction of blood flow, and significant risk for emboli.

Unfortunately, due to the incompatibility of the device surface with the blood, clinicians must manage the interactions of blood components at the material surface to avoid severe consequences such as surface clotting or inflammation. To date, the standard of care to prevent thrombus formation on devices is to administer systemic anticoagulants such as heparin intravenously or subcutaneously.[4–6] For certain patients, heparin use may result in excessive

[2] The following was adapted with permission from Zang Y, Popat KC, Reynolds MM. Nitric Oxide-Mediated Fibrinogen Deposition Prevents Platelet Adhesion and Activation. *Biointerphases*. 2018;13(6):E403. Copyright 2018 American Vacuum Society. All experiments were performed by Yanyi Zang. Dr. Patrick McCurdy from Central Instrument Facility at Colorado State University assisted scanning electron microscopy and X-ray photoelectron spectrometry. Dr. Alec Lutzke assisted in preparation for the manuscript. This work was supported by Monfort research funding awarded to Dr. Melissa Reynolds in 2017.

bleeding and further complications.[7] Antidotes such as protamine sulfate can neutralize the effects of heparin; however, it is necessary to adjust dosage on a case by case basis. Other anticoagulants such as direct thrombin inhibitors and Factor Xa inhibitors have been used for patients; however, no antidote exists that can reverse their effects.[8,9] Since these systemic anticoagulants have severe drawbacks, the development of new surfaces that prevent thrombus formation *in vivo* is vital.

There are three common approaches that researchers use to disrupt specific processes in the coagulation cascade: (i) controlling protein deposition, (ii) preventing platelet adhesion and activation, and (iii) reducing platelet aggregation. The first approach is to prevent protein adsorption on a material surface by changing surface wettability,[10–12] charge,[13,14] coating,[15–17] and other properties. For example, a modified surface with poly(2-methoxyethylacrylate) coating has been shown to reduce protein adhesion by creating a water boundary layer.[15,18] The second approach is to prevent platelet adhesion and activation by depositing precursor proteins or modifying the surface chemistry to delay or mitigate biological responses,[19–21] or by modifying the surface topography at a nanoscale to change surface properties, such as hydrophilicity/hydrophobicity via texturing the surface.[22,23] The third approach is to prevent platelet aggregation by inhibiting the activation of Factor Xa and further prevent fibrin formation by using direct Factor Xa inhibitors, such as rivaroxaban or apixaban, or by using indirect Factor Xa inhibitors, such as subcutaneous injection of fondaparinux.[24–26]

Over the past 25 years, nitric oxide (NO) has gained significant attention as an alternative strategy to surface modifications and systemic anticoagulants because of NO's ability to reversibly inhibit platelets and its short half-life in blood.[27] Indeed, many researchers have reported the ability of NO to prevent platelet adhesion, activation, and aggregation.[28–32] For example, the release of NO from NO donors embedded into polymer coatings has shown effectiveness in preventing platelet adhesion and activation on polymers such as silicone rubber, polyurethane, poly(vinyl

chloride) (PVC), and polymethacrylates.[33–42] These polymers have been tested in a range of devices including catheters, ECCs, vascular grafts, and sensors in mice, rabbit, sheep, and pig models. Taken together, the reports documenting NO's effectiveness as an antithrombotic agent are overwhelming. While much is known about the influence of NO on platelets, few studies have investigated the effects of NO on the first step of the coagulation cascade—protein adsorption. A surprising result has been shown that NO increases the amount of Fb adsorbed on the surface of PVC,[43] which is consistent with reports that plasma Fb decreased more after blood flow through NO-releasing silicone rubber ECC loops than controls.[33] These results subverted the traditional concept that NO reduces Fb adsorption to further prevent platelet adhesion and activation. However, the direct effect of NO on Fb adsorption and subsequent effects on platelet adhesion and activation on the surface of PVC remains unknown.

In this study, we examined the effect of NO on Fb adsorption and the subsequent ability of the NO-mediated Fb modified surfaces to bind platelets. A model system was designed for studying whether platelets would interact with an NO-mediated Fb modified surface. Plasticized PVC films containing NO donors were formulated to achieve three distinct NO surface fluxes: (i) $4.7 \pm 0.6 \times 10^{-10}$ mol NO cm^{-2} min^{-1} , (ii) 15.6 ± 0.9 × 10–10 mol NO cm^{-2} min^{-1} , and (iii) $33.2 \pm 0.7 \times 10^{-10}$ mol NO cm^{-2} min^{-1}. These values were selected based on the NO flux from the endothelium,[44] and the previously reported critical NO surface flux needed to reduce platelet activation and blood clot formation in an ECC rabbit model.[45] Direct NO measurements were made using a nitric oxide analyzer (NOA). The surfaces were characterized for roughness, contact angle, and elemental composition. Fb adsorption was determined by bicinchoninic acid (BCA) assay. Platelet adhesion was quantified and analyzed by using calcein-acetoxymethyl (AM) staining and IMAGEJ software. The results from this study demonstrate for the first time that NO may prevent platelet adhesion onto PVC surfaces through a pathway that involves protein deposition, confirming previous reports.[33,43] That is, NO directs Fb adsorption onto surfaces in a

manner that subsequently reduces platelet adhesion and activation even after NO release has ceased.

4.2 Materials and Methods

4.2.1 Materials

All reagents and solvents were purchased from commercial vendors and used without further purification unless noted otherwise. Reduced glutathione and phosphate buffered saline (PBS; 137 mM NaCl, 2.7 mM KCl, 10 mM phosphate, pH = 7.3–7.5) were purchased from VWR International (Radnor, PA, USA). Hydrochloric acid (HCl), dioctyl sebacate (DOS), tetrahydrofuran (THF), calcein-AM, sodium cacodylate, sucrose, a Pierce BCA protein assay kit, and Environmental Protection Agency (EPA) vials were purchased from Thermo Fisher Scientific (Waltham, MA, USA). Sodium nitrite and human plasma Fb were purchased from EMD Millipore (Burlington, MA, USA). High molecular weight PVC was purchased from Sigma-Aldrich (St. Louis, MO, USA). Ethylenediaminetetraacetic acid (EDTA)-coated vacuum tubes were purchased from BD Biosciences (Franklin Lakes, NJ, USA). A lactate dehydrogenase (LDH) cytotoxicity assay kit was purchased from Cayman Chemical (Ann Arbor, MI, USA). Glutaraldehyde was purchased from Ted Pella (Redding, CA, USA). Hexamethyldisilazane (HMDS) was purchased from KMG Chemicals (Fort Worth, TX, USA). Ultrahigh purity N_2 and O_2 gases were supplied by Airgas (Denver, CO, USA). Water (H_2O) was purified (18.2 MΩ cm) using a Millipore Direct-Q5 ultrapure water purification system purchased from EMD Millipore (Burlington, MA, USA) for all experiments.

4.2.2 Synthesis and characterization of *S*-nitrosoglutathione

The NO donor used in this study was *S*-nitrosoglutathione (GSNO). GSNO was synthesized based on a previously reported method.[46] In brief, 5 mmol (1.53 g) of reduced glutathione was added into 8 ml of cold H2O and 2.5 ml of 2 M HCl and was stirred on ice for 10 min. To initiate nitrosation, 5 mmol (0.345 g) of sodium nitrite was added into this solution. The

solution was stirred further for 40 min on ice. This was followed by the addition of 10 ml of cold acetone, and the mixture was stirred for another 10 min. The resulting GSNO was collected through gravity filtration. The filtered GSNO was washed with 5 ml of cold H_2O and 5 ml of cold acetone. Finally, GSNO was transferred into an EPA amber vial and dried under vacuum for at least 3 h. GSNO purity was characterized using an Evolution 300 UV-vis spectrophotometer (Thermo Fisher Scientific Inc., Waltham, MA, USA) by measuring the absorbance at 336 nm which is associated with the S-nitrosothiol (RSNO) functional group.[47] The GSNO was stored in an EPA amber vial to prevent light exposure and kept at –20 °C to prevent thermal decomposition until further use.

4.2.3 Fabrication of polymer films

Polymer solutions of varying concentrations of PVC, DOS, and GSNO in THF were prepared as shown in **Table 4.1** to make different films. Six hundred microliters of each solution was aliquoted into a 10 ml beaker and allowed to cure for approximately 40 min. This was repeated two more times to fabricate films with three layers. The films were then cut into 8 mm disks for further use. To prevent GSNO leaching and ensure slow release of NO, the NO-releasing polymer films were further coated on both top and bottom sides by curing with 300 µl of PVC control polymer solution. The films were dried overnight to evaporate solvent prior to further use.

Table 4.1 Composition of NO-releasing polymer films.

Polymer films	Polymer solution		Concentration of GSNO in polymer solution (w/v %)
	Total amount of PVC and DOS in THF (mg ml^{-1})	Ratio of PVC to DOS in THF (PVC:DOS)	
PVC control	150	2:1	0
Low NO flux	86	2:1	3
Mid NO flux	70	2:1	6.5

High NO flux	75	1:1	15

4.2.4 Measurement of NO surface flux from polymer films

NO surface flux of the GSNO incorporated films was measured using Sievers 280i nitric oxide analyzers (GE Analytical Instruments, Boulder, CO, USA). The instrument was calibrated with N_2 and 43.6 ppm NO/N_2 prior to all experiments using a flow rate of 200 ml min^{-1}. Baseline measurements were taken 4 min prior to introducing polymer films into the NOA sample cell. The film was placed in 2 ml of PBS in a sample cell connected to the NOA chamber and purged with N2 to deoxygenate the cell. The released NO is swept into a chamber where it reacts with ozone (O_3) to generate excited-state nitrogen dioxide (NO_2) and O_2. As NO_2 relaxes, a photon is released and passes through a red filter into a photomultiplier tube where the signals are multiplied and converted from millivolt (mV) into part per billion (ppb). These ppb values are converted to mols of NO using a calibration constant. All NO surface flux data points were collected for 5 h at 15 s intervals at 37 °C.

4.2.5 Isolation of platelet-rich plasma

Human whole blood was drawn from healthy donors who did not take thromboxane inhibitors for at least two weeks. The protocol of blood isolation from healthy human donors was approved by Colorado State University Institutional Review Board. In brief, venous phlebotomy blood was drawn into 10 ml EDTA-coated vacuum tubes by a trained phlebotomist. Platelet-rich plasma (PRP) was isolated by centrifuging whole blood at 150 g for 15 min. The PRP was allowed to rest for 10 min prior to further use. For all PRP studies, polymer films were incubated in PBS at 37 °C for 1 h to ensure a steady-state NO release rate. The films were then incubated in PRP for 2 h at 37 °C, 5% CO_2 with 100 rpm shaking.

4.2.6 Cytotoxicity of polymer films

Platelet cytotoxicity was measured using a commercially available LDH cytotoxicity assay kit. After 2 h incubation, 100 µl of film-exposed PRP and standards was transferred into a 96-well plate, followed by the addition of 100 µl of LDH Reaction Solution which contained 1% (v/v) of NAD^+ , 1% (v/v) of lactic acid, 1% (v/v) of tetrazolium salt (INT), and 1% (v/v) of reconstituted diaphorase in assay buffer. The solution was incubated for 30 min at 37 °C, 5% CO_2 with 100 rpm shaking. PRP lysed with 2% (v/v) Triton X-100 was used as the negative control, and assay buffer without cells was used as the noncytotoxic control. The absorbance of the red formazan product was measured at 490 nm using a FLUOstar Omega microplate reader (BMG LABTECH, Ortenburg, Germany).

4.2.7 Blood cell interaction with polymer films

Platelet adhesion on different polymer films was investigated by staining the cells with calcein-AM and imaging using an AXIO Imager A2 fluorescence microscope (Carl Zeiss, Inc., Thornwood, NY, USA). After 2 h incubation with PRP, the films were rinsed twice with PBS and stained with calcein-AM. The films were incubated in 1 ml of 5 µM calcein-AM solution at room temperature for 25 min. This was followed by gently rinsing the surfaces twice with PBS. All the films were imaged using a fluorescence microscope with 493/514 nm filters and processed using IMAGEJ software to obtain percentage of coverage.

Platelet activation was evaluated using a JEOL JSM-6500F scanning electron microscope (SEM; Peabody, MA, USA). After 2 h of incubation in PRP, the films were rinsed twice with PBS and were fixed with a primary fixative containing 7.2% glutaraldehyde, 0.1 M sodium cacodylate, and 0.1 M sucrose for 45 min at room temperature. The films were then transferred into a secondary fixative (primary fixative without glutaraldehyde) for 10 min. This was followed by exposing the films to consecutive solutions of ethanol (35%, 50%, 70%, and 100%) for 10 min

each and a final incubation in HMDS for 10 min at room temperature. The films were then air-dried in the fume hood and stored in a desiccator until imaging by SEM. All films were sputtered with 10 nm layer of gold and imaged at 15 kV.

4.2.8 Surface characterization of high NO flux films

Surface characterization of the high NO flux films was measured after 1 h incubation, 5 h incubation, and incubation until all NO was released. Incubation was done in PBS at 37 °C with 100 rpm shaking. Postincubation, films were vacuum dried and covered from light at room temperature before measurement.

An optical profilometer (Zygo Corporation, Middlefield, CT, USA) was used to determine surface roughness of films at room temperature. Average surface roughness (Ra) was measured from two single map squares 0.375 mm × 0.281 mm at –20× magnification.

The static water contact angle of films was measured using a Ramé-hart 200F-1 contact angle goniometer (Raméhart Instrument Co., Succasunna, NJ, USA) at room temperature. The static contact angle was obtained by placing a 2 µl drop of H_2O on the surface of films and measuring the angle between solid–liquid and liquid–vapor interfaces.

Surface elemental compositions were measured by a PE-5800 x-ray photoelectron spectrometer (XPS; Chanhassen, MN, USA). All spectra were collected using a monochromatic Al 7 mm filament with $h\nu$ = 187.85 eV and with a photoelectron takeoff angle of 45°. Survey scans were taken over a range of 10–1100 eV. High-resolution scans were taken for C 1s, O 1s, Cl 2p, N 1s, and S 2p using 23.50 eV analyzer pass energy with 0.1 eV per step. All scans were taken using a low-energy electron gun for charge neutralization set at 20.5 µA. Spectra curve fitting was done using Phi Electronics Multipak version 9.3 (Chanhassen, MN, USA).

4.2.9 Fb adsorption on high NO flux films

A commercially available Pierce BCA protein assay kit was used to quantify Fb adsorption on films. After films were incubated with Fb, Fb solution was removed and films were rinsed with PBS to remove excess and unabsorbed Fb. The films were transferred into a new 24-well plate and incubated with 1% sodium dodecyl sulfate (SDS) in PBS for 1.5 h at 37 °C to desorb Fb from the surfaces.[48] This was repeated twice to ensure all Fb was desorbed from the surface. Twenty-five microliters of the solution was mixed with 200 µl of BCA Working Reagent in a 96-well plate and incubated further for 30 min at 37 °C. The absorbance of the purple-colored reaction product was measured at 562 nm using a Synergy Mx Microplate reader (BioTek; Winooski, VT, USA). The amount of Fb adsorbed was calculated based on Fb standard curves.

To determine Fb adsorption on high NO flux films and to evaluate if incubation affects the amount of adsorbed Fb, two sets of films were used. First, films were incubated in a 24-well plate in PBS at 37 °C for 1 h to reach a steady-state NO release rate, and then incubated in 1.5 mg ml^{-1} Fb solution at 37 °C for 2 h with 100 rpm shaking. After incubation, Fb on one set of films was directly measured as described, and the other set of films was incubated in PBS at 37 °C until all NO was released and Fb was measured as described. To determine if surface roughness or NO release affects Fb adsorption, two sets of high NO flux films were used. One set of high NO flux films was incubated in PBS at 37 °C with 100 rpm shaking for 15 days to release all NO before incubated in Fb solution. The other set of high NO flux films was used directly after fabrication. The amount of Fb adsorbed on two sets of high NO flux films was measured as described.

4.2.10 Blood interaction with high NO flux films with pre-adsorbed Fb

To evaluate effects of NO-mediated pre-adsorbed Fb on platelet adhesion and activation, PVC control and high NO flux films with pre-adsorbed Fb were incubated in PBS at 37 °C with

100 rpm shaking for 15 days. After incubation, platelet adhesion and activation were evaluated as described earlier.

4.2.11 Statistical analysis

One-way analysis of variance (ANOVA) was performed to identify statistically significant differences between polymer films for measurements related to surface characterization, cytotoxicity, Fb adsorption, and platelet adhesion data. ANOVA was followed by post hoc Tukey–Kramer multiple comparison test to determine the statistically significant differences between films at 99% confidence levels ($p < 0.01$). All potential outliers were determined based on Grubb's test with a 99% confident level ($p < 0.01$). For NO surface flux, surface roughness, and static contact angle, three samples of each group were measured. For cytotoxicity, Fb adsorption, and platelet adhesion, five samples of each group were evaluated. Data are reported as mean with standard deviation. For XPS and platelet activation studies, two samples for each group were measured, and representative XPS spectra and SEM images are presented.

4.3 Results and discussion

4.3.1 Measurement of NO surface flux of polymer films

To investigate the effect of NO-mediated Fb deposition on platelet activation, surfaces with different NO surface fluxes were fabricated. NO generated from natural microvascular endothelial cells is $0.5 – 4.0 \times 10^{-10}$ mol NO cm^{-2} min^{-1},[44] whereas the NO surface flux needed to improve hemocompatibility of ECCs is 13.7×10^{-10} mol NO cm^{-2} min^{-1}.[49] Therefore, polymer films with varied NO surface flux were investigated in this study. NO surface flux of polymer films was measured using an NOA with the NOA sample cell maintained at 37 °C for 5 h. It took 1 h for all the films to reach a steady-state of NO release rate (**Figure 4.1**). **Figure 4.2** shows the NO surface flux over a 4 h period after the experiment had been performed for 1 h. All the low NO flux, mid NO flux, and high NO flux films maintained a steady-state NO release rate during the entire 4 h

period. Achieving a steady-state of NO release rate for all films allows for a better understanding of the effects of NO on Fb adsorption, and platelet adhesion and activation. During the 4 h period, NO surface flux of low NO flux films ($4.7 \pm 0.6 \times 10^{-10}$ mol NO cm^{-2} min^{-1}) was near the upper range of NO surface flux from natural microvascular endothelial cells, mid NO flux films ($15.6 \pm 0.9 \times 10^{-10}$ mol NO cm^{-2} min^{-1}) were similar to the known beneficial NO surface flux that improves the performance of ECCs, and high NO flux films ($33.2 \pm 0.7 \times 10^{-10}$ mol NO cm^{-2} min^{-1}) can provide information about Fb adsorption, and platelet adhesion and activation at a higher range of NO surface flux.

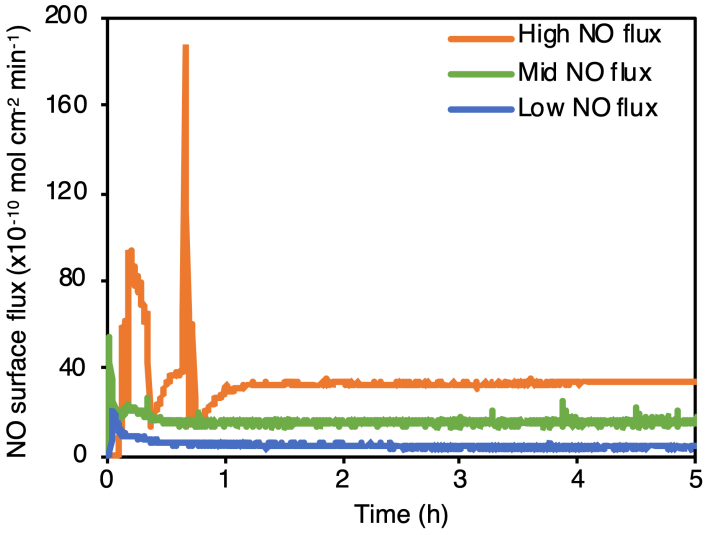

Figure 4.1 Representative 0 h to 5 h NO surface flux of low NO flux (blue), mid NO flux (green), and high NO flux (orange) films.

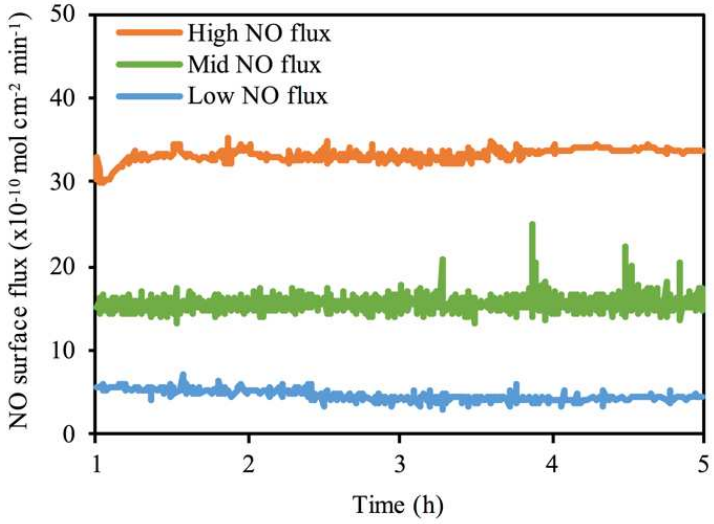

Figure 4.2 Representative 1-5 h NO surface flux of low NO flux (blue), mid NO flux (green), and high NO flux (orange) films after allowed to release for 1 h in PBS at 37 °C with 100 rpm shaking to reach steady-state of NO release rate.

4.3.2 Cytotoxicity of polymer films

Cytotoxicity of different films was determined after 2 h incubation in human platelet-rich plasma using an LDH assay kit. The amount of LDH released from dead cells, as well as the level of cytotoxicity, is directly proportional to the amount of red formazan product which can be measured spectrophotometrically at 490 nm. All the polymer films, polystyrene (PS) (nontoxic), and assay buffer (no platelets) were significantly less cytotoxic than Triton X-100 (cytotoxic) (**Figure 4.3**). There was no significant difference among PS, polymer films, and assay buffer. Since PS and assay buffer are noncytotoxic, none of the polymer films are expected to have short-term cytotoxic effects on platelets. Indeed, none of the NO films had a negative effect on platelet function.

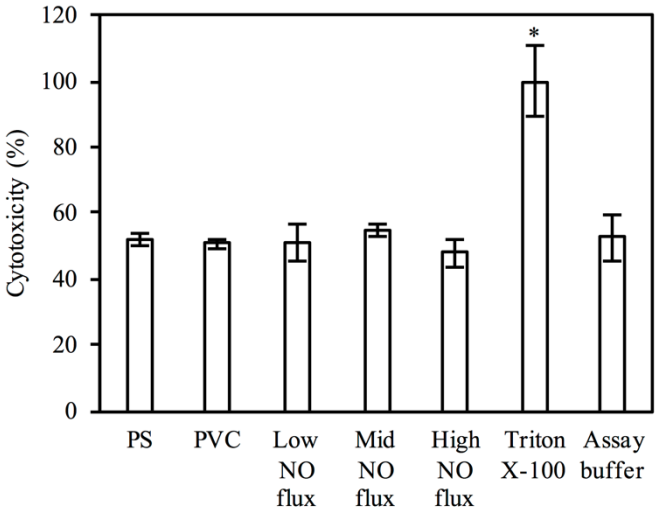

Figure 4.3 Quantification of LDH after 2 h incubation in human platelet-rich-plasms. No significant difference among PS control (noncytotoxic), polymer films and assay buffer control (no platelet). Triton X-100 is significant different than other groups (* indicates $p < 0.01$).

4.3.3 Blood cell interaction with polymer films

For platelet adhesion study, polymer films were incubated in PBS at 37 °C with 100 rpm shaking for 1 h to reach a steady-state of NO release and incubated in PRP for 2 h at 37 °C with 100 rpm shaking. Platelets adhered on film surfaces were stained with calcein-AM, which stains the cytoplasm of live cells and is converted to green fluorescent calcein. The fluorescent images were further processed and analyzed using IMAGEJ to quantify platelet coverage. As expected, significantly lower platelet adhesion was observed on PVC control, low NO flux, mid NO flux, and high NO flux films compared to PS ($p < 0.01$) (**Figure 4.4 and Figure 4.5**). PS has a tissue-culture treated surface, which is designed for platelets to adhere. High NO flux films have the least platelet adhesion. This is likely due to the increased concentration of NO, which is well known to have antiplatelet function.[49]

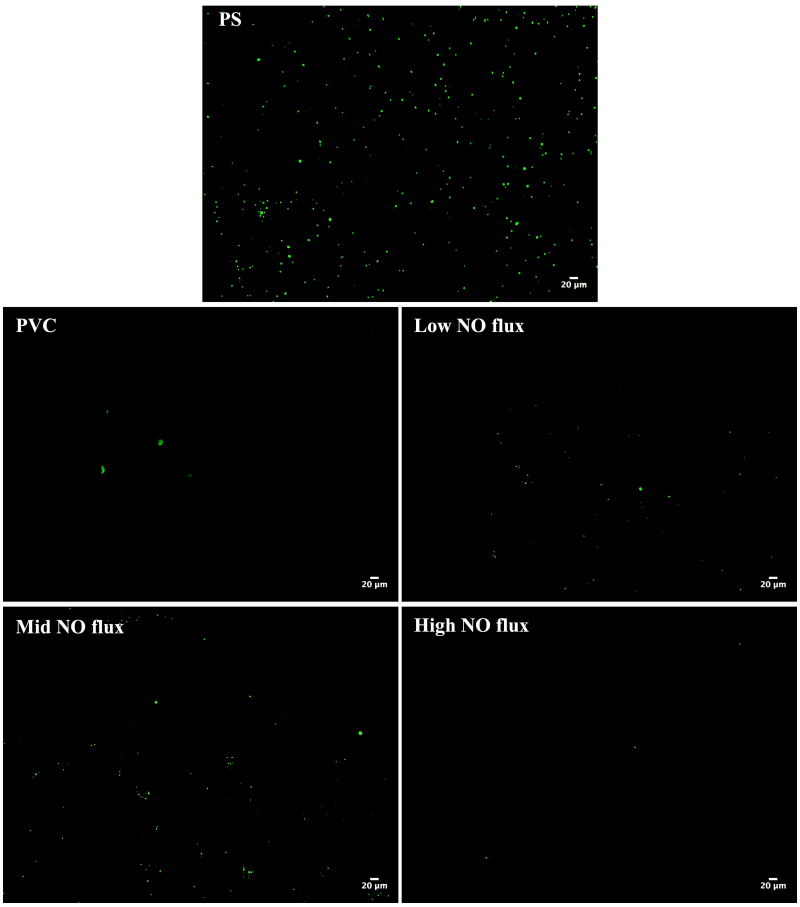

Figure 4.4 Representative (median from at least 5 samples for each group) fluorescence images of adhered platelets stained with calcein-AM on PS, PVC controls, low NO flux, mid NO flux, and high NO flux films.

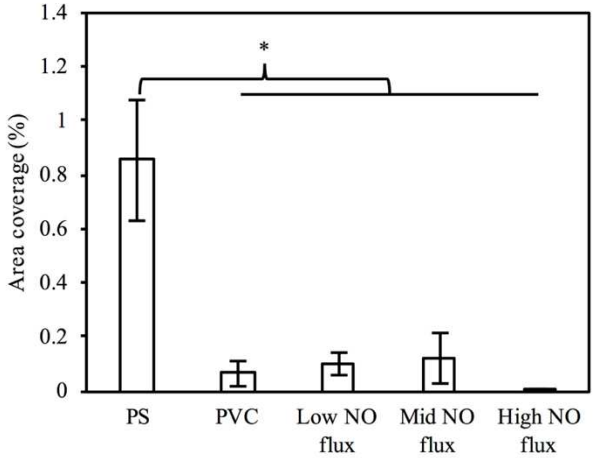

Figure 4.5 Percentage of platelet coverage was analyzed on PS, PVC control, low NO flux, mid NO flux, and high NO flux films. PS has a significant higher coverage than other groups (* indicates $p < 0.01$).

Platelet adhesion and activation were characterized qualitatively by SEM. During activation, the shape of the platelet membrane changes. Five morphologies with four levels of activation have been distinguished on implant surfaces, and each activation level has unique dendritic expression: round with no pseudopodia present (unactivated); short reversible dendritic extension with early pseudopodia (partially activated); spread dendritic extension with some pseudopodia flattening (moderately activated); almost fully flattening pseudopodia and hyaloplasmic spreading (fully activated); and fully hyaloplasmic spreading without pseudopodia present (fully activated).[50,51] (**Figure 4.6**) Control films exhibit a small amount of partially activated platelet aggregates with short dendritic extensions. Low NO flux films exhibit morphologies ranging from partially activated platelets with short dendritic extensions to fully activated platelets with fully flattening pseudopodia. This may be because of the combined effects of film surface properties and NO release. Mid NO flux films exhibit partially activated platelets with aggregation. High NO flux films have less platelets than the other groups, and the platelets are unactivated. The reduction of platelets and less activated morphology may be due to the increasing NO surface flux as previously reported. Based on these results, the high NO flux formulation was selected for further surface characterization, Fb adsorption, and blood cell interaction with pre-adsorbed Fb to determine the effect of NO on Fb.

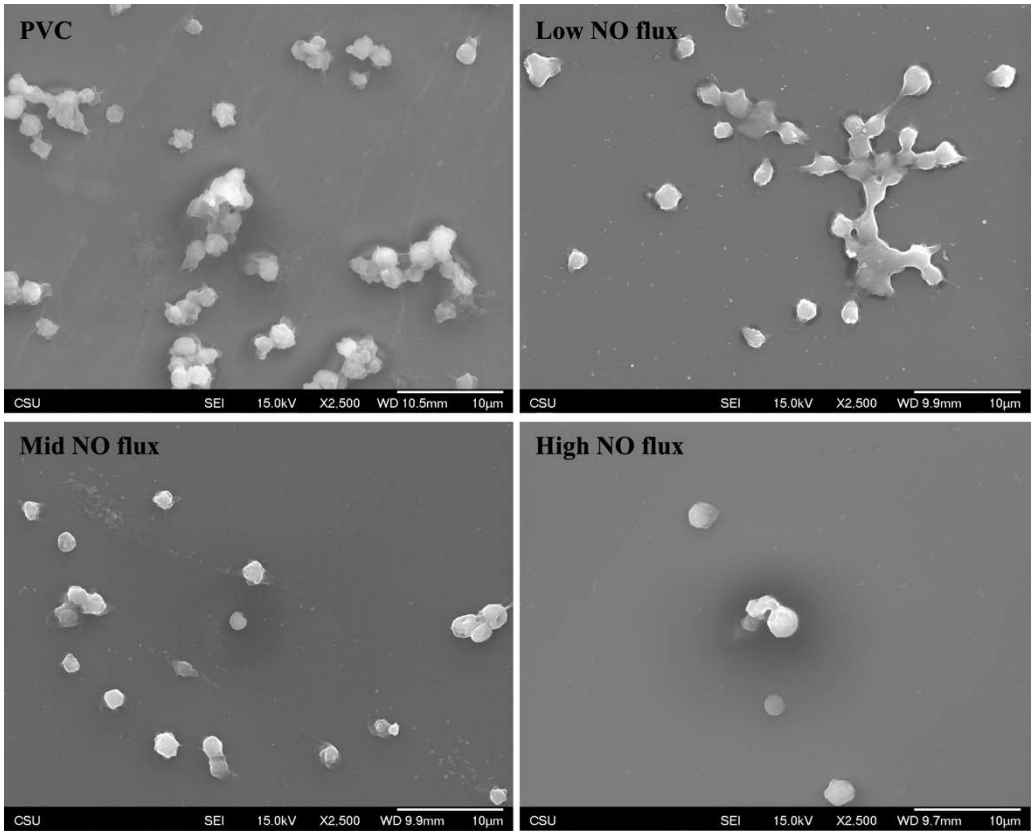

Figure 4.6 Representative SEM images of adhered cells on PVC control, low NO flux, mid NO flux, and high NO flux films.

4.3.4 Surface characterization of high NO flux films

To eliminate the potential effects of NO release on surface properties during Fb adsorption and blood cell interaction studies, high NO flux films were characterized after 1h incubation, after 5 h incubation, and after incubation until all NO was released, which covers the entire incubation period needed for this study.

For each incubation period, high NO flux films had significantly higher surface roughness than PVC control films. However, high NO flux films were found to have consistent surface roughness during the entire incubation period, as well as PVC control films (**Table 4.2**). However, high NO flux films have significantly higher roughness than PVC control films. This is due to the

settling of GSNO, which imparts a surface texture that remains detectable even after application of a polymer top coat.

The static water contact angle for both PVC control and high NO flux films showed similar wettability after 1 h incubation, 5 h incubation, and incubation until all NO was released (**Table 4.2**). Both PVC control films and high NO flux films are hydrophilic; however, the high NO flux films exhibited a greater degree of wettability ($p < 0.01$), which suggests a more hydrophilic surface than the PVC control films. These results are consistent with the Wenzel statement that adding surface roughness will enhance wettability.[52]

Table 0.2 Roughness and wettability of PVC control and high NO flux films.

Polymer films	Incubation status	Ra (nm)	Static contact angle (°)
PVC control	1 h incubation	3.9 ± 2.6	88.3 ± 0.9
	5 h incubation	7.4 ± 0.3	89.5 ± 0.6
	Incubation until all NO was released	4.9 ± 2.6	88.1 ± 0.8
High NO flux	1 h incubation	191.9 ± 36.5	85.2 ± 1.6
	5 h incubation	169.0 ± 39.1	83.2 ± 2.4
	Incubation until all NO was released	191.6 ± 26.9	85.4 ± 2.9

XPS was used to ensure surface composition does not change over the entire time period of Fb adsorption and platelet adhesion and activation. This was done by evaluating surface elemental composition of C, O, Cl, N, and S after 1 h incubation, 5 h incubation, and incubation until all NO was released. (**Figure 4.7**) The overall binding environment of PVC control and high NO flux films remains the same. This confirms that PVC control and high NO flux films have the same surface chemistry, and incubation will not affect the surface composition. To determine if

GSNO mixes with or leaches from the film surface, the high-resolution scans of S and N were evaluated. For all groups, the peaks of N 1s and S 2p to noise have average between 0 and 1, indicating no peak for N 1s and S 2p, which indicated GSNO remains under the surface of films.

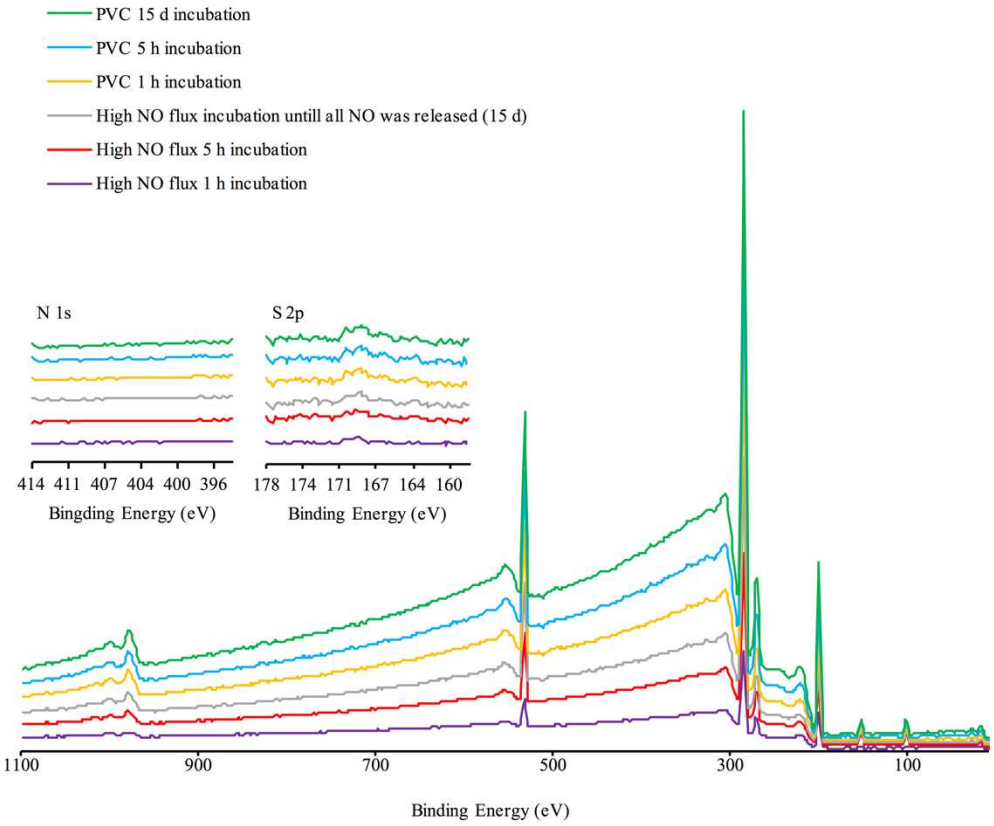

Figure 4.7 Representative survey scan of polymer film surfaces.

4.3.5 Fb adsorption on high NO flux films

Fb adsorption on films was detected and quantified using a BCA assay kit. This assay relies on the reduction of Cu^{2+} to Cu^{1+} by protein in an alkaline medium. Cu^{1+} can bind with two molecules of BCA and form a purple-colored product which can be measured at 562 nm. The amount of purple-colored product is proportional to the amount of Fb. Fb adsorbed on films can be calculated using Fb standard curves. PS is used as a negative control for Fb adsorption. PS

has a tissue-culture treated surface which is hydrophilic and has a net negative charge on the surface and is therefore not favorable for protein attachment.

To evaluate the effects of high NO flux films on Fb adsorption compared to control films, films were incubated for 1 h in PBS to reach a steady-state of NO release rate and then 2 h in Fb before use. To investigate the effects of NO-mediated pre-adsorbed Fb on platelet adhesion and activation, films with pre-adsorbed Fb that have released all NO were used to determine the amount of adsorbed Fb during the incubation period. High NO flux films have a significantly higher Fb adsorption than PS and PVC control films for both 1 h incubation and incubation until all NO was released groups ($p < 0.01$), and there is no significant difference between PS and PVC control films (**Figure 4.8**). Although PVC control films have less wettable surfaces, they are still not preferable for Fb. Since protein adsorption induces platelet adhesion and NO is known to have antiplatelet properties, a lower Fb adsorption was expected. This high Fb adsorption may be due to the surface roughness of high NO flux films which creates more surface area for Fb to bind, or this may be due to the release of NO as a previous study has shown that NO release can increase Fb adsorption on polymer films.[43]

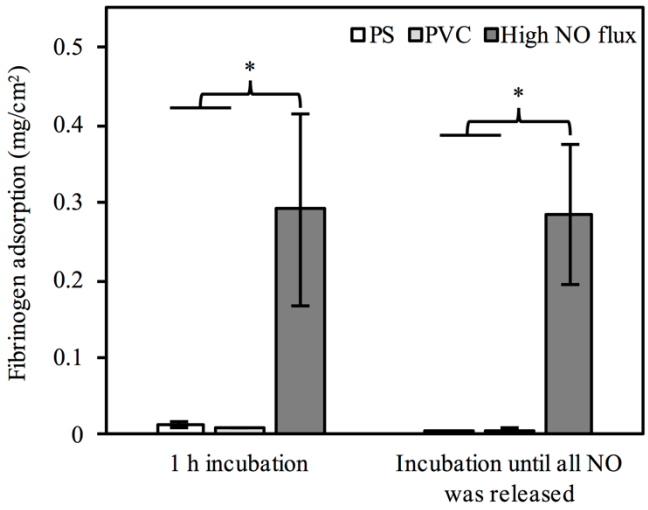

Figure 4.8 Amount of Fb adsorbed on PS, PVC control, and high NO flux films (* indicates $p < 0.01$).

To determine if the surface roughness or the NO release affects Fb adsorption, high NO flux films without NO release and high NO flux films with NO release were used. These two films were shown to have the same surface characterization in previously reported results; therefore, only NO release is anticipated to affect Fb adsorption between these two films. High NO flux films incubated until all NO was released, eliminates the effect of NO release on Fb adsorption, which isolates the effects of surface roughness. High NO flux films with NO release have the effect of both surface roughness and NO release on Fb adsorption. High NO flux films without NO release have significantly higher adsorbed Fb than PS and PVC control ($p < 0.01$), which indicates that surface roughness increases Fb adsorption (**Figure 4.9**). High NO flux films with NO release have significantly higher Fb adsorption than PS, PVC control, and high NO flux films without NO release ($p < 0.01$), which shows that NO release can significantly increase Fb adsorption. While surface roughness is clearly correlated with greater Fb adsorption, these results support that NO independently produces an increase in Fb adsorption.

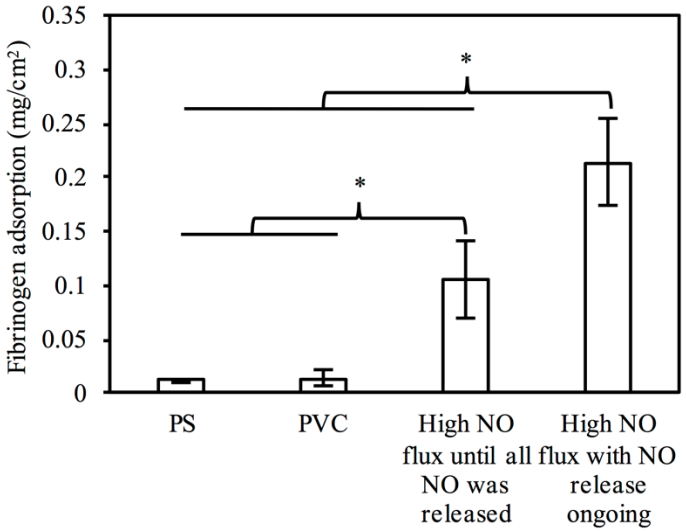

Figure 4.9 Amount of Fb adsorbed on PS, PVC control, high NO flux films without NO release, and high NO flux films with NO release ongoing (* indicates $p < 0.01$).

To determine if the surface roughness or NO release contributes more to the increase in Fb adsorption, the amount of adsorbed Fb was compared. High NO flux films without NO release exhibit Fb adsorption of 0.11 ± 0.04 mg cm^{-2} due to surface roughness, and high NO flux films with NO release have 0.21 ± 0.04 mg cm^{-2} due to both surface roughness and NO release, so the amount of Fb adsorption due to NO release is 0.10 ± 0.04 mg cm^{-2}. Therefore, surface roughness and NO release result in similar increases in Fb adsorption.

4.3.6 Blood cell interaction with high NO flux films with pre-adsorbed Fb

To determine the effects of surface roughness and the NO release on pre-adsorbed Fb, and further on platelet adhesion and activation, films were treated with Fb and incubated in PBS at 37 °C with 100 rpm shaking until all NO was released. This eliminates the direct effects of NO on platelet and activation. **Figure 4.10** shows fluorescence images of the adhered cell on PS, PVC control, and high NO flux films. As shown in **Figure 4.11**, PS has significantly higher platelet adhesion than PVC control and high NO flux films, and PVC control films have significantly higher platelet adhesion than high NO flux films. Combined with Fb adsorption results, high NO flux films are found to have the most adsorbed Fb, but have the least platelet adhesion. Platelet adhesion and activation were characterized qualitatively by SEM. PS exhibits irreversible long-dendritic extension moderately activated platelets and spreading fully activated platelets, and PVC control films exhibit small partially activated platelet aggregates and some moderately activated platelets with long dendrites (**Figure 4.12**). This is due to the pre-adsorbed Fb, which can promote platelet adhesion and activation. After extensively scanning the surfaces, fewer platelets were observed on high NO flux films.

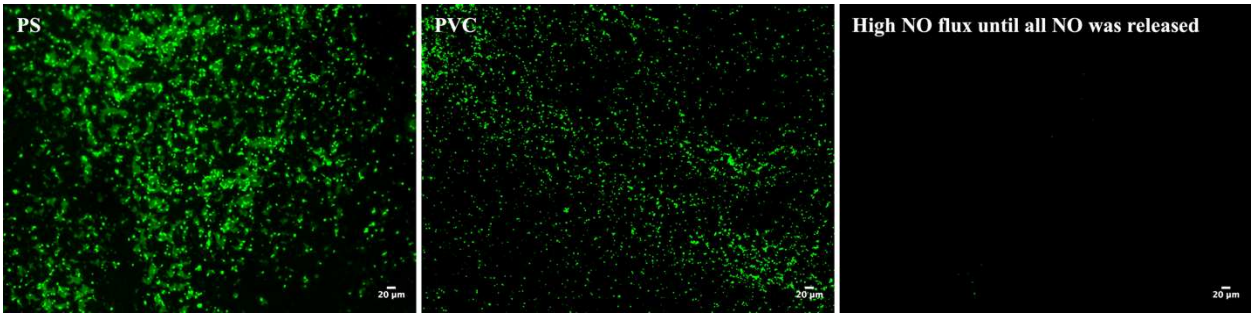

Figure 4.10 Representative (median from at least five samples for each group) fluorescence images of adhered platelets stained with calcein-AM on PS, PVC control, and high NO flux films with NO-mediated pre-adsorbed Fb.

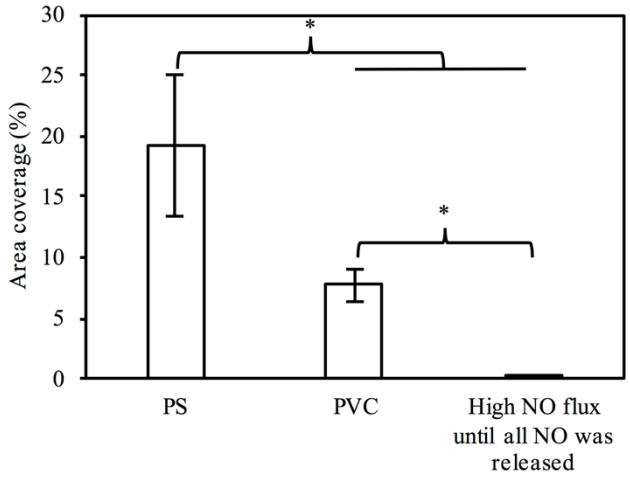

Figure 4.11 Percent coverage analysis of platelet adhered to surfaces visualized by calcein-AM staining on PS, PVC control, and high NO flux films with NO-mediated pre-adsorbed Fb. PS has a significantly high platelet adhesion than PVC control and high NO flux films, and PVC control films have a significantly higher platelet adhesion than high NO flux films (* indicates $p < 0.01$).

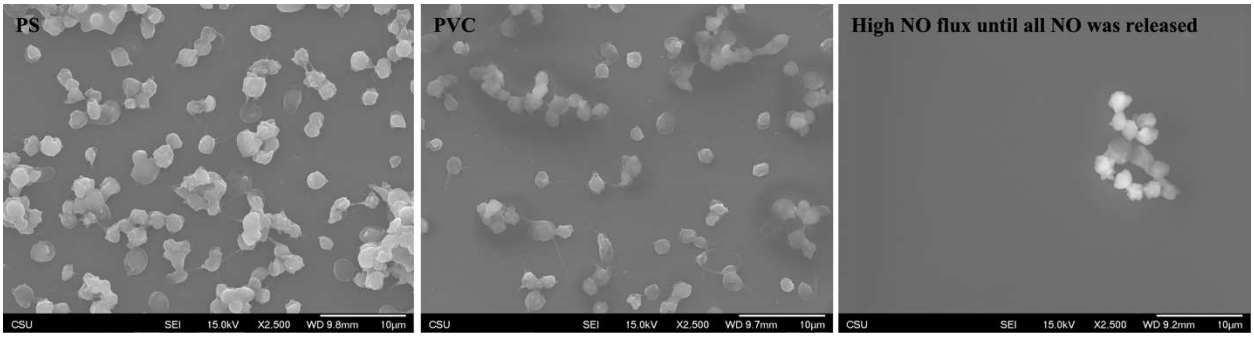

Figure 4.12 Representative SEM images of adhered platelets on PS, PVC control, and high NO flux films with NO-mediated pre-adsorbed Fb.

Since Fb is the connection between the surface of the material and platelets, the increase of Fb would presumably coincide with increased platelet adhesion.[1] Surprisingly, the results were counterintuitive. Studies have shown that surface roughness greater than 50 nm increases platelet adhesion,[53] so surface roughness is not likely to be the cause of the reduction of platelet adhesion on high NO flux films that have a measured roughness around 184.2 nm during the incubation period.

Based upon the findings of this study, NO mediates Fb binding to the surface and in turn, this NO-mediated Fb binding prevents platelet activation. While the mechanism through which NO influences Fb deposition requires further investigation, it is feasible that NO may change the Fb structure or conformation rendering the surface nonreactive to platelets. Excitingly, this is the first study to show that NO increases Fb adsorption, but still exerts its antiplatelet properties, which provides a new perspective on how NO-releasing materials can prevent platelet adhesion and activation.

4.4 Conclusions

In this work, the results have shown that constant NO surface flux with $33.2 \pm 0.7 \times 10^{-10}$ mol NO cm^{-2} min^{-1} can increase Fb adsorption, but still improves the hemocompatibility of NO-releasing polymer films by reducing the likelihood of platelet adhesion and activation. With NO-releasing surfaces, this inhibition of platelet adhesion and activation is accompanied by an increase in Fb adsorption. A greater degree of Fb adsorption has been previously theorized to induce more platelet adhesion and activation, but this study reveals the opposite outcome. Furthermore, the exposure of adsorbed Fb to NO is able to inhibit platelet adhesion and activation even in the absence of continuing NO release. It is possible that NO alters Fb conformation or structure in a manner that lowers the binding affinity to platelets. This may be a key factor in the

ability of NO-releasing synthetic materials to prevent the blood clot formation in comparison to traditional biomaterials.

REFERENCES

1. Baier RE, Dutton RC. Initial events in interactions of blood with a foreign surface. *J Biomed Mater Res*. 1969;3(1):191-206. doi:10.1002/jbm.820030115
2. Xu L-CC, Bauer JW, Siedlecki CA. Proteins, platelets, and blood coagulation at biomaterial interfaces. *Colloids Surfaces B Biointerfaces*. 2014;124:49-68.
3. Scheraga HA, Laskowski M. The Fibrinogen-Fibrin Conversion. *Adv Protein Chem*. 1957;12(C):1-131. doi:10.1016/S0065-3233(08)60115-1
4. Coughlin MA, Bartlett RH. Anticoagulation for Extracorporeal Life Support. *ASAIO J*. 2015;61(6):652-655. doi:10.1097/MAT.0000000000000273
5. Schömig A, Neumann F-J, Kastrati A, et al. A Randomized Comparison of Antiplatelet and Anticoagulant Therapy after the Placement of Coronary-Artery Stents. *N Engl J Med*. 1996;334(17):1084-1089. doi:10.1056/NEJM199604253341702
6. Brismar B, Hårdstedt C, Jacobson S, Kager L, Malmborg AS. Reduction of Catheter-Associated Thrombosis in Parenteral Nutrition by Intravenous Heparin Therapy. *Arch Surg*. 1982;117(9):1196-1199. doi:10.1001/archsurg.1982.01380330054013
7. Oliver WC. Anticoagulation and coagulation management for ECMO. *Semin Cardiothorac Vasc Anesth*. 2009;13(3):154-175. doi:10.1177/1089253209347384
8. Beiderlinden M, Treschan T, Görlinger K, Peters J. Argatroban in Extracorporeal Membrane Oxygenation. *Artif Organs*. 2007;31(6):461-465. doi:10.1111/j.1525-1594.2007.00388.x
9. Maul TM, Massicotte MP, Wearden PD. ECMO Biocompatibility: Surface Coatings, Anticoagulation, and Coagulation Monitoring. In: *Extracorporeal Membrane Oxygenation: Advances in Therapy*. InTech; 2016. doi:10.5772/63888
10. Koc Y, De Mello AJ, McHale G, Newton MI, Roach P, Shirtcliffe NJ. Nano-scale

superhydrophobicity: Suppression of protein adsorption and promotion of flow-induced detachment. *Lab Chip*. 2008;8(4):582-586. doi:10.1039/b716509a

11. Zhao J, Song L, Yin J, Ming W. Anti-bioadhesion on hierarchically structured, superhydrophobic surfaces. *Chem Commun*. 2013;49(80):9191-9193. doi:10.1039/c3cc44971h
12. Stallard CP, McDonnell KA, Onayemi OD, O'Gara JP, Dowling DP. Evaluation of protein adsorption on atmospheric plasma deposited coatings exhibiting superhydrophilic to superhydrophobic properties. *Biointerphases*. 2012;7(1-4):1-12. doi:10.1007/s13758-012-0031-0
13. Evans-Nguyen KM, Schoenfisch MH. Fibrin proliferation at model surfaces: Influence of surface properties. *Langmuir*. 2005;21(5):1691-1694. doi:10.1021/la047303h
14. Hartvig RA, van de Weert M, Østergaard J, Jorgensen L, Jensen H. Protein Adsorption at Charged Surfaces: The Role of Electrostatic Interactions and Interfacial Charge Regulation. *Langmuir*. 2011;27(6):2634-2643. doi:10.1021/la104720n
15. Tanaka M, Motomura T, Kawada M, et al. Blood compatible aspects of poly(2-methoxyethylacrylate) (PMEA)-relationship between protein adsorption and platelet adhesion on PMEA surface. *Biomaterials*. 2000;21(14):1471-1481. doi:10.1016/S0142-9612(00)00031-4
16. Malmsten M, Emoto K, Van Alstine JM. Effect of chain density on inhibition of protein adsorption by poly(ethylene glycol) based coatings. *J Colloid Interface Sci*. 1998;202(2):507-517. doi:10.1006/jcis.1998.5513
17. Amiji M, Park K. Prevention of protein adsorption and platelet adhesion on surfaces by PEO/PPO/PEO triblock copolymers. *Biomaterials*. 1992;13(10):682-692. doi:10.1016/0142-9612(92)90128-B
18. Yoshizaki T, Tabuchi N, Van Oeveren W, Shibamiya A, Koyama T, Sunamori M. PMEA

polymer-coated PVC tubing maintains anti-thrombogenic properties during in vitro whole blood circulation. *Int J Artif Organs*. 2005;28(8):834-840. doi:10.1177/039139880502800809

19. Mulvihill JN, Faradji A, Oberling F, Cazenave J-P. Surface passivation by human albumin of plasmaperesis circuits reduces platelet accumulation and thrombus formation. Experimental and clinical studies. *J Biomed Mater Res*. 1990;24(2):155-163. doi:10.1002/jbm.820240203

20. Zimmermann AK, Weber N, Aebert H, Ziemer G, Wendel HP. Effect of biopassive and bioactive surface-coatings on the hemocompatibility of membrane oxygenators. *J Biomed Mater Res Part B Appl Biomater*. 2007;80B(2):433-439. http://doi.wiley.com/10.1002/jbm.b.30614. Accessed February 6, 2020.

21. Reser D, Seifert B, Klein M, et al. Retrospective analysis of outcome data with regards to the use of Phisio®-, Bioline®- or Softline®-coated cardiopulmonary bypass circuits in cardiac surgery. *Perfusion*. 2012;27(6):530-534. doi:10.1177/0267659112454558

22. Chen L, Liu M, Bai H, et al. Antiplatelet and Thermally Responsive Poly(N -isopropylacrylamide) Surface with Nanoscale Topography. *J Am Chem Soc*. 2009;131(30):10467-10472. doi:10.1021/ja9019935

23. Sun T, Tan H, Han D, Fu Q, Jiang L. No Platelet Can Adhere—Largely Improved Blood Compatibility on Nanostructured Superhydrophobic Surfaces. *Small*. 2005;1(10):959-963. doi:10.1002/smll.200500095

24. Connors JM. Antidote for Factor Xa Anticoagulants. *N Engl J Med*. 2015;373(25):2471-2472. doi:10.1056/NEJMe1513258

25. De Vriese AS, Caluwé R, Bailleul E, et al. Dose-finding study of rivaroxaban in hemodialysis patients. *Am J Kidney Dis*. 2015;66(1):91-98. doi:10.1053/j.ajkd.2015.01.022

26. Rupprecht HJ, Blank R. Clinical pharmacology of direct and indirect factor xa inhibitors. *Drugs*. 2010;70(16):2153-2170. doi:10.2165/11538030-000000000-00000

27. Moncada S, Palmer RM, Higgs EA. Nitric oxide: physiology, pathophysiology, and pharmacology. *Pharmacol Rev*. 1991;43(2).

28. Radomski M., Palmer RM., Moncada S. Endogenous nitric oxide inhibits human platelet adhesion to vascular endothelium. *Lancet*. 1987;330(8567):1057-1058.

29. Radomski MW, Palmer RMJ, Moncada S. The role of nitric oxide and cGMP in platelet adhesion to vascular endothelium. *Biochem Biophys Res Commun*. 1987;148(3):1482-1489. doi:10.1016/S0006-291X(87)80299-1

30. Annich GM, Meinhardt JP, Mowery KA, et al. Reduced platelet activation and thrombosis in extracorporeal circuits coated with nitric oxide release polymers. *Crit Care Med*. 2000;28(4):915-920. doi:10.1097/00003246-200004000-00001

31. Simon-Walker R, Romero R, Staver JM, et al. Glycocalyx-Inspired Nitric Oxide-Releasing Surfaces Reduce Platelet Adhesion and Activation on Titanium. *ACS Biomater Sci Eng*. 2017;3(1):68-77. doi:10.1021/acsbiomaterials.6b00572

32. Radomski MW, Palmer RMJ, Moncada S. Comparative pharmacology of endothelium-derived relaxing factor, nitric oxide and prostacyclin in platelets. *Br J Pharmacol*. 1987;92(1):181-187. doi:10.1111/j.1476-5381.1987.tb11310.x

33. Brisbois EJ, Major TC, Goudie MJ, Bartlett RH, Meyerhoff ME, Handa H. Improved hemocompatibility of silicone rubber extracorporeal tubing via solvent swelling-impregnation of S-nitroso-N-acetylpenicillamine (SNAP) and evaluation in rabbit thrombogenicity model. *Acta Biomater*. 2016;37:111-119. doi:10.1016/j.actbio.2016.04.025

34. Frost MC, Rudich SM, Zhang H, Maraschio MA, Meyerhoff ME. In Vivo Biocompatibility and Analytical Performance of Intravascular Amperometric Oxygen Sensors Prepared

with Improved Nitric Oxide-Releasing Silicone Rubber Coating. *Anal Chem*. 2002;74(23):5942-5947. doi:10.1021/ac025944g

35. Zhang H, Annich GM, Miskulin J, et al. Nitric oxide releasing silicone rubbers with improved blood compatibility: preparation, characterization, and in vivo evaluation. *Biomaterials*. 2002;23(6):1485-1494. doi:10.1016/S0142-9612(01)00274-5
36. Taite LJ, Yang P, Jun H-W, West JL. Nitric oxide-releasing polyurethane–PEG copolymer containing the YIGSR peptide promotes endothelialization with decreased platelet adhesion. *J Biomed Mater Res Part B Appl Biomater*. 2008;84B(1):108-116. doi:10.1002/jbm.b.30850
37. Reynolds MM, Hrabie JA, Oh BK, et al. Nitric oxide releasing polyurethanes with covalently linked diazeniumdiolated secondary amines. *Biomacromolecules*. 2006;7(3):987-994. doi:10.1021/bm060028o
38. Fleser PS, Nuthakki VK, Malinzak LE, et al. Nitric oxide-releasing biopolymers inhibit thrombus formation in a sheep model of arteriovenous bridge grafts. *J Vasc Surg*. 2004;40(4):803-811. doi:10.1016/j.jvs.2004.07.007
39. Handa H, Major TC, Brisbois EJ, Amoako KA, Meyerhoff ME, Bartlett RH. Hemocompatibility comparison of biomedical grade polymers using rabbit thrombogenicity model for preparing nonthrombogenic nitric oxide releasing surfaces. *J Mater Chem B*. 2014;2(8):1059-1067.
40. Handa H, Brisbois EJ, Major TC, et al. Invitro and in vivo study of sustained nitric oxide release coating using diazeniumdiolate-doped poly(vinyl chloride) matrix with poly(lactide-co-glycolide) additive. *J Mater Chem B*. 2013;1(29):3578-3587. doi:10.1039/c3tb20277a
41. Parzuchowski PG, Frost MC, Meyerhoff ME. Synthesis and characterization of polymethacrylate-based nitric oxide donors. *J Am Chem Soc*. 2002;124(41):12182-12191. doi:10.1021/ja020268l

42. Zhou Z, Meyerhoff ME. Polymethacrylate-based nitric oxide donors with pendant N-diazeniumdiolated alkyldiamine moieties: Synthesis, characterization, and preparation of nitric oxide releasing polymeric coatings. *Biomacromolecules*. 2005;6(2):780-789. doi:10.1021/bm049462l

43. Lantvit SM, Barrett BJ, Reynolds MM. Nitric oxide releasing material adsorbs more fibrinogen. *J Biomed Mater Res - Part A*. 2013;101(11):3201-3210. doi:10.1002/jbm.a.34627

44. Vaughn MW, Kuo L, Liao JC. Estimation of nitric oxide production and reaction rates in tissue by use of a mathematical model. *Am J Physiol - Hear Circ Physiol*. 1998;274(6 43-6). doi:10.1152/ajpheart.1998.274.6.h2163

45. Major TC, Brant DO, Reynolds MM, et al. The attenuation of platelet and monocyte activation in a rabbit model of extracorporeal circulation by a nitric oxide releasing polymer. *Biomaterials*. 2010;31(10):2736-2745. doi:10.1016/j.biomaterials.2009.12.028

46. Hart TW. Some observations concerning the S-nitroso and S-phenylsulphonyl derivatives of L-cysteine and glutathione. *Tetrahedron Lett*. 1985;26(16):2013-2016. doi:10.1016/S0040-4039(00)98368-0

47. Williams DLH. The chemistry of S-nitrosothiols. *Acc Chem Res*. 1999;32(10):869-876. doi:10.1021/ar9800439

48. Kratz F, Grass S, Umanskaya N, et al. Cleaning of biomaterial surfaces: Protein removal by different solvents. *Colloids Surfaces B Biointerfaces*. 2015;128:28-35. doi:10.1016/j.colsurfb.2015.02.016

49. Skrzypchak AM, Lafayette NG, Bartlett RH, et al. Effect of varying nitric oxide release to prevent platelet consumption and preserve platelet function in an in vivo model of extracorporeal circulation. *Perfusion*. 2007;22(3):193-200. doi:10.1177/0267659107080877

50. Goodman SL, Grasel TG, Cooper SL, Albrecht RM. Platelet shape change and cytoskeletal reorganization on polyurethaneureas. *J Biomed Mater Res*. 1989;23(1):105-123. doi:10.1002/jbm.820230109

51. Ko T-M, Cooper SL. Surface properties and platelet adhesion characteristics of acrylic acid and allylamine plasma-treated polyethylene. *J Appl Polym Sci*. 1993;47(9):1601-1619. doi:10.1002/app.1993.070470908

52. Wenzel RN. Resistance of solid surfaces to wetting by water. *Ind Eng Chem*. 1936;28(8):988-994. doi:10.1021/ie50320a024

53. Linneweber J, Dohmen PM, Kerzscher U, Affeld K, Nosé Y, Konertz W. The Effect of Surface Roughness on Activation of the Coagulation System and Platelet Adhesion in Rotary Blood Pumps. *Artif Organs*. 2007;31(5):345-351. doi:10.1111/j.1525-1594.2007.00391.x

CHAPTER 5

METAL–ORGANIC FRAMEWORK POLYMER COATING ON EXTRACORPOREAL LIFE SUPPORT COMPONENTS AND ITS ANTIBACTERIAL ATTACHMENT PERFORMANCE[3]

5.1 Introduction

Extracorporeal life support (ECLS) has been used as a life-saving therapy to replace organ function for trauma patients and combat casualties with acute lung failure or severe heart and/or lung injuries.[1,2] Currently, both U.S. civilian and military hospitals are seeking the establishment of standardized ECLS protocols. However, thrombosis, thrombocytopenia or even hemorrhage, and infection are the major challenges that impede early initiation and wider utilization of ECLS.

Initiation of the coagulation cascade occurs due to interaction between blood components (e.g., blood serum proteins and platelets) and ECLS material surfaces (e.g., oxygenation fibers and circulation tubing). When human whole blood comes into contact with ECLS material surfaces, blood will respond to the material surface as a foreign body and trigger immune responses. Within seconds to minutes, blood serum proteins such as fibrinogen and albumin will adsorb to the material surface and induce platelet adhesion. Adsorbed fibrinogen will be converted into fibrin clots in the presence of thrombin, inducing further platelet adhesion, platelet activation and

[3] Part of the following work was adapted with permission from Zang Y, Roberts TR, Batchinsky AI, Reynolds MM. Metal-Organic Framework Polymer Coating Inhibits *Staphylococcus aureus* Attachment on Medical Circulation Tubing under Static and Dynamic Flow Conditions. *ACS Appl. Bio Mater.* 2020;XXXX,XXX,XXX-XXX. H_3BTTri synthesis and characterization were performed by Jonathan Thai. ICP-AEC analysis was performed by the Soil, Water and Plant Testing Laboratory at Colorado State University. All other experiments were performed by Yanyi Zang. Dr. Patrick McCurdy and Dr. Roy Geiss from Central Instrument Facility at Colorado State University assisted scanning electron microscopy. Dr. Alec Lutzke assisted in preparation for the manuscript. This work was funded by the Assistant Secretary of Defense for the Health Affairs endorsed by the Department of Defense through the Peer Reviewed Medical Research Program – Technology/Therapeutic Development Award, under Grant number W81XWH-18-2-0048.

platelet aggregation. After several hours, blood clots will form on the surface. Without effective and proper intervention, blood clot formation will lead to the failure of ECLS.[3]

Several strategies have been used to prevent medical device-induced thrombosis. Anticoagulants such as heparin are commonly administered during ECLS procedures. However, anticoagulants increase the risk of hemorrhage, especially for patients who already have severe bleeding injuries. Commercially available heparinized ECLS is another approach. The limitation of heparinized surfaces is that their inhibitory effects may not be enough to compensate for the coagulative activation that results from the foreign reaction with the artificial surface.[4] Polymer coatings that release nitric oxide (NO) have also shown a promising ability to inhibit platelet activation and aggregation.[5–7] However, none of these studies have been performed using a full ECLS circuit (circulation tubing, catheters, and membrane lung) under conditions that simulate clinical ECLS applications for trauma patients and lack sufficient information for further coating development. There is an urgent need to seek new surface treatment to prevent thrombus formation and reduce the use of anticoagulants.

Among all ECLS components, blood-contacting circulation tubing used in hemodialysis and other forms of extracorporeal organ support has a large surface area that permits the attachment and spread of bacteria. This significant foreign-surface exposure that occurs during extracorporeal organ support places these patients at an elevated risk of bacterial infection. For example, instances of nosocomial infection in chronic hemodialysis patients were significantly higher than patients who did not require chronic hemodialysis but were hospitalized for the same duration.[8] Additionally, in adult patients requiring extracorporeal pulmonary support for >14 days, instance of nosocomial infection (52%) was significantly higher than patients requiring support for <7 days (13%).[9] These findings emphasize the need for antibacterial materials for extracorporeal organ support with sufficient stability and longevity of function for the duration of therapy required.

Medical device-associated bacterial infection involves multiple strains of bacteria. However, *Staphylococci aureus* (*S. aureus*) is one of the most virulent, common organisms isolated from infected implanted medical devices.[10] Specific to hemodialysis, *S. aureus* was selected as it is the leading cause of access infections and bacteremia.[11,12] For example, a prospective single center study reported that 40% of hemodialysis patients were *S. aureus* carriers versus 27% in the general population.[13] A major contributing factor in the prevalence of *S. aureus* infections is their unique ability to attach to surfaces and develop into a biofilm.[14,15] The removal of the medical device and antibiotic treatments are the two most common methods for prevention or mitigation of medical device-associated bacterial infections. Unfortunately, the removal of a device requires urgent replacement for long-term applications and is sometimes impossible because the patient relies on its performance to survive.[16] Antibiotics can be provided by oral or intravenous administration, through the use of antibiotic releasing-medical devices or other approaches. Regrettably, antibiotic resistance has been recognized as one of the biggest public health challenges facing the world and effectively voids the use of current antibiotic treatments.[17] These disadvantages have necessitated the development of new methods to combat medical device-associated bacterial attachment. Antibacterial drug delivery systems have been widely developed for wound healing, surgeries, and water disinfection applications. For example, silver has been regarded as the “antimicrobial gold standard” when used in antibacterial applications.[18,19] However, silver-based treatments have caused allergic reactions in some individuals, creating toxicity concerns for silver and silver-derived products.[20] Surface modification can also confer antibacterial properties to medical devices. For example, superhydrophobic surfaces and micropatterned surfaces have shown promising antibacterial properties.[21–30] Unfortunately, the majority of studies that assess the antibacterial properties of these modified surfaces have used substrates that were not commercial medical devices or were performed

under static or shaking conditions that do not simulate the blood flow rate and shear conditions that occur during clinical use, providing insufficient information for medical device development.

One alternative approach is to use metal–organic frameworks (MOFs) in polymer coatings to confer antibacterial function to medical tubing under dynamic flow conditions. MOFs are hybrid high-porosity crystalline structures containing metal centers and organic linkers. Various MOFs have been widely utilized as gas-storage/-separation agents and catalysts.[31,32] Recently, increased understanding of the biological effects of MOFs has led to interest for medical applications. For example, water-unstable copper-based MOFs have been shown to inhibit *S. aureus* and *Escherichia coli (E. coli)* activity on polymeric substrates such as silk and cotton fibers with the observed effects attributed to the release of copper ions.[33,34] Water-stable copper-based MOF/polymer films have also been seen to inhibit bacterial attachment but without significant degradation and release of copper ions.[35,36]

In this study, we report the first custom-designed coating process for application of a water-stable copper-based MOF, CuBTTri ($H_3[(Cu_4Cl)_3(BTTri)_8]$ where H_3BTTri = 1,3,5-tris(1*H*-1,2,3-triazol-5-yl)benzene), to standard seven-foot-long extracorporeal circulation tubing. The CuBTTri coating was characterized using optical profilometry for coating roughness, scanning electron microscopy (SEM) for coating thickness and CuBTTri distribution, and SEM coupled with energy-dispersive X-ray spectroscopy (SEM-EDS) for copper content analysis. The coating stability was examined by inductively coupled plasma-atomic emission spectroscopy (ICP-AES) for copper release after 24 h incubation. SEM was used to assess changes to the coating morphology after circulating phosphate-buffered saline (PBS) with a 300 mL min^{-1} flow rate for 24 h. We also report the first bacterial attachment study of CuBTTri-coated 0.25 in inner diameter (ID) medical tubing with a 300 mL min^{-1} flow rate. Our study simulates the blood flow rate utilized during hemodialysis, a procedure used to replace kidney function via removal of metabolites and water from blood. Bacterial attachment studies were carried out by circulating a *S. aureus*

suspension in both CuBTTri-coated medical tubing and uncoated controls for 24 h under static and dynamic flow conditions. This is the first report of a successful application of a MOF coating to seven-foot-long medical tubing, a length commonly used in hemodialysis and circuitry for other forms of extracorporeal organ support. The bacterial results demonstrate for the first time that *S. aureus* attachment was reduced by 52 ± 15% (static conditions) and 53 ± 29% (dynamic conditions) on the CuBTTri-coated tubing compared to uncoated controls, and *S. aureus* attachment was reduced by 52 ± 12% (CuBTTri coating) and 52 ± 30% (uncoated controls) under dynamic flow compared to static conditions.

5.2 Materials and methods

5.2.1 Materials

All chemicals and solvents were purchased from commercial vendors and used without further purification unless otherwise noted. Plasticizer-free Tygon® ND-100-65 medical tubing (1/4 inch ID) was purchased from Saint Gobain (Courbevoie, France). Tecophilic® polyurethanes were purchased from Lubrizol (SP-80A-150, SP-60D-60; Wickliffe, OH, USA). PBS tablets was purchased from VWR (Radnor, PA, USA). 1,3,5-Triethynylbenzene (98%), trimethylsilylazide ($(CH_3)_3SiN_3$, 94%), copper(II) chloride dihydrate ($CuCl_2{\cdot}2H_2O$, >99%), and m-cresol (99%) were purchased from Alfa Aesar (Ward Hill, MA, USA). Copper(I) iodide (CuI, 99.5%) was purchased from Sigma-Aldrich (St. Louis, MO, USA). Methanol, *N,N*-dimethylformamide (DMF), tetrahydrofuran (THF), 50 mL conical tubes, microcentrifuge tubes, nutrient broth medium (NBM), and nutrient agar were purchased from Fisher Scientific (Hampton, NH, USA). Dopamine hydrochloride (>98%) was purchased from Tokyo Chemical Industry (Tokyo, Japan). Diethyl ether was purchased from EMD Millipore (Burlington, MA, USA). *S. aureus* was purchased from ATCC (Manassas, VA, USA). Deionized water (18.2 MΩ·cm) (H_2O) was prepared using a Millipore Direct-Q5 ultrapure water purification system purchased from EMD Millipore (Burlington, MA,

USA). Raumedic ECC noDOP® tubing, Avalon Elite® Bi-Caval Dual Lumen Catheters (Avalon catheters), OriGen Reinforced Dual Lumen VV Catheters (OriGen catheters), and BIOLINE coated membrane oxygenation fibers in the Getinge HLS Set Advance (membrane oxygenation fibers) were provided by Dr. Andriy I. Batchinsky from The Geneva Foundation (Tacoma, WA, USA). *S*-nitrosoglutathione (GSNO) was synthesis and characterized based on previously reported methods.[36] Characterization data of GSNO that match reported value were used in this study.[36]

5.2.2 CuBTTri synthesis and characterization

The ligand, 1,3,5-tris(1*H*-1,2,3-triazol-5-yl)-benzene (H_3BTTri), was synthesized using a simplified method adapted from literature.[37] Briefly, 1,3,5-triethynylbenzene (5.3 g , 35.29 mmol), and CuI (1.011 g, 5.31 mmol) were measured out. A solvent system of DMF (180 mL) and methanol (20 mL) was then added under nitrogen. Then, $(CH_3)_3SiN_3$ (21 mL, 158.95 mmol) was added into the above mixture. The reaction was heated at 100 ° C for at least 36 h. Once collected, the filtrate was concentrated to approximately 10 mL with rotary evaporation. After concentration, 30 mL of H_2O was added to the filtrate to produce a pale green precipitate. The resulting pale green precipitate was filtered through a coarse porosity fritted glass funnel under vacuum and washed with 500 mL of H_2O followed by 500 mL of diethyl ether. The final product was dried under vacuum overnight and characterized by proton nuclear magnetic resonance spectroscopy (^{1}H NMR) and time-of-flight mass spectrometry (TOFMS). CuBTTri synthesis followed a method from the same paper.[37] H_3BTTri (1.2375 g, 5.1535 mmol) was suspended into 220 mL DMF and sonicated for 1 h. $CuCl_2{\cdot}2H_2O$ (2.1065 g, 12.36 mmol) was added into the mixture and shaken until fully dissolved. CuBTTri-DMF, a dark purple precipitate, was formed after the mixture was heated to 100 ° C for 72 h. CuBTTri-DMF was filtered using a fine porosity fritted glass funnel under vacuum and washed with 150 mL of 100 ° C DMF and 150 mL of 85 ° C H_2O. Then,

CuBTTri-DMF was heated in H_2O at 95 ° C for 5 days with H_2O being changed every 24 h to replace DMF with H_2O. The resulting product CuBTTri, a light purple solid, was dried using reduced pressure and characterized using attenuated total reflectance-Fourier transform infrared spectroscopy (ATR-FTIR) and powder X-ray diffraction (pXRD). H_3BTTri and CuBTTri that matched reported characterization values were used in this study.[37]

5.2.3 Circulation tubing coating and characterization

Colored Tygon® polymer solution preparation. 1.0 g of Tygon® ND-100-65 medical tubing was added into 10 mL of THF to form 10 w/v % Tygon® polymer solution. Before the coating process, 10 w/v % Tygon® polymer solution was diluted to1 w/v % using THF and mixed with green dye to form a colored Tygon® polymer solution. The volume ratio of 1 w/v % Tygon® polymer solution to green dye was 10 to 1.

CuBTTri coating solution preparation. Tygon® tubing pieces (approximately 1/4 inch length with 0.125 inch width) were cut from Tygon® ND-100-65 medical tubing. Tygon® tubing pieces were added into THF and stirred overnight at room temperature until fully dissolved to form Tygon® polymer solution. Two methods were used to process CuBTTri into Tygon® polymer solution. The first method was adding CuBTTri directly into Tygon® polymer solution and sonicated the mixture for 1 h to form CuBTTri coating solution. The second method was mixing CuBTTri into THF to form CuBTTri solution and sonicated the mixture for 1 h. After sonication, CuBTTri solution was gently added into Tygon® polymer solution while stirring and sonicated for another 1 h to form CuBTTri coating solution. The formulation of CuBTTri coating solution was shown in **Table 5.1**.

Table 5.1 Composition of tubing CuBTTri coating solution.

Tygon® (g)	CuBTTri (g)	THF (ml)	Concentration of Tygon® in coating solution (w/v %)	Concentration of CuBTTri in coating solution (w/v %)
0.16	0.016	16	1.0	0.1
0.16	0.08	16	1.0	0.5

0.16	0.16	16	1.0	1.0
0.16	0.8	16	1.0	5.0

Tubing coating process 1. The coating process is shown in **Figure 5.1**. Approximately one-foot-long middle section of a night-foot-long tubing was inserted into the head of a peristaltic pump. Half-foot-long tubing from each end of the eight-foot-long tubing was inserted into 50 mL of colored Tygon® polymer solution. The colored Tygon® polymer solution was circulated in the tubing via peristaltic pump at 300 mL min^{-1}. After coating, tubing sections merged inside the polymer solution were removed, and the remaining coated eight-foot-long tubing was dried in the fume hood.

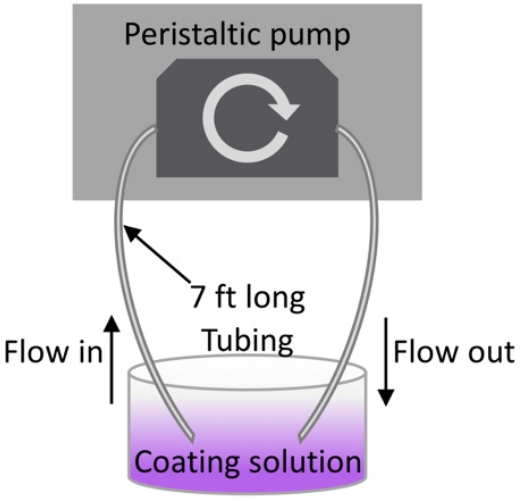

Figure 5.1 Tubing coating process 1.

Tubing coating process 2. Two-foot-long tubing sample in pump head was connected two seven and half-foot-long tubing on each end in Design 2 as shown in **Figure 5.2**. Half-foot-long tubing from each of the seven and half-foot-long tubing was merged into 50 mL of colored Tygon® polymer solution. After coating, tubing sections in the polymer solution were removed and two coated seven-foot-long tubing were disconnected from the tubing sample in pump head. The coated tubing were dried in fume hood.

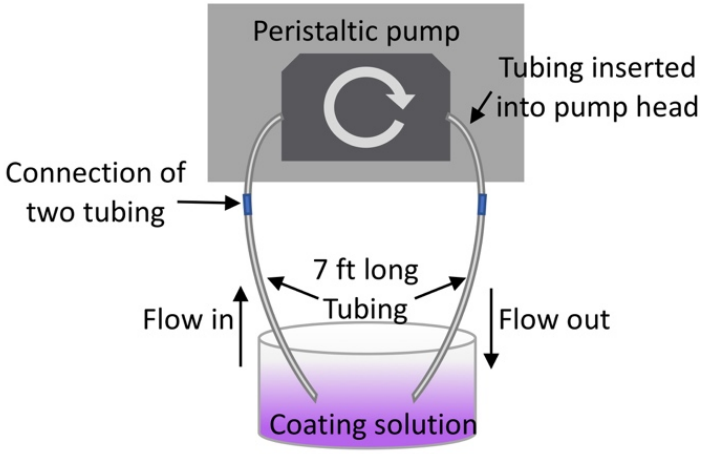

Figure 5.2 Tubing coating process 2.

Tubing coating process 3. A two-foot-long tubing sample was inserted into the pump head and connected to the seven-foot-long tubing using connector as shown in **Figure 5.3**. The end of seven-foot-long tubing was inserted into colored Tygon® polymer solution, and the end of two-foot-long tubing sample was inserted into waste coating solution container. 16 mL of colored Tygon® polymer solution was pumped through the tubing. After coating process, the seven-foot-long tubing was disconnected from the two-foot-long tubing sample and dried in fume hood.

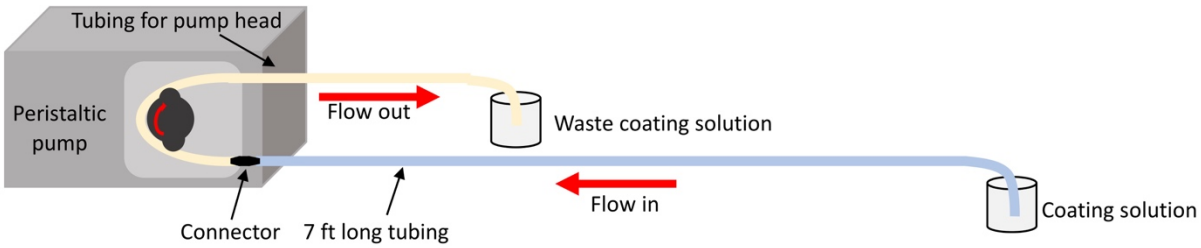

Figure 5.3 Tubing flow loop coating process 3.

Tubing coating process 4. The seven-foot-long tubing was adhered onto a stainless steel rod using parafilm as shown in **Figure 5.4**. The seven-foot-long tubing was then connected with two-foot-long tubing using parafilm on top of tape. 16 mL of colored Tygon® polymer solution passed through the tubing via the peristaltic pump. After coating, the coated seven-foot-long tubing was disconnected from the two-foot-long tubing and rod before dried in the fume hood.

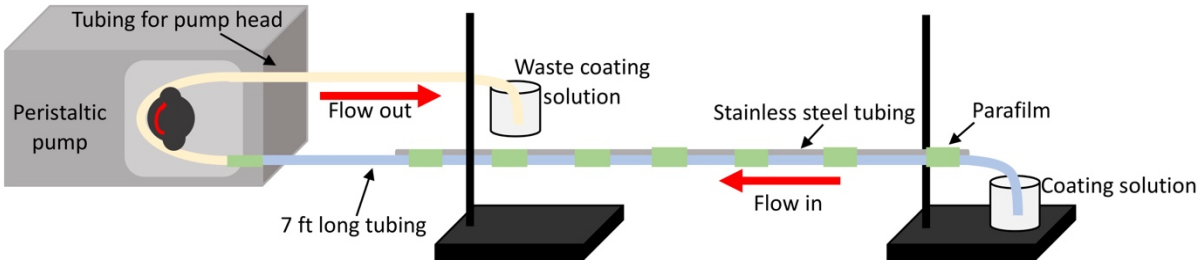

Figure 5.4 Tubing flow loop coating process 4.

Tubing coating process 5. The stainless steel rod was connected to a mechanical rotator with a slope angle of 30° as shown in **Figure 5.5**. 20 mL of colored Tygon® polymer solution was manually added into one end of the tubing with a rotation speed at 65 rpm. After coating, the tubing was disconnected from the rod and dried in fume hood.

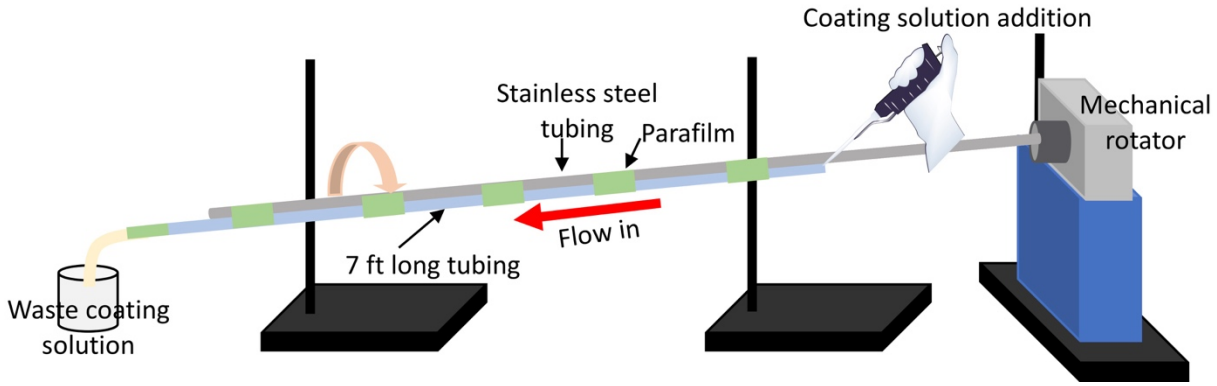

Figure 5.5 Tubing flow loop coating process 5.

Tubing coating process 6. One end of the seven-foot-long tubing was connected to a two-foot-long tubing using a swivel connector and adhered to the stainless steel rod using parafilm as shown in **Figure 5.6**. The open end of the two-foot-long tubing was inserted into the colored Tygon® polymer solution. The two-foot-long tubing was inserted into the pump head. The rod was connected to a mechanical rotator. 16 mL of colored Tygon® polymer solution was moved through the tubing while the tubing was rotated at 65 rpm.

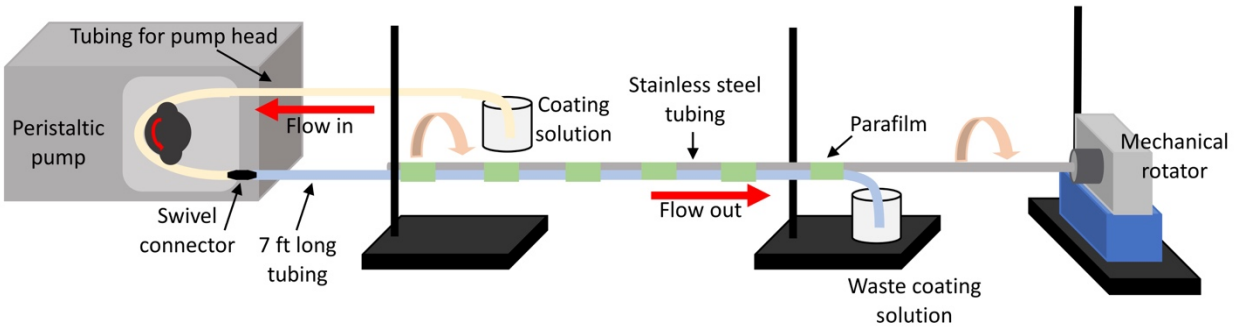

Figure 5.6 Tubing flow loop coating process 6.

Tubing coating process 7 (successful). The coating process is shown in **Figure 5.7**. One end of the seven-foot-long tubing segment was connected to a two-foot tubing segment for connection with a peristaltic pump. An additional four-inch tubing segment was connected on the opposite end for insertion into a vial of the coating solution. 16 mL of CuBTTri coating solution was pumped from one end of the tubing to the other end via a peristaltic pump at 900 mL min^{-1} (**Figure 5.7a**). The coated tubing was then rotated on a mechanical rotator at 65 rpm for 10 min to ensure coating uniformity (**Figure 5.7b**). Finally, the coated tubing was placed under vacuum (~0.05 Torr) for 48 h to remove residual solvent.

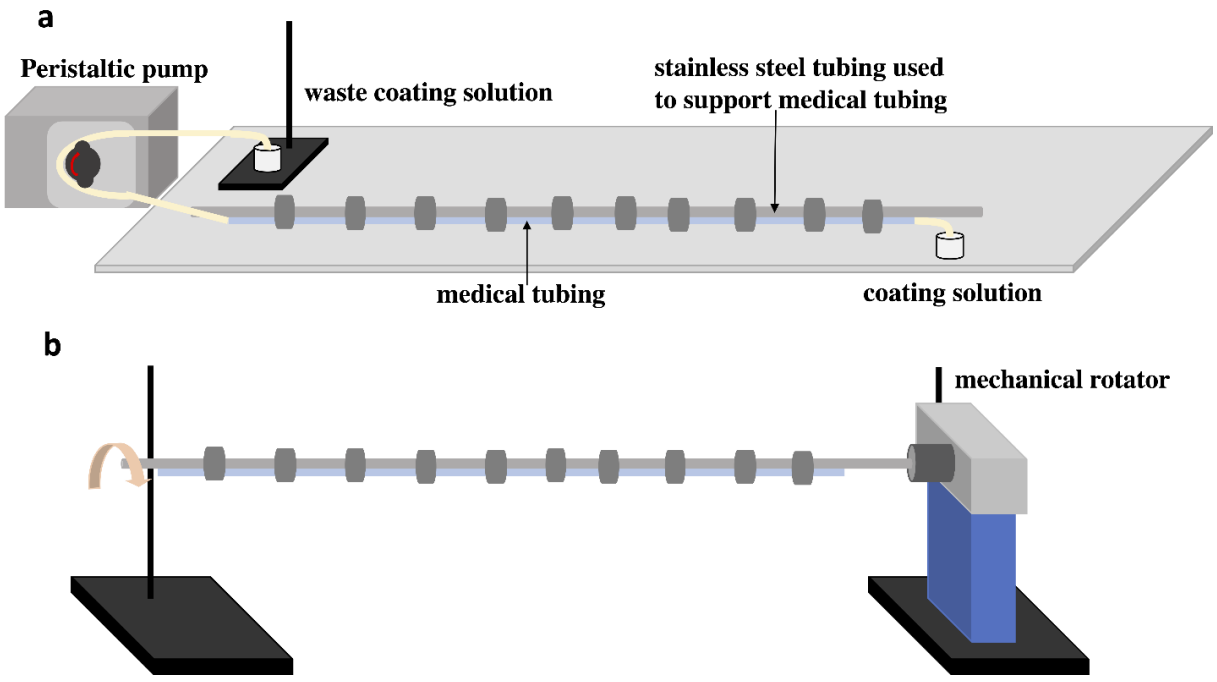

Figure 5.7 Tubing flow loop coating process 7. (a) A peristaltic pump was used to pump the coating solution from one end of the tubing to the other end. (b) A mechanical rotator was used to create uniform coating.

Coating catalytic property evaluation before and after sterilization by nitric oxide analyzer (NOA). To remove potential copper ions in the PBS solution, one PBS tablet was dissolved in 100 mL of water containing 0.1g Chelex resin and sit for two days. After two days, resin was removed through centrifugation. The resulting PBS solution (pH = 7.4) was used for NO generation study. The ethylene oxide sterilization was performed with the help from Dr. Jeremiah Easley (Department of Clinical Sciences, Colorado State University, Fort Collins, CO, USA). The amount of NO generation promoted by CuBTTri coating was measured via NOA using previously reported methods.[38] 2 cm CuBTTri-coated tubing was immersed into 5 mL of water containing 10 μM of GSNO at 37 °C until the amount of NO was not detectable. Control experiments were performed with 10 μM of GSNO in 5 mL of water in the absence of tubing and were performance with 2 cm uncoated tubing in water without GSNO. All experiments were protected from light. The data points were collected at 15 intervals until NO signal was not detectable (n = 3).

Surface roughness by optical profilometer. Before characterization, the seven-foot-long CuBTTri-coated medical tubing was cut into seven one-foot segments as shown in **Figure 5.8** using titanium-bonded non-stick scissors. The average surface roughness (Ra) of coated tubing was measured on three locations at each length interval by optical profilometer (Zygo Corporation, Middlefield, CT, USA). The measurements were taken from central rough scan of a square 0.3 mm × 0.3 mm at 20x magnification with a frontier filter applied. Measurements were done on three different spots from each segment and three different tubing samples were used (n = 3).

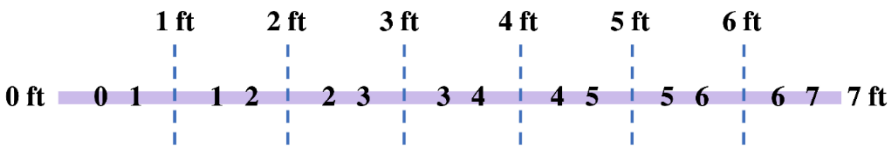

Figure 5.8 Sampling schematic of seven-foot-long CuBTTri-coated medical tubing for coating surface characterization. Seven segments were sliced before characterization. The numbers on the tubing corresponded to measured length point.

Coating thickness and CuBTTri distribution by SEM. Coating thickness was measured by JEOL JSM-6500F SEM using 5 kV with 1500x magnification. CuBTTri particle distribution was visualized by SEM using 10 kV with 100x, 1000x, and 10000x magnification. The sample surfaces were sputter-coated with 20 nm of gold before imaging. All measurements and images were obtained on three different spots from each tubing sample and three different seven-foot-long tubing pieces were used (n = 3).

Copper content analysis by SEM-EDS. Copper content was analyzed by JEOL JSM-6500F SEM-EDS using 2 and 10 kV with 100x magnification. All measurements were obtained on two different spots from each tubing sample and three different seven-foot-long tubing pieces were used (n = 3).

Coating stability (determination of CuBTTri degradation) by ICP-AES. Copper ion concentration from CuBTTri degradation in the coating was examined by immersing 2 cm length CuBTTri-coated medical tubing samples into 5 mL PBS at room temperature for 24 h. The following day, tubing samples were removed from PBS and the solution was diluted five times before the copper concentration was measured using ICP-AES (n = 3).

Coating stability (morphology change) by SEM. Coating morphology changes after flow were visualized by SEM. A custom-designed flow system shown in **Figure 5.9** was used to circulate PBS in the tubing. The CuBTTri-coated medical tubing was cut into six-inch-long segments from four different seven-foot-long CuBTTri-coated medical tubing segments. The coated tubing pieces were connected to one and half-foot-long tubing on each end; one end was inserted into the peristaltic pump and the other end was inserted into PBS. The PBS was pumped from one end to the other end. All experiments were performed for 24 h at room temperature in

the absence of bubbles in the tubing with a 300 mL min^{-1} flow rate which simulates a typical blood flow rate utilized for hemodialysis. After 24 h, tubing samples were dried under vacuum after removing PBS. The coating morphology was visualized by SEM using 10 kV with 10000x magnification before and after 24 h flow. The sample surfaces were sputter-coated with 20 nm of gold before imaging. All images were obtained on three different spots from each tubing sample and four different tubing samples were used (n = 4).

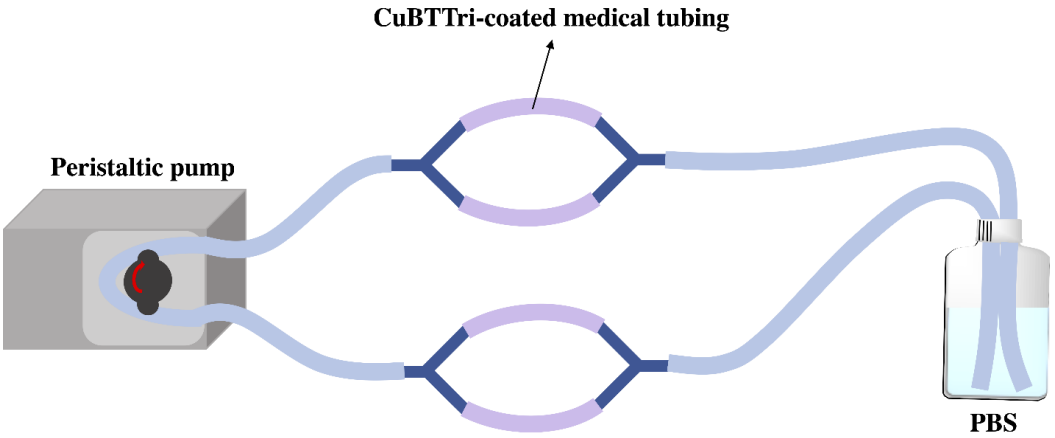

Figure 5.9 Schematic of the custom flow system for CuBTTri stability study under dynamic flow conditions. (For bacterial attachment study, PBS was replaced by *S. aureus* solution).

5.2.4 Avalon catheter coating and characterization

Evaluation the compatibility between Avalon Catheter polymer and various solvents. Acetone, diethyl ether, and methanol were used to dissolve Avalon Catheter samples. The compatibility between Avalon Catheter polymer and each of the solvents was evaluated by visual inspection.

Nonaqueous turbidimetric titration test. The turbidity of solvent having no/minimum effect to Avalon Catheter sample were tested in 1.0 w/v % Avalon Catheter polymer solution via a nonaqueous turbidimetric titration method. 0.13 g of Avalon Catheter was added into 13 mL of THF and stirred overnight at room temperature until fully dissolved to form 1 w/v % Avalon Catheter polymer solution. 5 mL of the polymer solution was transferred into a 15 mL beaker and

stirred. Methanol was added dropwise into the beaker until the mixture became turbid. The volume of methanol used during the test was recorded.

CuBTTri coating solution preparation. 1 g of Avalon Catheter was dissolved in 20 mL THF to form a 5 w/v % of polymer solution. 0.4 g of CuBTTri was added into 32 mL of THF and sonicated for 1 h to for 1.25 w/v % CuBTTri solution. 8 mL of polymer solution and 32 mL of CuBTTri solution were added into 160 mL of THF. The mixture was sonicated for 1 h. After sonication, 200 mL of methanol was added into the mixture dropwise and sonicated for 1 h to form CuBTTri coating solution.

Avalon Catheter coating method. The custom-designed dip-coating process was shown in **Figure 5.10**. Briefly, Avalon catheter was hung on a stainless steel rod. The rod was inserted into a mechanical rotator so that the catheter could be moved up and down at 65 rpm. After dip-coating, the catheter was dried in the fume hood for two days and then dried under vacuum for 3 days.

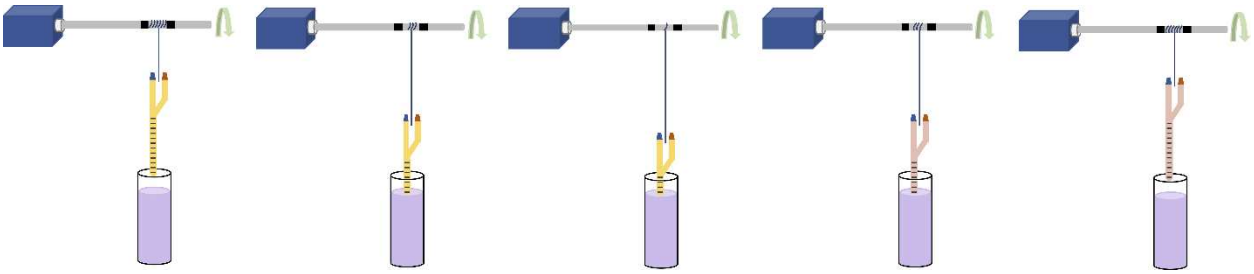

Figure 5.10 Avalon catheter dip-coating process.

Coating catalytic property evaluation before and after sterilization by nitric oxide analyzer (NOA). Same sample preparation and experimental process were performed as “coating catalytic property evaluation before and after sterilization by nitric oxide analyzer (NOA) in **1.2.3**.

5.2.5 OriGen catheter coating

Evaluation of compatibility between OriGen Catheter polymer and various solvents. Ethanol, acetone, THF, toluene, hexane, and dichloromethane were used to dissolve OriGen

Catheter samples at room temperature, respectively. The compatibility between OriGen Catheter polymer and each solvent was evaluated by visual inspection.

Polyurethane polymer solution preparation and evaluation. Tecophilic® polyurethane SP-80A-150 and Tecophilic® polyurethane SP-60D-60 were used to make polymer solution. Polyurethane was added into 50 °C THF and stirred until polyurethane completely dissolved. The concentration of two types of polyurethane polymer solution were shown in **Table 5.2**. 300 mL of polyurethane polymer solution was applied to the surface of a OriGen catheter sample. The coated sample was dried in a fume hood overnight. To test coating delamination, surgical tweezers were used to scratch and peel off the polyurethane coating from the catheter surface before and after soaking in water for 1 h.

Table 5.2 Various concentration of Tecophilic® polyurethane (SP-80A-150 and SP-60D-60) in THF.

Polyurethane (g)	THF (mL)	Concentration of polyurethane in polymer solution (w/v %)
0.05	5	1
0.15	5	3
0.25	5	5
0.35	5	7
0.5	5	10

Pebax polymer solution preparation and evaluation. 0.1 g of Pebax polymer was added into 10 mL dichloromethane and stirred at 37 °C overnight. The solubility of Pebax polymer in dichloromethane was evaluated by visual inspection. 0.1 g of Pebax polymer was added into 10 mL of m-cresol and stirred at room temperature until fully dissolved to form 1.0 w/v % Pebax polymer solution. 1 cm length of OriGen® Catheter sample was dipped into Pebax polymer solution for 10 sec, and then dipped into ethyl ether to remove m-cresol. The coated sample was dried in fume hood and evaluated by visual inspection.

5.2.6 Membrane oxygenation fiber coating

CuBTTri with solvent coating solution preparation and evaluation. 0.1 g CuBTTri was added into 10 mL of solution containing various concentration of THF and methanol as shown in **Table 5.3** and sonicated for 1 h to form 1.0 w/v % CuBTTri coating solution. 1 inch x 1 inch membrane oxygenator fiber sheet was merged into coating solution for 5 sec and dried in fume hood. The coated fiber sheet was evaluated by visual inspection.

Table 5.3 Composition of membrane lung fiber CuBTTri coating solution.

CuBTTri (g)	Volume of THF (mL)	Volume of methanol (mL)	Concentration of CuBTTri in coating solution (w/v %)
0.1	10	0	1.0
0.1	5	5	1.0

Layer-by-layer CuBTTri growth and evaluation. 0.012 g of H_3BTTri and 0.012 g of $CuCl_2 \cdot 2H_2O$ were individually dissolved in 5 mL of ethanol. 1 inch x 1 inch membrane oxygenator fiber sheet was soaked into 15 mM 10 mL NaOH overnight. Next day, the soaked fiber sheet was rinsed with water three time and dried in fume hood before use. Fiber sheet was soaked in H3BTTri solution for 30 min and rinsed with water and soaked in $CuCl_2 \cdot 2H_2O$ solution for 30 min and rinsed with water. These two steps were repeated for 5 times. The fiber sheet surface was evaluated by visual inspection.

Dopamine coating evaluation. 10 mM of Tris buffer was prepared by adding 0.5 g Tris buffer into 318 mL of water and adjust to pH 8.5 using 0.1 mM NaOH. 0.01g of dopamine was added into 5 mL Tris buffer solution to form 2 mg/mL polydopamine solution. 1 inch x 1 inch membrane oxygenator fiber sheet was soaked into polydopamine solution for 24 h with shaking in the absence of light. After 24 h, the fiber sheet was rinsed with water for 3 times and soaked in 5 mL of water for 24 h with shaking to remove unbounded polydopamine. These two steps repeated for 3 times. The polydopamine coating on fiber sheet surface was evaluated by visual inspection.

5.2.7 Bacterial attachment study

Bacterial solution preparation. Commercial *S. aureus* solution was thawed at room temperature and streaked onto an agar plate, which was incubated overnight at 37 ° C until colony formation. A single colony was chosen and inoculated into NBM, which was allowed to grow overnight at 37 ° C until an optical density at 600 nm (OD_{600}) ≈ 1 was reached. The resulting *S. aureus* solution was mixed with 30% v/v glycerol in a 1:1 volume ratio and stored at −80 ° C until further use. Prior to each bacterial experiment, the frozen *S. aureus* solution was thawed and centrifuged at 4700 rpm for 10 min. The upper solution was discarded, and the remaining *S. aureus* pellet was resuspended in NBM and incubated overnight at 37 ° C until OD_{600} ≈ 1. The next day, *S. aureu*–NBM solution was centrifuged at 4700 rpm for 10 min. The supernatant was discarded, and the remaining bacterial pellet was resuspended in PBS. The *S. aureus*–PBS solution was diluted with PBS until OD_{600} ≈ 0.033 corresponding to $(4.7 \pm 1.4) \times 10^6$ cfu/mL with approximate total volume of 125 mL before use.

Bacterial attachment study. The bacterial attachment study was carried out using the same custom-designed flow system with modification. Briefly, six-inch-long uncoated medical tubing segments were used as controls. The coated or uncoated control tubing pieces were connected to one and half-foot-long tubing, which was inserted into the peristaltic pump on one end and one-foot-long tubing, which was inserted into the bacterial solution on the other end. The bacterial solution was pumped from one end to the other end. All experiments were performed in the absence of bubbles in the tubing. For the bacterial attachment study performed under dynamic flow conditions, the flow rate was 300 mL min^{-1}, which simulated a typical blood flow rate utilized for hemodialysis. For the bacterial attachment study under static condition, the bacterial suspension was incubated in the loop for 24 h without active pumping. After 24 h, 150 mL of PBS was used to wash the entire loop at a flow rate of 300 mL min^{-1}. Four inch-long CuBTTri-coated

or uncoated control tubing pieces were cut from the system and moved into 25 mL of PBS in a 50 mL conical tube, which was then sonicated for 15 min and vortexed for 10 s to completely detach *S. aureus* from the tubing surface. The bacterial solution in the tube was transferred into a microcentrifuge tube and diluted 10 times. Diluted bacterial solution (20 μL) was streaked onto an agar plate and incubated overnight at 37 °C until colonies formed for enumeration. The amount of bacterial attachment was normalized into cfu mm^{-2} (n = 12).

5.2.8 Statistical analysis

Potential outliers were detected by Grubb's test with a 95% confidence interval ($p < 0.05$). The statistical differences in data were evaluated using one-way analysis of variance (ANOVA) followed by post-hoc Tukey-Kramer multiple comparison test at a 95% confidence interval ($p < 0.05$). All reported values were expressed as either mean ± standard deviation or spread range of 95% confidence interval.

5.3 Results and discussion

5.3.1 Circulation tubing coating and characterization

CuBTTri coating solution preparation. Larger CuBTTri agglomerates were observed in CuBTTri coating solution with direct addition of CuBTTri into polymer solution compared to by mixing CuBTTri solution into polymer solution. Using the second CuBTTri coating solution preparation method, sonication was able to reduce the size of CuBTTri agglomerates. The additional sonication after mixing allowed the evenly distribution CuBTTri particles inside Tygon® polymer network, which helped to create a relatively well-dispersed CuBTTri coating solution.

Tubing coating process 1 - 7. In tubing coating process 1, tubing section in the pump head was deformed, which was due to the compression created by the rollers that allowed the partially soften tubing change its configuration. Tubing coating process 2 was able to solve this issue by discarding the tubing used in pump head. However, bubbles formed in the flow-out tubing after

coating solution passing through the pump head. In addition to bubble formation, the coating solution tended to settle at the bottom of the tubing due to gravity. These two issues resulted in unevenly coated tubing. In tubing coating process 3, bubble formation was not a concern by removing flow-out tubing. However, coating solution still settled at the bottom of the tubing and tubing kept bending due to vibration resulting in unevenly coating. The connector needed to be changed each time after use which increased the cost. In tubing coating process 4, parafilm was used instead of connector. However, coating solution settlement remained a challenge. In tubing coating process 5, since the peristaltic pump was removed and coating solution was manually added into the tubing, a constant speed of addition of coating solution was hard to control and spilled coating solution while the tubing was rotating which created safety concerns. To keep tubing rotated and reduce safety concerns at the same time, peristaltic pump and a swivel connector was used in tubing coating process 7. However, the coating solution leaked from the swivel connector and tubing was twisted during rotation. In addition, a surface coating formed inside the swivel connector which needed to be changed each time of use and increased the cost. These issues found in tubing coating process 1 – 6 were solved in tubing coating process 7 which is currently used in our lab, including Raumedic ECC tubing (1/4 inch ID) coating and Tygon® ND-100-65 medical tubing (0.25 inch ID).

Interconnection between CuBTTri coating and surface of medical tubing. In this study, CuBTTri was coated onto the inner surface of the medical tubing by casting from the coating solution containing dissolved Tygon®. The Tygon® in the coating solution serves as a bonding agent, which blends with and penetrates the medical tubing, to prevent delamination of the CuBTTri-coating layer, and to avoid the introduction of new chemicals and additional bonding chemistries. THF dissolves a wide variety of polymers such as polyvinyl chloride and thermoplastic polyurethane and has a relatively low boiling point.[40,41] Over a short contact time, THF in the CuBTTri-coating solution is able to penetrate the rubbery surface of medical tubing,

leading to the formation of a gel layer that promotes adhesion of the coating solution.[40] Since the coating polymer is identical to the polymer used to manufacture the substrate tubing, the CuBTTri coating was deposited on the surface of the medical tubing without concern of delamination due to shear stress under flow conditions. Due to the volatility of THF, residual solvent was easily removed under vacuum.[42] In addition, no cytotoxic effects were observed when CuBTTri particles were added directly to human whole blood in an *in vitro* assessment of the effects of CuBTTri on coagulation and platelet aggregation.[43] CuBTTri/PVC composite membrane extracts also do not show any toxic effects to fibroblast or hepatocyte cultures.[44] Therefore, we expect that the coating method used in this work reduces the risk of cytotoxic effects.

CuBTTri-coating. CuBTTri (**Figure 5.11a**) maintained the same purple color after being mixed with a transparent polymer solution, which made the interior surface of CuBTTri-coated tubing appear the same purple color (**Figure 5.11c**) compared to clear uncoated controls (**Figure 5.11b**). The color change was an indicator of the distribution of CuBTTri particles in CuBTTri coating. CuBTTri coating solution containing 0.1 w/v%, 0.5 w/v%, and 1.0 w/v% were successfully coated onto the interior surface of tubing using Coating process 7.

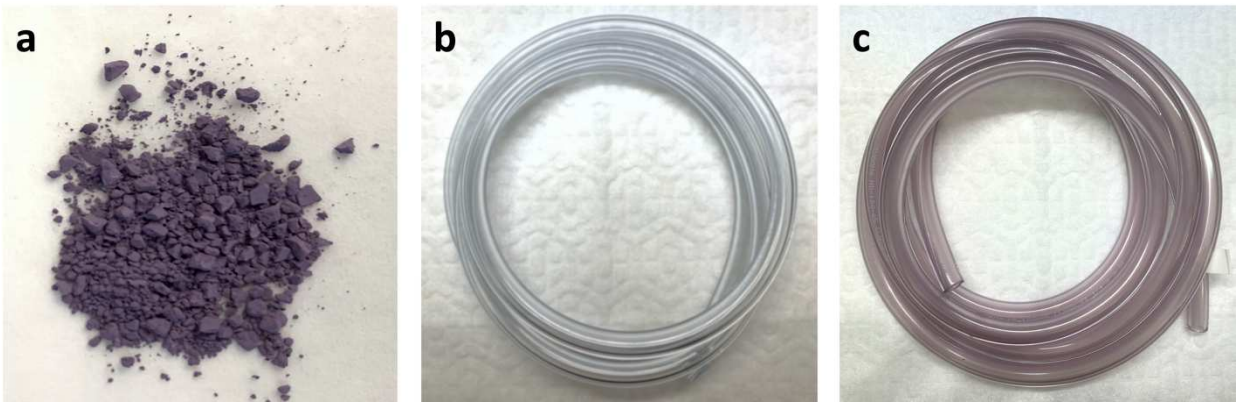

Figure 5.11 Representative images of (a) purple color CuBTTri particles; (b) clear uncoated medical tubing control; and (c) CuBTTri-coated medical tubing.

Coating catalytic property by nitric oxide analyzer (NOA). The real-time enhanced NO production from GSNO with CuBTTri coating containing various concentration of CuBTTri were

shown in **Figure 5.12**. CuBTTri-coated tubing was able to promote NO production from 10 μM GSNO in the solution. 1.0 w/v% CuBTTri-coated tubing induced a faster NO generation compared to 0.5 w/v % and 0.1 w/v % CuBTTri-coated tubing. The drop of NO production in the figure indicated that all NO was generated from GSNO through the CuBTTri coating.

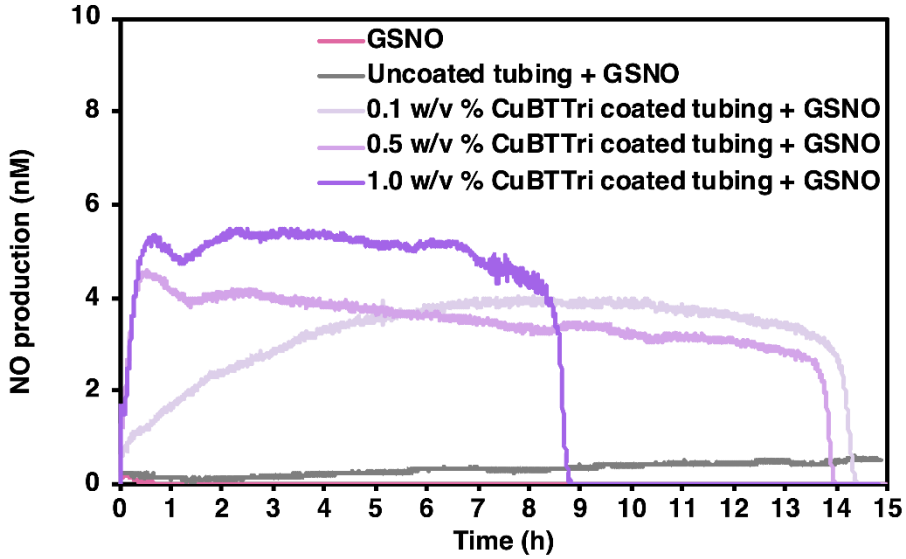

Figure 5.12 Representative real-time enhanced NO production from GSNO with CuBTTri-coated tubing containing various concentration of CuBTTri.

Coating post-sterilization catalytic property change by NOA. The real-time enhanced NO production from GSNO with CuBTTri coating containing various concentration of CuBTTri after ethylene oxide sterilization were shown in **Figure 5.13**. The CuBTTri coating was still able to promote NO production from GSNO, which indicated the ethylene oxide sterilization won't affect the catalytic properties of CuBTTri coating on tubing.

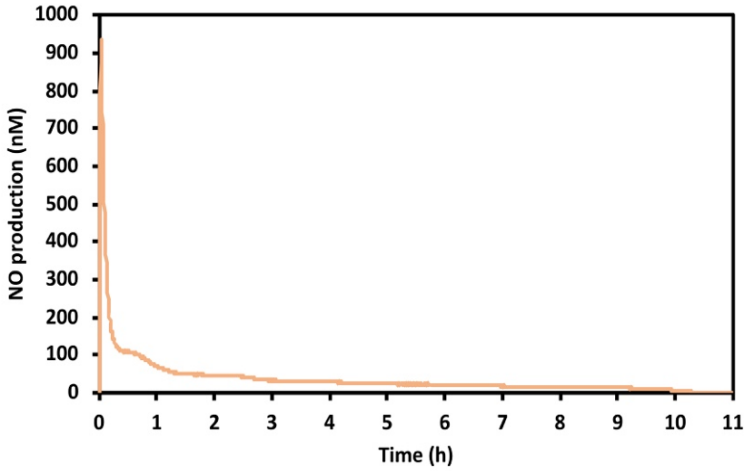

Figure 5.13 Representative real-time enhanced NO production from GSNO with CuBTTri-coated tubing after ethylene oxide sterilization.

Surface roughness by optical profilometer. It is essential that the seven-foot-long medical tubing exhibits a uniform thin coating after processing. The coating uniformity was evaluated based on coating surface roughness, coating thickness, and CuBTTri particle distribution in the coating. There were no significant differences in coating surface roughness among the seven segments of one inch-long tubing that were cut from the same tubing sample as shown in **Figure 5.14**. The average roughness (Sa) of coated tubing pieces was 0.50 ± 0.06 μm, approximately eight-fold greater than the roughness of uncoated control tubing which was 0.06 ± 0.005 μm.

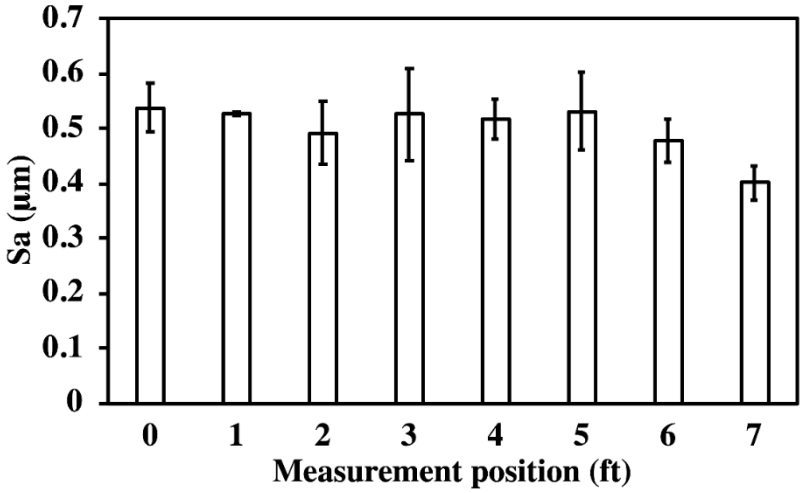

Figure 5.14 Surface roughness was measured on each segment from the CuBTTri-coated tubing. No significant difference was observed in surface roughness along the seven-foot long tubing (n = 3, $p < 0.05$) which indicated that the coating was evenly applied along the entire length of tubing.

Coating thickness and CuBTTri distribution by SEM. The coating thickness was roughly 20 μm, which is less than a 1.3% increase in wall thickness or less than 0.63% decrease in tubing inner diameter. The octahedral morphology of CuBTTri particles (**Figure 5.15a**) was partially lost during the coating process, as shown in **Figure 5.15b**. This change in particle morphology resulted from sonication during preparation of the coating solution. Sonication also separates larger CuBTTri agglomerates into smaller particles and disperses these uniformly in the polymer solution. Due to the distinct physical and chemical properties of CuBTTri and the Tygon® solution, CuBTTri particles tended to aggregate and form small agglomerates between 0.5 to 3.0 μm in size (**Figure 5.15b**). An industrial extrusion method would be able to solve this issue by melting CuBTTri particles and Tygon® into polymer pellets, similar to the CuBTC/polyurethane pellets previously reported by our group.[45] Furthermore, as shown in **Figure 5.15c and 5.15d**, CuBTTri particles were embedded in the coating matrix and distributed across the entire surface without regular micropatterning. Portions of the CuBTTri particles were merged into the surface of the tubing while the remaining portion of CuBTTri particles was on the surface of tubing but covered by Tygon® polymer which is able to protect CuBTTri particles under flow conditions. Overall, based on the results of coating thickness, surface roughness and surface morphology analysis, the CuBTTri coating was relatively uniform and thin but not fully homogenous.

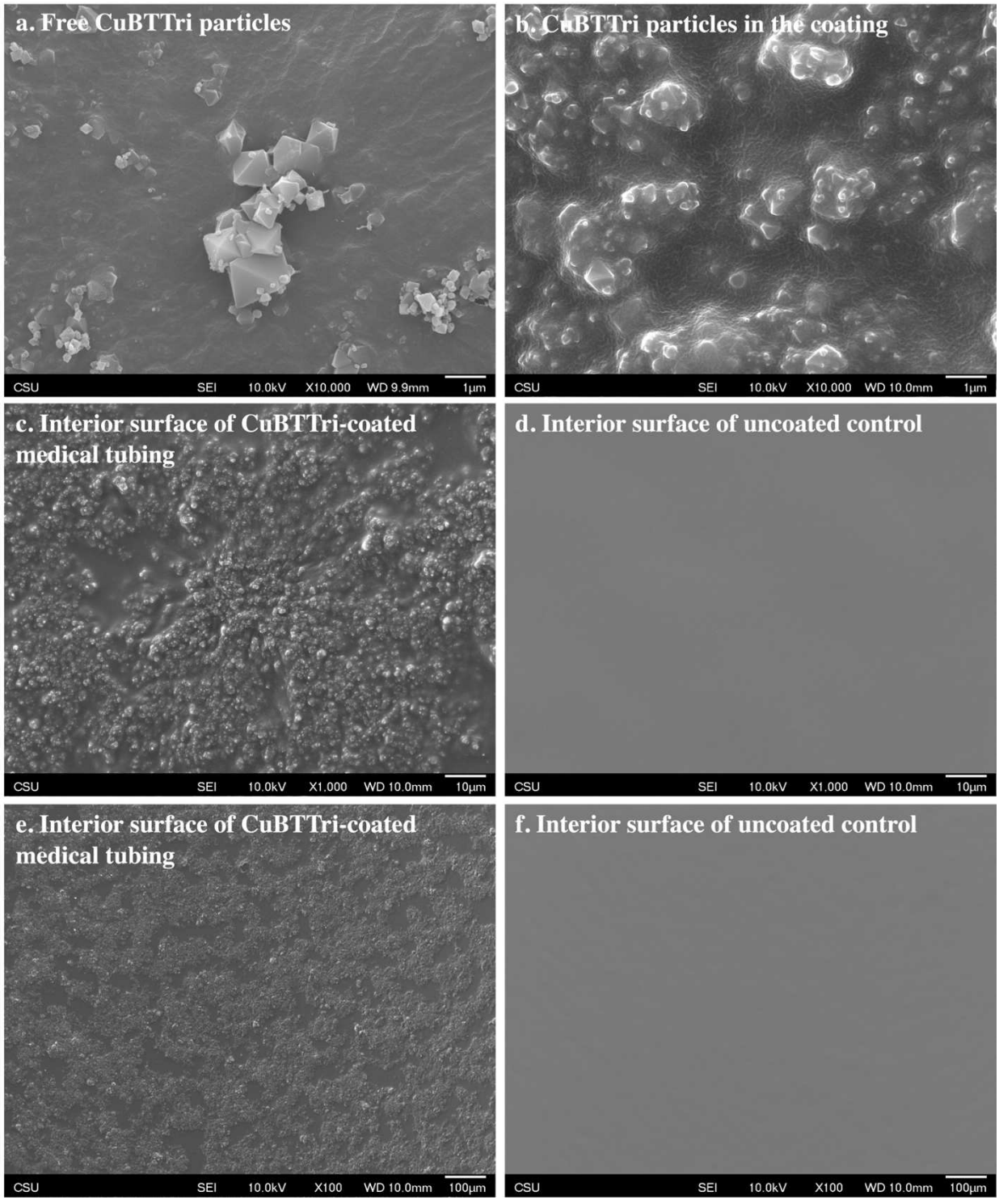

Figure 5.15 Representative SEM images of (a) free CuBTTri particles after synthesis; (b) CuBTTri particles in the coating at 10000x magnification; (c) and (d) interior surfaces of CuBTTri-coated medical tubing and uncoated control at 1000x magnification; (e) and (f) interior surfaces of CuBTTri-coated medical tubing and uncoated control at 100x magnification.

Copper content analysis by SEM-EDS. The incorporation of CuBTTri in the coating matrix was further evaluated via the elemental analysis of copper ion in the framework using SEM-EDS. The weight percentage of copper content in the coating matrix after scanning the sample surface was 3.9%. This results indicates the presence of CuBTTri particles in the coating matrix, which was consistent with the observation in **Figure 5.15**.

Coating stability (determination of CuBTTri degradation) by ICP-AES. For use in extracorporeal organ support, the stability of CuBTTri in the coating must be maintained to preserve function and protect patient safety. When copper-based MOF breaks down, it will release copper ions and organic linkers.[46,47] CuBTTri degradation from the coating was evaluated based on measurement of the copper ion concentration in PBS after 24 h incubation. The presence of dissolved copper in this medium may indicate breakdown of CuBTTri particles from the coating matrix or leaching of residual copper ions from the MOF synthesis that were trapped in the framework.[48] Using ICP-AES, the concentration of copper ions in this solution was determined to be $(3.3 \pm 0.1) \times 10^{-6}$ M, corresponding to 0.28% of the theoretical total copper in the coating. This result indicates that CuBTTri in the coating matrix is stable with negligible leached copper.

Coating stability (coating morphology change) by SEM. Changes in coating morphology were visualized using SEM. CuBTTri particles maintained a similar size and crystal structure in the CuBTTri-coating matrix before and after flow as shown in **Figure 5.16**. This outcome supports that the CuBTTri coating remains stable under flow conditions over 24 h. However, the CuBTTri coating in **Figure 5.16b** looked more uniform than in **Figure 5.16a**. After the coating was exposed to flowing PBS for 24 h, the PBS was trapped within the coating matrix and induced some swelling. SEM measurements were made under high vacuum, which causes surface dehydration. The dehydrated surface would either turn to its original appearance or become deformation. In addition, the samples used for SEM before and after flow were not the same but from similar

locations. From the surface roughness results, this was a ± 0.06 μm variability from location to location. These are the reason why the two surfaces look slightly different.

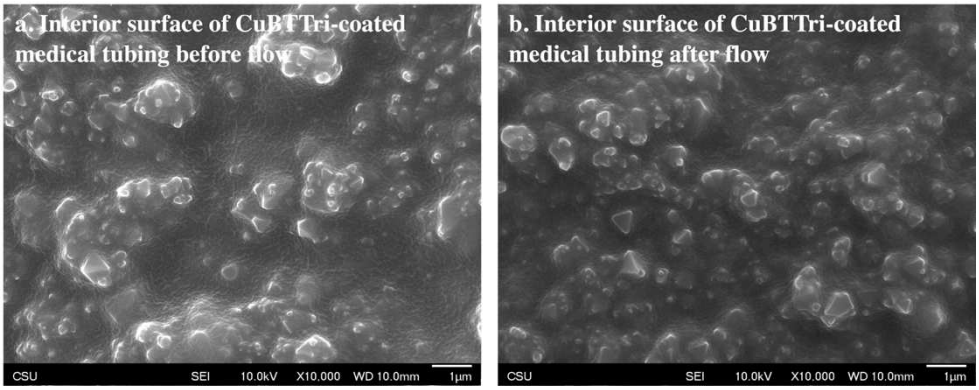

Figure 5.16 Representative SEM images of (a) interior surface of CuBTTri-coated medical tubing before flow at 10000x magnification (same image as Figure 6b); and (b) interior surfaces of CuBTTri-coated medical tubing after flow at 10000x magnification.

5.3.2 Avalon catheter coating and coating catalytic property evaluation

Evaluation the compatibility between Avalon Catheter polymer and various solvents. To reduce the effects of THF on the catheter surface, solvent that is miscible with THF and compatible with the Avalon Catheter polymer was used to dilute THF. The volatility of this second solvent was selected to be similar to THF so that they can be removed by evaporation at similar rates. Acetone, diethyl ether, and methanol were tested. Methanol satisfied all of the previously mentioned criteria and was therefore used to dilute THF.

Nonaqueous turbidimetric titration test. The volume of methanol used during turbidimetric titration test was 5 mL which was exactly the same volume of polymer solution. Because of these results, the ratio of THF to methanol used in CuBTTri coating solution was 1 to 1.

Assessment of catalytic property by NOA. Real-time enhanced NO production from GSNO is shown in **Figure 5.17**. Without light exposure, NO production from GSNO was minimal either in solution without any coated sample or in the presence of uncoated catheter. Both of reinfusion port and tubing section from CuBTTri-coated catheter were able to promote NO production from

GSNO. Again, the decline in NO release indicated that all NO was released from GSNO in the presence of CuBTTri coating.

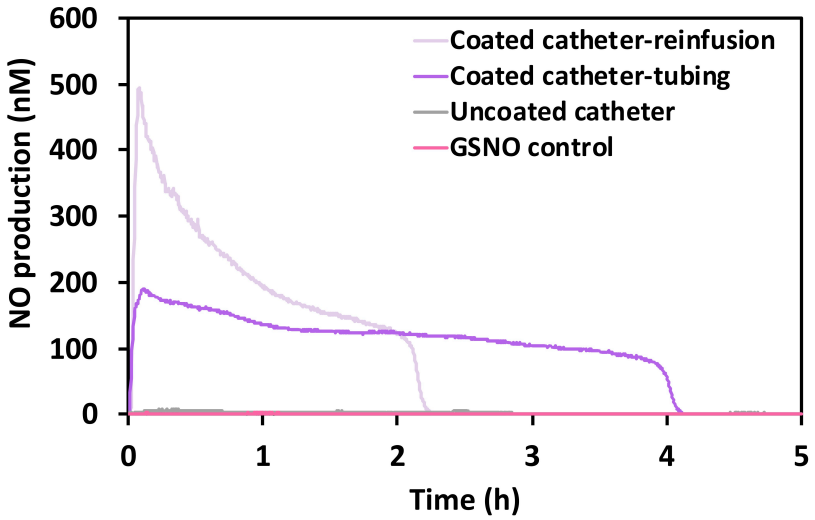

Figure 5.17 Representative real-time enhanced NO production from GSNO with CuBTTri-coated catheter.

Assessment of post-sterilization catalytic property changes by NOA. Real time enhanced NO production from sterilized CuBTTri-coated catheter is shown in **Figure 5.18**. This result indicates that ethylene oxide sterilization is unlikely to affect the catalytic properties of CuBTTri coating on catheters.

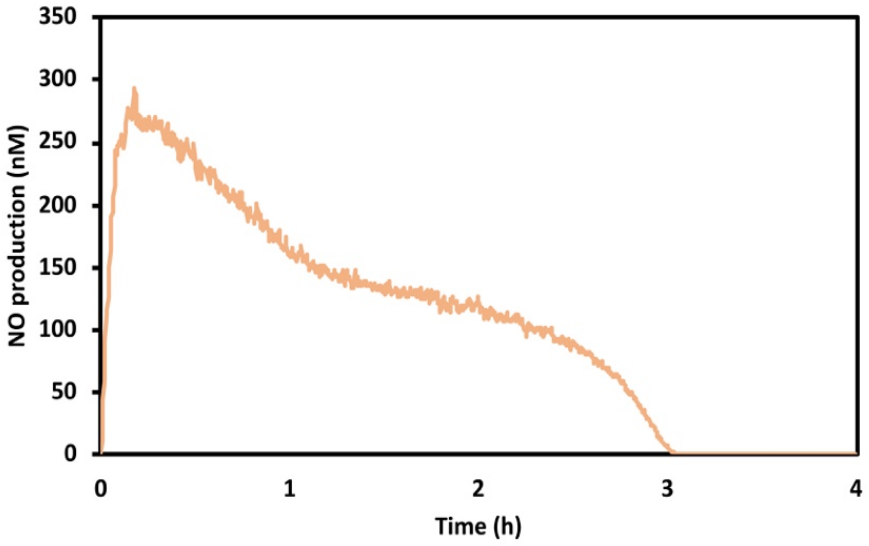

Figure 5.18 Representative real-time enhanced NO production from GSNO with CuBTTri-coated tubing after ethylene oxide sterilization. Compared to pre-sterilization results, CuBTTri-coating was still able to promote NO production.

5.3.3 OriGen catheter coating

Evaluation of compatibility between OriGen Catheter polymer and various solvents. To prepare a coating solution of the OriGen Catheter polymer, different solvents were used to dissolve OriGen Catheter samples. Ethanol, acetone, toluene, hexane, and dichloromethane had no effect on the surface of OriGen Catheter sample after 12 h exposure by visual inspection. OriGen Catheter samples softened after 12 h in THF, but did not dissolve.

Polyurethane polymer solution evaluation. Both types of polyurethane polymer coating layer on Origen Catheter sample surface were removed by scratching using a steel implement and delaminated after soaking in water for 1 h.

Pebax polymer solution evaluation. Pebax polymers failed to dissolve in dichloromethane, but slightly swelled. The colorless *m*-cresol became yellow when this solvent was exposed to air, which is attributable to oxidation of phenols.[44] *m*-Cresol was able to fully dissolve Pebax polymers and the polymer solution was a light yellow color. The boiling point of *m*-cresol is 203 °C under atmospheric pressure, making it difficult to remove from the polymer coating and creating

biological toxicity concerns. Diethyl ether dissolves *m*-cresol and is very volatile with a boiling point of 34.6 °C. By dipping the coated sample in diethyl ether, *m*-cresol can be removed from the coating matrix. However, phenol tarring odor persisted after several dipping cycles and the polymer coating was not uniform by visual inspection.

Because the composition of OriGen Catheters is proprietary, the exact polymer or mixture of polymers used in their fabrication is unknown. Without this information, it was challenging to identify chemicals that would effectively dissolve or promote coating of OriGen Catheters. Different methods were tested to prepare a coating solution in the absence of this information. However, none of the methods worked well on these catheters. Because of the known formulation of Avalon catheters , we were focused on them instead.

5.3.4 Membrane oxygenation fiber coating

Coating solution evaluation. Membrane lung fibers were deformed in both coating solutions. This outcome likely results from incomplete removal of THF from the hollow structure of fibers, leading to deformation.

Layer-by-layer CuBTTri growth and evaluation. In this study, no CuBTTri formation was observed on the fiber sheet surface. However, copper-based MOFs, such as CuBTC, have been successfully grown on silk and cotton fibers using layer-by-layer growth methods.[32,33,45] Chemical bonds could first form between the fiber surface and ligand by the interaction of functional groups. Metal ions could coordinate with the ligand on the fiber surface and start the nucleation process to form the frameworks. To protect membrane oxygenation fibers from deformation, the solvent used for the ligand and metal ions should be resistant to the fibers and the nucleation temperature should be below the fiber melting point. The chief difficulty is identifying useful nucleation conditions, such as solvent, temperature, and other factors.

Dopamine coating evaluation. Dopamine is a mussel-inspired chemical that contains both catechol and amine functional groups which mimic 3,4-dihydroxy-L-phenylalanine and lysine amino acids, two adhesive proteins in mussels. Dopamine can self-polymerize under marine condition and has been shown to successfully form thin polydopamine films on different substrates. After deposition, the polydopamine film can be used as an intermediate for secondary reactions. So far, dopamine has been shown to help the growth of CuBTC on metal surface. We expect dopamine can help either the adhesion or the growth of CuBTTri. In this study, a black color polydopamine layer was formed on a fiber surface. Further study involved in the incorporation of CuBTTri into polydopamine layer is needed.

5.3.5 Static and dynamic flow bacterial attachment studies on CuBTTri-coated tubing

Conventional hemodialysis is performed in routine treatments lasting 3-12 hours.[51] More intensive forms of renal support, such as continuous renal replacement therapy (CRRT), can be implemented over 24 hours to several days.[52] In this initial investigation, an intermediary 24 h duration study was selected with the results applicable to both conventional hemodialysis and CRRT. Bacterial attachment to foreign surfaces is highly flow dependent. For example, fluid shear forces can accelerate bacterial transport to the biomaterial surface and promote cell binding to an extent; however, significantly high flow rates can induce detachment and limit attachment once a critical flow limit is exceeded.[53] Further, lower flow rates are associated with random bacterial attachment and lower density of attached bacteria in specific regions.[54] This demonstrates the importance of evaluating bacterial attachment to biomaterials utilizing flow conditions that closely replicate the clinical scenario. Therefore, we used a flow rate of 300 ml L^{-1} to simulated a typical blood flow setting during hemodialysis procedures.

Under static conditions, the attachment of *S. aureus* on uncoated controls and CuBTTri-coated medical tubing was 1912 $\pm$ 490 cfu mm^{-2} and 916 $\pm$ 281 cfu mm^{-2}, respectively. Under

dynamic flow conditions the attachment of *S. aureus* on uncoated controls and CuBTTri-coated medical tubing was 925 ± 221 cfu mm^{-2} and 437 ± 272 cfu mm^{-2}, respectively. As shown in **Figure 5.19**, bacterial attachment was significantly reduced by 52 ± 15% and 53 ± 29% on CuBTTri-coated medical tubing compared to uncoated controls under static and dynamic flow conditions, respectively. Leaching of copper ions from the material surface could raise safety concerns for medical applications, so copper leaching was accessed in addition to bacterial attachment. Based on the dimensions of medical tubing samples and the volume of the solution used for the bacterial attachment study, the copper ion concentration in the system was calculated to be approximately 4 μM based on the coating stability test. This concentration is lower than concentrations (10-100 μM) reported to have an effect on both mammalian cells and *S. aureus*.[55–57] CuBTTri antibacterial properties have been reported by several groups, although the mechanism remains unclear.[35,36] In addition, Neufeld et al. demonstrates that the antimicrobial properties of CuBTTri/chitosan films are attributable to the material itself, not solvated copper ions or organic ligands.[35] CuBTTri contains copper centers both inside the framework and on the framework surface. Copper centers on the framework surface may be able to come into direct contact with bacterial membranes and induce oxidative damage to bacterial cells.[36,58,59] However, coating physiochemical properties, such as surface patterns and surface roughness, may also affect bacterial attachment.[60] Patterning surfaces, such as sharklet, are known to influence the interaction between bacteria and material surfaces.[30,61] In this study, a regular micropatterning was not observed on the CuBTTri coating surfaces (**Figure 5.15**). Coating surface roughness is another factor that may affect *S. aureus* attachment. The effects of surface roughness on bacteria attachment have been studied with a variety of biomaterials and bacterial strain. However, a surface roughness study has yet to be performed using CuBTTri coatings. It is possible that the combination of MOF

inherent antibacterial properties and surface roughness contribute to the reduction of *S. aureus* attachment. In general, the mechanism of antibacterial activity requires further investigation.

Bacterial attachment was also significantly reduced under dynamic flow conditions compared to static conditions for both the CuBTTri-coated medical tubing and uncoated controls. Both mass transport and shear stress can affect bacterial attachment in a flow system.[62] Mass transport refers to the process in which the rate of bacterial attachment is determined by the number of bacteria passing over the surfaces of medical devices.[63–65] It is believed that bacterial attachment will be increased if the number of bacteria is higher.[66] Shear stress can neutralize this phenomenon if flow occurs beyond a critical point where shear stress can decrease bacterial attachment.[67,68] In our study, we showed that bacterial attachment is reduced by 52 $\pm$ 12% (CuBTTri coating) and 52 $\pm$ 30% (uncoated controls) under dynamic flow compared to static conditions. Traditionally, pre-clinical assessment of antibacterial biomaterials is performed in a static benchtop setup with no flow on small fragments of tubing or isolated pieces of catheters. For this reason, it is difficult to compared the percent reduction in bacterial adhesion we observed in our study to other static, benchtop assays. A small number of dynamic flow bacterial attachment studies have been reported, but these studies do not use the same flow rate or clinically-relevant circuit test configuration as we have attempted to do in this study, so it is also difficult to compare the percent reduction in bacterial attachment observed in this study to other dynamic studies.[69–72]

The promising antibacterial activity of this CuBTTri-based coating may interest clinicians who are seeking new treatments and novel surfaces for the improvement of extracorporeal organ support performance. Further testing is required, including *in vivo* testing in animal models, to understand more about how these results translate to clinical applications.

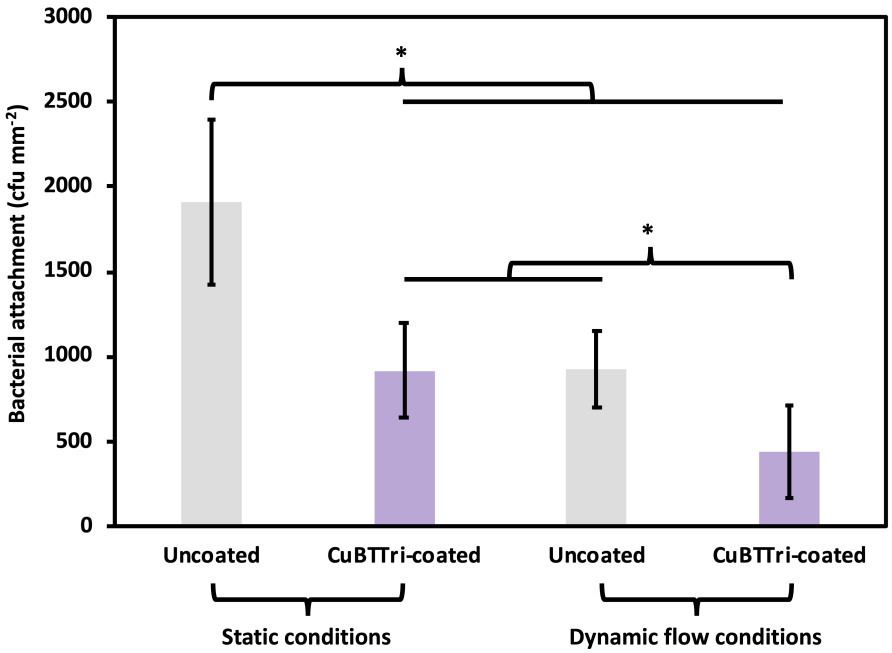

Figure 5.19 Bacterial attachment was significantly reduced on CuBTTri-coated medical tubing. Bacterial attachment was significantly reduced with dynamic flow (n = 12, * indicates $p < 0.05$).

In addition to antibacterial effects, CuBTTri has catalytic properties that enhance nitric oxide (NO) release from bioavailable donors in the blood, such as *S*-nitrosothiols (RSNOs).[44,45,50,73,74] NO has potent antimicrobial and antibacterial effects that are implicated in a healthy host response to infection.[75] In addition, NO can effectively inhibit platelet activation and aggregation at the blood-biomaterial interface.[5] Generation of NO at the biomaterial surface using CuBTTri could be extremely beneficial to prevent infections and blood clot formation during hemodialysis and other forms of extracorporeal organ support such as ECMO. The anticoagulant effects of CuBTTri were demonstrated *ex vivo* using whole blood from healthy human donors where CuBTTri reduced the time to start of clot formation and reduced clot strength, as measured by thromboelastography.[43] Additionally, CuBTTri added to platelet-rich plasma with an RSNO reduced platelet aggregation by approximately 35% when compared to addition of the RSNO alone.[43] Further testing using the CuBTTri-coated medical tubing we have detailed in this study

is required to examine the effects of the coating on both foreign surface-induced thrombus deposition and bacterial adhesion when exposed to blood and RSNOs.

5.4 Conclusion

This is the first study to report methods for coating a MOF-polymer composite layer on catheters and medical tubing at a length normally used during extracorporeal organ support procedures. The CuBTTri-coated medical tubing combined with typical hemodialysis flow conditions can maximize inhibition of bacterial attachment compared to uncoated medical tubing under static conditions. The CuBTTri coating is not limited to medical tubing and can conceivably be used to coat other polymeric medical devices. Since CuBTTri also has catalytic properties conferring antibacterial and platelet inhibitory effects, the CuBTTri coating is a promising multifunctional coating for medical devices.

REFERENCES

1. Hemmila MR, Rowe SA, Boules TN, et al. Extracorporeal Life Support for Severe Acute Respiratory Distress Syndrome in Adults. *Ann Surg*. 2004;240(4):595-607. doi:10.1097/01.sla.0000141159.90676.2d
2. Neff LP, Cannon JW, Stewart IJ, et al. Extracorporeal organ support following trauma. *J Trauma Acute Care Surg*. 2013;75(2):S120-S129. doi:10.1097/TA.0b013e318299d0cb
3. Gorbet MB, Sefton M V. Biomaterial-associated thrombosis: roles of coagulation factors, complement, platelets and leukocytes. *Biomaterials*. 2004;25(26):5681-5703. doi:10.1016/j.biomaterials.2004.01.023
4. Lappegård KT, Fung M, Bergseth G, et al. Effect of complement inhibition and heparin coating on artificial surface–induced leukocyte and platelet activation. *Ann Thorac Surg*. 2004;77(3):932-941. doi:10.1016/S0003-4975(03)01519-4
5. Major TC, Brant DO, Reynolds MM, et al. The attenuation of platelet and monocyte activation in a rabbit model of extracorporeal circulation by a nitric oxide releasing polymer. *Biomaterials*. 2010;31(10):2736-2745. doi:10.1016/j.biomaterials.2009.12.028
6. Skrzypchak AM, Lafayette NG, Bartlett RH, et al. Effect of varying nitric oxide release to prevent platelet consumption and preserve platelet function in an in vivo model of extracorporeal circulation. *Perfusion*. 2007;22(3):193-200. doi:10.1177/0267659107080877
7. Major TC, Brant DO, Burney CP, et al. The hemocompatibility of a nitric oxide generating polymer that catalyzes S-nitrosothiol decomposition in an extracorporeal circulation model. *Biomaterials*. 2011;32(26):5957-5969. doi:10.1016/j.biomaterials.2011.03.036
8. D'Agata EMC, Mount DB, Thayer V, Schaffner W. Hospital-acquired infections among chronic hemodialysis patients. *Am J Kidney Dis*. 2000;35(6):1083-1088.

doi:10.1016/S0272-6386(00)70044-8

9. Bizzarro MJ, Conrad SA, Kaufman DA, Rycus P. Infections acquired during extracorporeal membrane oxygenation in neonates, children, and adults. *Pediatr Crit Care Med*. 2011;12(3):277-281. doi:10.1097/PCC.0b013e3181e28894

10. Van Epps JS, Younger JG. Implantable device-related infection. *Shock*. 2016;46(6):597-608. doi:10.1097/SHK.0000000000000692

11. Piraino B. Staphylococcus Aureus Infections in Dialysis Patients: Focus on Prevention. *ASAIO J*. 2000;46(6):S13-S17. doi:10.1097/00002480-200011000-00031

12. Hoen B, Paul-Dauphin A, Hestin D, Kesslerr M. EPIBACDIAL: A Multicenter Prospective Study of Risk Factors for Bacteremia in Chronic Hemodialysis Patients. *J Am Soc Nephrol*. 1998;9(5):869-876.

13. Scheuch M, Freiin Von Rheinbaben S, Kabisch A, et al. Staphylococcus aureus colonization in hemodialysis patients: A prospective 25 months observational study. *BMC Nephrol*. 2019;20(1):153. doi:10.1186/s12882-019-1332-z

14. Paharik AE, Horswill AR. The Staphylococcal Biofilm: Adhesins, Regulation, and Host Response. *Microbiol Spectr*. 2016;4(2):529-566. doi:10.1128/microbiolspec.VMBF-0022-2015

15. Otto M. Staphylococcal Biofilms. In: *Current Topics in Microbiology and Immunology*. Vol 322. ; 2008:207-228. doi:10.1007/978-3-540-75418-3_10

16. von Eiff C, Jansen B, Kohnen W, Becker K. Infections Associated with Medical Devices. *Drugs*. 2005;65(2):179-214. doi:10.2165/00003495-200565020-00003

17. *ANTIBIOTIC RESISTANCE THREATS in the United States*.; 2013. https://www.cdc.gov/drugresistance/threat-report-2013/pdf/ar-threats-2013-508.pdf. Accessed September 16, 2019.

18. A Brief History of The Health Support Uses of Silver. http://www.silver-

colloids.com/Pubs/history-silver.html. Accessed September 18, 2019.

19. Clement JL, Jarrett PS. Antibacterial Silver. *Met Based Drugs*. 1994;1:467-482.

20. Lansdown ABG. Silver in Health Care: Antimicrobial Effects and Safety in Use. In: *Biofunctional Textiles and the Skin*. Vol 33. Basel: KARGER; 2006:17-34. doi:10.1159/000093928

21. Shateri Khalil-Abad M, Yazdanshenas ME. Superhydrophobic antibacterial cotton textiles. *J Colloid Interface Sci*. 2010;351(1):293-298. doi:10.1016/j.jcis.2010.07.049

22. Fadeeva E, Truong VK, Stiesch M, et al. Bacterial Retention on Superhydrophobic Titanium Surfaces Fabricated by Femtosecond Laser Ablation. *Langmuir*. 2011;27(6):3012-3019. doi:10.1021/la104607g

23. Bhadra CM, Khanh Truong V, Pham VTH, et al. Antibacterial titanium nano-patterned arrays inspired by dragonfly wings. *Sci Rep*. 2015;5:16817. doi:10.1038/srep16817

24. Patil D, Aravindan S, Kaushal Wasson M, P. V, Rao P V. Fast Fabrication of Superhydrophobic Titanium Alloy as Antibacterial Surface Using Nanosecond Laser Texturing. *J Micro Nano-Manufacturing*. 2018;6(1):011002. doi:10.1115/1.4038093

25. Bartlet K, Movafaghi S, Dasi LP, Kota AK, Popat KC. Antibacterial activity on superhydrophobic titania nanotube arrays. *Colloids Surfaces B Biointerfaces*. 2018;166:179-186. doi:10.1016/j.colsurfb.2018.03.019

26. Spasova M, Manolova N, Markova N, Rashkov I. Superhydrophobic PVDF and PVDF-HFP nanofibrous mats with antibacterial and anti-biofouling properties. *Appl Surf Sci*. 2016;363:363-371. doi:10.1016/j.apsusc.2015.12.049

27. Schlaich C, Li M, Cheng C, et al. Mussel-Inspired Polymer-Based Universal Spray Coating for Surface Modification: Fast Fabrication of Antibacterial and Superhydrophobic Surface Coatings. *Adv Mater Interfaces*. 2018;5(5):1701254. doi:10.1002/admi.201701254

28. Eduok U, Szpunar J, Ebenso E. Superhydrophobic antibacterial polymer coatings. In: *Superhydrophobic Polymer Coatings*. Elsevier; 2019:245-279. doi:10.1016/B978-0-12-816671-0.00012-6

29. Dundar Arisoy F, Kolewe KW, Homyak B, Kurtz IS, Schiffman JD, Watkins JJ. Bioinspired Photocatalytic Shark-Skin Surfaces with Antibacterial and Antifouling Activity via Nanoimprint Lithography. *ACS Appl Mater Interfaces*. 2018;10(23):20055-20063. doi:10.1021/acsami.8b05066

30. May RM, Hoffman MG, Sogo MJ, et al. Micro-patterned surfaces reduce bacterial colonization and biofilm formation in vitro: Potential for enhancing endotracheal tube designs. *Clin Transl Med*. 2014;3(1):8. doi:10.1186/2001-1326-3-8

31. Li H, Wang K, Sun Y, Lollar CT, Li J, Zhou HC. Recent advances in gas storage and separation using metal–organic frameworks. *Mater Today*. 2018;21(2):108-121. doi:10.1016/j.mattod.2017.07.006

32. Isaeva VI, Kustov LM. The application of metal-organic frameworks in catalysis (review). *Pet Chem*. 2010;50(3):167-180. doi:10.1134/S0965544110030011

33. Abbasi AR, Akhbari K, Morsali A. Dense coating of surface mounted CuBTC Metal–Organic Framework nanostructures on silk fibers, prepared by layer-by-layer method under ultrasound irradiation with antibacterial activity. *Ultrason Sonochem*. 2012;19(4):846-852. doi:10.1016/j.ultsonch.2011.11.016

34. Rubin HN, Neufeld BH, Reynolds MM. Surface-Anchored Metal–Organic Framework–Cotton Material for Tunable Antibacterial Copper Delivery. *ACS Appl Mater Interfaces*. 2018;10(17):15189-15199. doi:10.1021/acsami.7b19455

35. Neufeld BH, Neufeld MJ, Lutzke A, Schweickart SM, Reynolds MM. Metal-Organic Framework Material Inhibits Biofilm Formation of Pseudomonas aeruginosa. *Adv Funct Mater*. 2017;27(34):1702255. doi:10.1002/adfm.201702255

36. Wen Y, Chen Y, Wu Z, Liu M, Wang Z. Thin-film nanocomposite membranes incorporated with water stable metal-organic framework CuBTTri for mitigating biofouling. *J Memb Sci*. 2019;582(15):289-297. doi:10.1016/j.memsci.2019.04.016

37. Hart TW. Some observations concerning the S-nitroso and S-phenylsulphonyl derivatives of L-cysteine and glutathione. *Tetrahedron Lett*. 1985;26(16):2013-2016. doi:10.1016/S0040-4039(00)98368-0

38. Demessence A, D'Alessandro DM, Foo ML, Long JR. Strong CO 2 Binding in a Water-Stable, Triazolate-Bridged Metal–Organic Framework Functionalized with Ethylenediamine. *J Am Chem Soc*. 2009;131(25):8784-8786. doi:10.1021/ja903411w

39. Zang Y, Popat KC, Reynolds MM. Nitric oxide-mediated fibrinogen deposition prevents platelet adhesion and activation ARTICLES YOU MAY BE INTERESTED IN. *Biointerphases*. 2018;13(6):E403. doi:10.1116/1.5042752

40. Miller-Chou BA, Koenig JL. A review of polymer dissolution. *Prog Polym Sci*. 2003;28(8):1223-1270. doi:10.1016/S0079-6700(03)00045-5

41. Wu W-I, Sask KN, Brash JL, Selvaganapathy PR. Polyurethane-based microfluidic devices for blood contacting applications. *Lab Chip*. 2012;12:960-970. doi:10.1039/c2lc21075d

42. Brisbois EJ, Handa H, Major TC, Bartlett RH, Meyerhoff ME. Long-term nitric oxide release and elevated temperature stability with S-nitroso-N-acetylpenicillamine (SNAP)-doped Elast-eon E2As polymer. *Biomaterials*. 2013;34(28):6957-6966. doi:10.1016/j.biomaterials.2013.05.063

43. Roberts TR, Neufeld MJ, Meledeo MA, et al. A metal organic framework reduces thrombus formation and platelet aggregation ex vivo. *J Trauma Acute Care Surg*. 2018;85(3):572-579. doi:10.1097/TA.0000000000001982

44. Neufeld MJ, Ware BR, Lutzke A, Khetani SR, Reynolds MM. Water-Stable Metal–Organic

Framework/Polymer Composites Compatible with Human Hepatocytes. *ACS Appl Mater Interfaces*. 2016;8(30):19343-19352. doi:10.1021/acsami.6b05948

45. Harding JL, Metz JM, Reynolds MM. A Tunable, Stable, and Bioactive MOF Catalyst for Generating a Localized Therapeutic from Endogenous Sources. *Adv Funct Mater*. 2014;24(47):7503-7509. doi:10.1002/adfm.201402529

46. Chiericatti C, Basilico JC, Zapata Basilico ML, Zamaro JM. Novel application of HKUST-1 metal-organic framework as antifungal: Biological tests and physicochemical characterizations. *Microporous Mesoporous Mater*. 2012;162:60-63. doi:10.1016/j.micromeso.2012.06.012

47. Wyszogrodzka G, Marszałek B, Gil B, Dorożyński P. Metal-organic frameworks: mechanisms of antibacterial action and potential applications. *Drug Discov Today*. 2016;21(6):1009-1018. doi:10.1016/j.drudis.2016.04.009

48. Pöppl A, Kunz S, Himsl D, Hartmann M. CW and Pulsed ESR Spectroscopy of Cupric Ions in the Metal–Organic Framework Compound Cu3(BTC)2. *J Phys Chem C*. 2008;112(7):2678-2684. doi:10.1021/jp7100094

49. Joglekar HS, Samant SD, Joshi JB. Kinetics of wet air oxidation of phenol and substituted phenols. *Water Res*. 1991;25(2):135-145. doi:10.1016/0043-1354(91)90022-I

50. Neufeld MJ, Harding JL, Reynolds MM. Immobilization of Metal–Organic Framework Copper(II) Benzene-1,3,5-tricarboxylate (CuBTC) onto Cotton Fabric as a Nitric Oxide Release Catalyst. *ACS Appl Mater Interfaces*. 2015;7(48):26742-26750. doi:10.1021/acsami.5b08773

51. Rocco M, Daugirdas JT, Depner TA, et al. KDOQI Clinical Practice Guideline for Hemodialysis Adequacy: 2015 Update. *Am J Kidney Dis*. 2015;66(5):884-930. doi:10.1053/j.ajkd.2015.07.015

52. Karkar A, Ronco C. Prescription of CRRT: a pathway to optimize therapy. *Ann Intensive*

Care. 2020;10(1):32. doi:10.1186/s13613-020-0648-y

53. Busscher HJ, Van Der Mei HC. Microbial adhesion in flow displacement systems. *Clin Microbiol Rev*. 2006;19(1):127-141. doi:10.1128/CMR.19.1.127-141.2006

54. Liu Y, Wang J-C, Ren L, et al. Microfluidics-based assay on the effects of microenvironmental geometry and aqueous flow on bacterial adhesion behaviors. *J Pharm Anal*. 2011;1(3):175-183. doi:10.1016/j.jpha.2011.06.001

55. Baker J, Sitthisak S, Sengupta M, Johnson M, Jayaswal RK, Morrissey JA. Copper Stress Induces a Global Stress Response in Staphylococcus aureus and Represses sae and agr Expression and Biofilm Formation. *Appl Environ Microbiol*. 2010;76(1):150-160. doi:10.1128/AEM.02268-09

56. Burghardt I, Lüthen F, Prinz C, et al. A dual function of copper in designing regenerative implants. *Biomaterials*. 2015;44:36-44. doi:10.1016/j.biomaterials.2014.12.022

57. Ning C, Wang X, Li L, et al. Concentration Ranges of Antibacterial Cations for Showing the Highest Antibacterial Efficacy but the Least Cytotoxicity against Mammalian Cells: Implications for a New Antibacterial Mechanism. *Chem Res Toxicol*. 2015;28(9):1815-1822. doi:10.1021/acs.chemrestox.5b00258

58. Cady NC, Behnke JL, Strickland AD. Copper-Based Nanostructured Coatings on Natural Cellulose: Nanocomposites Exhibiting Rapid and Efficient Inhibition of a Multi-Drug Resistant Wound Pathogen, A. baumannii, and Mammalian Cell Biocompatibility In Vitro. *Adv Funct Mater*. 2011;21(13):2506-2514. doi:10.1002/adfm.201100123

59. Hans M, Mathews S, Mücklich F, Solioz M. Physicochemical properties of copper important for its antibacterial activity and development of a unified model. *Biointerphases*. 2016;11(1):018902. doi:10.1116/1.4935853

60. Katsikogianni M, Missirlis Y. Concise review of mechanisms of bacterial adhesion to biomaterials and of techniques used in estimating bacteria-material interactions. *Eur Cells*

Mater. 2004;8:37-57. doi:10.22203/eCM.v008a05

61. Reddy ST, Chung KK, McDaniel CJ, Darouiche RO, Landman J, Brennan AB. Micropatterned surfaces for reducing the risk of catheter-associated urinary tract infection: An in vitro study on the effect of sharklet micropatterned surfaces to inhibit bacterial colonization and migration of uropathogenic Escherichia coli. *J Endourol*. 2011;25(9):1547-1552. doi:10.1089/end.2010.0611

62. Busscher HJ, Van Der Mei HC. Microbial adhesion in flow displacement systems. *Clin Microbiol Rev*. 2006;19(1):127-141. doi:10.1128/CMR.19.1.127-141.2006

63. Marshall KC. Mechanisms of Bacterial Adhesion at Solid-Water Interfaces. In: *Bacterial Adhesion*. Boston, MA: Springer US; 1985:133-161. doi:10.1007/978-1-4615-6514-7_6

64. van Loosdrecht MCM, Lyklema J, Norde W, Zehnder AJB. Bacterial adhesion: A physicochemical approach. *Microb Ecol*. 1989;17:1-15. doi:10.1007/BF02025589

65. Korber DR, Lawrence JR, Zhang L, Caldwell DE. Effect of gravity on bacterial deposition and orientation in laminar flow environments. *Biofouling*. 1990;2(4):335-350. doi:10.1080/08927019009378155

66. Sjollema J, Busscher HJ, Weerkamp AH. Deposition of oral streptococci and polystyrene latices onto glass in a parallel plate flow cell. *Biofouling*. 1988;1(2):101-112. doi:10.1080/08927018809378100

67. Rutter PR, Vincent B. Attachment Mechanisms in the Surface Growth of Microorganisms. In: *Physiological Models in Microbiology*. CRC Press; 2018:87-108. doi:10.1201/9781351075640-4

68. Morisaki H. Measurement of the force necessary for removal of bacterial cells from a quartz plate. *J Gen Microbiol*. 1991;137(11):2649-2655. doi:10.1099/00221287-137-11-2649

69. Bruinsma GM, Van Der Mei HC, Busscher HJ. Bacterial adhesion to surface hydrophilic

and hydrophobic contact lenses. *Biomaterials*. 2001;22(24):3217-3224. doi:10.1016/S0142-9612(01)00159-4

70. Cheng G, Zhang Z, Chen S, Bryers JD, Jiang S. Inhibition of bacterial adhesion and biofilm formation on zwitterionic surfaces. *Biomaterials*. 2007;28(29):4192-4199. doi:10.1016/j.biomaterials.2007.05.041

71. Hetrick EM, Schoenfisch MH. Antibacterial nitric oxide-releasing xerogels: Cell viability and parallel plate flow cell adhesion studies. *Biomaterials*. 2007;28(11):1948-1956. doi:10.1016/j.biomaterials.2007.01.006

72. Hopkins SP, Pant J, Goudie MJ, Schmiedt C, Handa H. Achieving Long-Term Biocompatible Silicone via Covalently Immobilized S-Nitroso- N-acetylpenicillamine (SNAP) That Exhibits 4 Months of Sustained Nitric Oxide Release. *ACS Appl Mater Interfaces*. 2018;10(32):27316-27325. doi:10.1021/acsami.8b08647

73. Neufeld MJ, Lutzke A, Jones WM, Reynolds MM. Nitric Oxide Generation from Endogenous Substrates Using Metal–Organic Frameworks: Inclusion within Poly(vinyl alcohol) Membranes To Investigate Reactivity and Therapeutic Potential. *ACS Appl Mater Interfaces*. 2017;9(41):35628-35641. doi:10.1021/acsami.7b11846

74. Neufeld MJ, Lutzke A, Tapia JB, Reynolds MM. Metal–Organic Framework/Chitosan Hybrid Materials Promote Nitric Oxide Release from S-Nitrosoglutathione in Aqueous Solution. *ACS Appl Mater Interfaces*. 2017;9(6):5139-5148. doi:10.1021/acsami.6b14937

75. Fang FC. Perspectives series: host/pathogen interactions. Mechanisms of nitric oxide-related antimicrobial activity. *J Clin Invest*. 1997;99(12):2818-2825. doi:10.1172/JCI119473

CHAPTER 6

CONCLUSIONS AND FUTURE DIRECTIONS

6.1 Conclusions

In this work, three strategies were achieved to improve the performance of blood-contacting medical device surfaces: (1) nitric oxide (NO)-releasing surfaces, (2) NO-mediated fibrinogen surfaces, and (3) NO-generating surfaces. In addition, platelet-rich plasma, human whole blood and bacteria were used to evaluate the biological responses on these coated surfaces.

Chapter 3 achieves the synthesis of a multifunctional glycocalyx-mimetic surface with three features: (1) surface nano- and micro topography to provide high surface area, (2) a heparin-chitosan polyelectrolyte multilayer coating to provide glycosaminoglycan functionalization, and (3) modified chitosan with NO donor chemistry to provide an important antithrombotic small-molecule signal. Chapter 3 also demonstrates that the multifunctional glycocalyx-mimetic surfaces are nontoxic to platelets and are able to inhibit platelet adhesion and platelet activation. In addition, the NO-releasing surface can delay the blood clotting process. This work presents a successful and innovative strategy to coat medical devices with metallic surfaces.

Chapter 4 addresses the effects of a NO-mediated fibrinogen surface on platelet adhesion and activation. It is surprising that fibrinogen adsorption increases in the presence of NO, because the assumption has been that NO would inhibit fibrinogen adsorption. Interestingly, it was also observed that NO-exposed fibrinogen is able to inhibit platelet adhesion and platelet activation in the absence of continuing NO release. This observation could lead to a new approach to coat blood-contacting medical devices using fibrinogen and NO gas. It also allows consideration of whether NO-releasing surfaces are necessary at all, since platelet inhibition can be mediated by

a layer of NO-treated fibrinogen without continuous NO release. As an example of this approach, a thin fibrinogen layer can be deposited onto the surface of medical devices. The surface of the fibrinogen-coated device can then be swept with NO gas, presumably altering the structure and behavior of the protein in order to reduce the binding affinity between fibrinogen and receptors on platelet membranes. This approach overcome the limitations of NO-releasing surfaces, such as finite NO release, photo- and thermo sensitivities, NO cytotoxicity concerns, and sterilization incompatibility.

Chapter 5 demonstrates different coating methods for extracorporeal life support (ECLS) components using a copper-based metal–organic framework (MOF) as a NO-generating catalyst. The coatings promote NO generation from endogenous NO donors and are stable both after sterilization and under dynamic flow conditions. This is the first report of a successful ECLS tubing and catheter coating with catalytic properties and inherent antibacterial properties under both static and dynamic conditions. These coatings are also improve upon the disadvantages of NO-releasing surfaces as described above.

6.2 Future directions

6.2.1 NO-releasing PEM coating

Currently, the NO-releasing surfaces described in Chpater 3 can only release NO for approximately 20 min which is not ideal for implanted medical devices. For example, the achievement of re-endothelialization after coronary stent implantation is a strategy to minimize undesired immune response and smooth muscle cell de-differentiation and proliferation.[1] However, the time taken from after implantation to complete re-endothelialization various on a case-by-case basis. Two methods can be used to prolong NO release: (1) deposition of more PEM layers, and (2) modification of the nitrosation step used to form the NO donor. *tert*-Butyl nitrite is able to penetrate PEM layers and react with chitosan-thioglycolic acid (chitosan-TGA) to

form *S*-nitrosothiol functional groups. The increased chitosan-TGA layer may lead to the formation of more nitrosated chitosan-TGA, which may extend the NO release time. The additional PEM layers will also result in a rougher surface, which has been shown to reduce blood protein adsorption and prevent fibrin clot formation.[2] Modification of the nitrosation step is another approach that may improve overall nitrosation of chitosan-TGA and perhaps extend NO release capabilities. For example, nitrosation of PEM layers multiple times during the PEM coating process. However, it is unclear if additional nitrosation steps or the release of NO will change the structure of PEM layers, such as undesired reaction between reactive nitrogen species and heparin.[3,4] Dynamic blood studies with a simulated physiological flow rate are recommended. Coating stability tests under dynamic flow conditions should also be included. In addition, this NO-releasing surface is photo- and thermo- sensitive, which limits its application in clinical procedures. An alternative approach with a more robust NO donor may be considered, such as *N*-diazeniumdiolate.

6.2.2 NO-mediated fibrinogen coating

The mechanism of how NO affects fibrinogen is still unclear. It is possible that NO forms reactive nitrogen species in aqueous condition and induces changes the structure of fibrinogen. With new a structure, fibrinogen may have low binding affinity to the receptor on platelet membranes. It would be beneficial to distinguish the effects of NO and reactive nitrogen species on fibrinogen. NO gas can be used instead of a NO-releasing surfaces. However, NO gas is not stable, reacting rapidly with oxygen in the presence of air. A glovebox may or may not solve this issue. To examine structure change, several methods may help, such as circular dichroism, single-pair fluorescence resonance energy transfer, partial proteolysis, immunochemical analysis, and others.[5]

6.2.3 NO-generating MOF-coating

Currently, the MOF-coated ECLS circuit is being tested using an *ex vivo* blood flow model that simulates anticipated clinical conditions. With the exception of thromboelastographic performance, the coating integrity and catalytic properties will also be evaluated after *ex vivo* studies. The coating will then be optimized based on the results from *ex vivo* studies. For examples, the amount of MOF in each coating matrix will be adjusted if the thromboelastographic results are the same or worse than control groups. After optimization, the coated ECLS circuit will be tested using animal models for up to 72 h, which is the time required for prolonged field care. The decision on further development of MOF-coated ECLS will be based on the results from animal studies.

REFERENCES

1. Bedair TM, ElNaggar MA, Joung YK, Han DK. Recent advances to accelerate re-endothelialization for vascular stents. *J Tissue Eng*. 2017;8. doi:10.1177/2041731417731546
2. Hedayati M, Reynolds MM, Krapf D, Kipper MJ. Nanostructured Surfaces That Mimic the Vascular Endothelial Glycocalyx Reduce Blood Protein Adsorption and Prevent Fibrin Network Formation. 2018. doi:10.1021/acsami.8b09435
3. Shively JE, Conrad HE. Formation of Anhydrosugars in the Chemical Depolymerization of Heparin. *Biochemistry*. 1976;15(18):3932-3942. doi:10.1021/bi00663a005
4. Vilar RE, Ghael D, Li M, et al. Nitric oxide degradation of heparin and heparan sulphate. *Biochem J*. 1997;324(2):473-479. doi:10.1042/bj3240473
5. Nadeau OW, Carlson GM. A review of methods used for identifying structural changes in a large protein complex. *Methods Mol Biol*. 2012;796:117-132. doi:10.1007/978-1-61779-334-9_7